Summer 7-15-2024

Chemical and Morphological Characterization of Airborne Particulate Matter at the Jackpile-Paguate Mine, Pueblo of Laguna, New Mexico: Implications for Potential Metals Exposure

Andreanna C. Roros

Andreanna Roros

Candidate

Earth and Planetary Sciences

Department

This thesis is approved, and it is acceptable in quality and form for publication:

Approved by the Thesis Committee:

Adrian Brearley, Chairperson

Jose Cerrato

Eliane El Hayek

Thomas De Pree

Joe Galewsky

CHEMICAL AND MORPHOLOGICAL CHARACTERIZATION OF AIRBORNE PARTICUALATE MATTER AT THE JACKPILE-PAGUATE MINE, PUEBLO OF LAGUNA, NEW MEXICO: IMPLICATIONS FOR POTENTIAL METALS EXPOSURES

BY

ANDREANNA ROROS

B.S., Geological Sciences, University of Delaware, 2022

THESIS

Submitted in Partial Fulfillment

of the Requirements for the Degree of

Master of Science

Earth and Planetary Sciences

The University of New Mexico

Albuquerque, New Mexico

July 2024

ACKNOWLEDGEMENTS:

I would first like to thank the Pueblo of Laguna community for allowing me to collect samples from their land, inviting me to their feast days, and informing me about how the Jackpile-Paguate abandoned uranium mine has impacted each of their lives. I especially want to acknowledge the collaboration with the Pueblo of Laguna Environmental Natural Resources Department and the continuous effort of Greg Jojola and Amy Garcia to accommodate their busy work schedules for field sampling days. It is because of their support and knowledge of the mine that we were able to collect this large array of dust samples. They also provided key insights into possibilities for potential metals release into the environment.

I would also like to thank the UNM Metals Exposure and Toxicity Assessment on Tribal Lands in the Southwest Superfund Research Program for allowing me to become a trainee and for the continued support to attend conferences and present new data. Furthermore, I would like to thank my advisor, Dr. Adrian Brearley, for taking me on as an M.S. student and giving me the opportunity to create these collaborations and participate in a meaningful research project that will hopefully provide insights to the Pueblo of Laguna community.

I am also grateful for the opportunity to have participated in the NSF-funded Museum Research Traineeship program which provided key mentorship, applicable classes, and multiple networking opportunities. Thank you to Dr. Cori Myers for initially reaching out to me about the program and encouraging me to apply. I would also like to thank Dr. Tom Turner, Loretta Esquibel, and everyone in the second MRT cohort for their endless support and ability to withstand my frankness.

I am also extremely appreciative of everyone in the Brearley lab group for their continuous help in answering my research questions, listening to me practice presentations, teaching me how to use the SEM, and always providing moral support.

I would like to thank my committee members, Dr. Jose Cerrato, Dr. Eliane El Hayek, Dr, Thomas De Pree, and Dr. Joe Galewsky for all their help and encouragement during these last two years.

I am also grateful to Dr. Abdul-Mehdi, Dr. Michael Splide, and Dr. Angelica Trevizo for helping me with important lab analyses during this project.

Lastly, I would like to thank my friends and family for supporting my goals of achieving higher education—even if that means moving across the country. Most importantly, I am grateful to Mr. Freckles for putting a smile on my face each day and helping me get through the stressors of life and graduate school.

This research was supported by the UNM METALS SRP (NIH Award No. P42ES025589), the Museum Research Traineeship Program (NSF Award No. A21-0084-001), the UNM Center for Regional Studies, and the Research Exploration Connection Program.

Chemical and Morphological Characterization of Airborne Particulate Matter at the Jackpile-Paguate Mine, Pueblo of Laguna, New Mexico: Implications for Potential Metals Exposure

By

Andreanna C. Roros

B.S. Geological Sciences, University of Delaware, 2022

M.S. Earth and Planetary Sciences, University of New Mexico, 2024

ABSTRACT

In this study, we sampled airborne particulate matter (PM) within the Jackpile abandoned uranium mine on the Pueblo of Laguna, New Mexico, using passive sampling to characterize dust within the mine. The objective was to determine the elemental concentrations, mineralogy, and morphology of PM in the mine. From August 2023 to May 2024, samples were collected monthly from five sites and analyzed using scanning electron microscopy (SEM) and inductively coupled plasma mass spectrometry (ICP-MS). Uranium-bearing minerals were not detected, and U and V concentrations were at or below their crustal averages. However, the dust contained Cu, Zn, Cr, Ni, Fe, and Sn-bearing PM_{10} and $PM_{2.5}$ particulates likely of anthropogenic origin. Mo, As, Cu, Zn, Ni, Cr, Sn, and Cd exceeded their crustal averages, further suggesting anthropogenic sources. Overall, the exposure risks from windblown hazardous minerals originating from the mine are minimal and like those experienced by the general U.S. population.

TABLE OF CONTENTS

LIST OF FIGURES viii

LIST OF TABLES xvi

1 INTRODUCTION: 1

2 MATERIALS AND METHODS: 6

2.1 Airborne Dust Sampling. 6

2.2 Dust Extraction from Filters. 7

2.3 Determination of Dust Mass. 8

2.4 Acid Digestion of Dust. 8

2.5 Inductively Coupled Mass Spectrometry (ICP-MS). 9

2.6 Scanning Electron Microscopy (SEM). 9

3 RESULTS: 11

3.1 Locations and Monthly Trends for Dust Mass Collection: 11

3.2 Particulate Matter Morphology & Elemental Composition: 14

3.3 Identification of Metal Concentrations in Dust: 18

4 DISCUSSION: 31

4.1 Temporal and Topographical Considerations on Dust Collection: 31

4.1.1 Collection Type: 31

4.1.2 Temporal Variations: 32

4.1.3 Geomorphic Differences: 35

4.2 Implications of Particulate Composition & Morphology: 36

4.3 Potential Metal Sources: 38

4.3.1 Molybdenum 40

4.3.2 Arsenic 41

4.3.3 Copper & Zinc 43

4.3.4 Chromium & Nickel 46

4.3.5 Tin & Cadmium 47

5 CONLCLUSIONS: 50

6 FUTURE DIRECTIONS: 53

REFERENCES.....96

LIST OF FIGURES

Figure 1. Aerial map, taken from Google Earth, of the five different sampling locations from where dust was collected throughout the Jackpile-Paguate Mine. Three dust samplers were placed in the Main Pit (Sites 1-3), one in the North Pit (Site 4), and one in the South Pit (Site 5). Proximity of the samplers to the Village of Paguate can also be seen on this map.....55

Figure 2. Ground-level images of each of the five sampling sites within the Jackpile-Paguate Mine and their surrounding topography. Site 1, in the Main Pit, was the most exposed out of all the samplers and located on a mesa top while Site 5 (South Pit) was the least exposed of all the samplers and located in a bowl-shaped depression surrounded by large sandstone cliffs. 56

Figure 3. Bar graphs showing the raw, logged, mass data by sampling period and filter type. Graph 3A shows the masses collected by the settler samplers throughout the 8 sampling periods. The highest settler masses occurred during September through October, February through March, and March through April and all at Site 1. The lowest settler mass occurred at Site 1 from January through February. October through December, January through December, and January through February tended to have smaller masses compared to the other sampling periods. Graph 3B shows the masses collected by the windblown samplers throughout the 8 sampling periods. Apart from a slight decreasing trend and a few outliers, the windblown masses remain similar throughout the sampling periods and at each of the sites. In general, when comparing graph 3A to 3B the settler masses are more variable when compared to the windblown masses by sampling period.....57

Figure 4. Bar graphs showing the raw, logged, mass data by site and filter type. Graph 4A shows the masses collected by the settler samplers at each of the 5 sites. Site 1 tended to collect the largest masses while Site 5 collected the smallest masses. The largest mass collected at Site 1 occurred during the March through April sampling period. The settler masses collected at Site 5 were consistent throughout the sampling period but varied for the other sites depending on the sampling month. Graph 4B shows the masses collected by the windblown samplers at each of the 5 sites. Apart from a few outliers, the windblown masses remained similar at each site during the different sampling periods. In general, when comparing graph 4A to 4B, the settler masses are more variable when compared to the windblown masses by site.....58

Figure 5. Bar and scatterplot showing the normalized average mass collected, on a logarithmic scale, by each site during the entire 10-month sampling period. These graphs show that the settler filters collected a larger mass than the windblown filters at each of the five sites. The settler masses varied more, sometimes by a whole order of magnitude, by site when compared to the windblown masses which stayed more consistent. The graphs also show that Site 1 collected the largest average settler mass while Site 5 collected the smallest average settler mass. 59

Figure 6. Bar and scatterplot showing the normalized average mass collected, on a logarithmic scale, by each sampling period. These graphs show that the settler filters

collected a larger mass than the windblown filters during each sampling period. The graphs show a bimodal distribution of masses. The peak mass occurred during September through October, followed by a general decrease in mass from October through December, and another peak mass in March through April. 60

Figure 7. Scanning electron microscopy (SEM) backscattered electron image (BSE) and corresponding montaged energy dispersive spectroscopy (EDS) X-ray map of dust grains collected in Filter 10 located at Site 5. Overlaying different colors for each element produces a semi-qualitative understanding of the composition of dust grains. For example, if Si is assigned the color orange, a quartz grain would show up as orange. If mixes of elements are present, there will be a combination of colors (see feldspar grains that contain both Si and K and/or Ca). This elemental X-ray map shows the bulk mineralogy of dust collected at the Jackpile-Paguate Mine. Silicates, such as quartz and feldspars, sulfates, carbonates, and oxides are common within the dust samples. These minerals are consistent with regional geology, especially sandstone bodies. The table shows the chemical formula of common minerals found within the dust. 61

Figure 8. Scanning electron microscopy (SEM) backscattered electron (BSE) images of naturally occurring minerals found within the dust collected throughout the mine. Corresponding energy dispersive spectroscopy (EDS) spectraa for each of the grains showing the peak elemental counts are also presented. Figure 8A shows an iron sulfide mineral found in the dust collected in the Main Pit that is about 15 μm. The spectrum in 8B shows high Fe and S intensity peaks indicating that the particulate is likely an iron-sulfide. Figure 8C and Figure 8E show barium-sulfate grains collected from the Main and South pit that are less than 5 μm. The spectrum in 8D and 8F shows high Ba and S intensity peaks indicating that the particulates are likely barium sulfate. 62

Figure 9. Scanning electron microscopy (SEM) backscattered electron (BSE) images of copper metal particulates in the dust collected throughout the mine. Corresponding energy dispersive spectroscopy (EDS) spectra for each of the grains showing the peak elemental counts are also presented. Figure 9A and 9C show Cu metal particulates found in dust collected from the Main Pit (Site 2 & 3) and are both less than 5 μm. Both spectra in Figure 9B and 9D show low oxygen intensity peaks but high Cu peaks indicating that the particulates are likely metal. 63

Figure 10. Scanning electron microscopy (SEM) backscattered electron (BSE) images of tin metal particulates in the dust collected throughout the mine. Corresponding energy dispersive spectroscopy (EDS) spectra for each of the grains showing the peak elemental counts are also presented. The Sn particulate in 10A and 10C were both collected in dust from the Main Pit (Site 3). The particulates in 10A and 10C are both less than 5 μm and have irregular morphologies. The spectrum in 10B, which corresponds to the particulate in 10A, shows low oxygen intensity peaks compared to higher intensity Sn peaks. The spectrum in 10D, which corresponds to the particulate in 10C, has multiple different elements present such as Al, Si, and O. However, since the Sn intensity peaks are larger, the EDS is likely picking up X-rays from other surrounding grains. The high intensity Sn peaks when compared to the other

elements present in spectra 10B and spectra 10D indicate that the grains in 10A and 10C are likely tin metal. 64

Figure 11. Scanning electron microscopy (SEM) backscattered electron image (BSE) of nickel metal particulate in the dust collected throughout the mine with corresponding energy dispersive spectroscopy (EDS) spectrra showing the peak elemental counts. The particulate in 11A was found in dust collected from the North Pit (Site 5). The Ni particulate is less than 2.5 μm and has an irregular morphology. The spectrum in 11B shows high intensity Ni peaks with a low intensity oxygen peak indicating that the particulate is likely a metal. 65

Figure 12. Scanning electron microscopy (SEM) backscattered electron images (BSE) of cerium-rich particulates in the dust collected throughout the mine. Corresponding energy dispersive spectroscopy (EDS) spectra for each of the grains showing the peak elemental counts are also present. The Ce-rich particulates in 12A, 12C, and 12E were all found in dust collected from the Main Pit (Site 3) located near the exposed U-bearing outcrop. Figure 12A shows a particulate that is less than 2.5 μm. The corresponding EDS spectrum in 12B shows Ce and O intensity peaks indicating that the particulate is likely ceria. Figure 12C shows a particulate that is less than a micron. The corresponding EDS spectrum in 12D shows a high Si intensity peak coupled with smaller Ce and O peaks indicating that the particulate is likely a Ce-rich silicate. Figure 12E shows a 10 μm particulate. The EDS spectrum in 12F reveals the presence of Ce and La, a rare earth element. There are also smaller intensity Al, Si, and P peaks. This composition is indicative of a monazite grain. 66

Figure 13. Scanning electron microscopy (SEM) backscattered electron images (BSE) of Cu & Zn-rich particulates in the dust collected throughout the mine. Corresponding energy dispersive spectroscopy (EDS) spectra for each of the grains showing the peak elemental counts are also presented. The particulates in 13A, 13C, 13E, and 13G, were all found in dust collected from the three sites within the Main Pit and range in size from 2.5 μm to 10 μm. The respective EDS spectra in 13B, 13D, 13F, and 13H show high intensity Cu and Zn peaks with low O peaks. This indicates that the particulates could be metal and associated with brass alloys. 67

Figure 14. Scanning electron microscopy (SEM) backscattered electron images (BSE) of Cr, Ni, and Fe-rich particulates in the dust collected throughout the mine. Corresponding energy dispersive spectroscopy (EDS) spectra for each of the grains showing the peak elemental counts are also present. The particulates in 14A, 14C, 14E, and 14G were found in dust collected from the Main Pit (Site 2) and the North Pit (Site 4). Each of the particulates are 2.5 μm or less (14A). Respective EDS spectra in 14B, 14D, 14F, and 14H show intensity peaks in multiple elements including Cr, Ni, and Fe. The co-occurrence of these elements is commonly associated with stainless-steel alloys. However, these spectra also show high O peaks and the presence of other elements such as Si, S, Al, and Co. This could be due to the EDS spectra picking up X-rays from nearby particles.....68

Figure 15. Scanning electron microscopy (SEM) backscattered electron images (BSE) of Cr, Ni, and Fe-rich particulates in the dust collected throughout the mine. Corresponding energy

dispersive spectroscopy (EDS) spectra for each of the grains showing the peak elemental counts are also presented. The particulates in 15A, 15C, and 15E were found in dust collected from the Main Pit (Site 3) and the North Pit (Site 4). The particles range from 2.5 μm to 5 μm. Respective EDS spectra in 15B, 15D and 15F show intensity peaks in multiple elements including Cr, Ni, and Fe. The co-occurrence of these elements is commonly associated with stainless-steel alloys. However, these spectra also show high O peaks and the presence of other elements such as Si, S, Al, and Co. This could be due to the EDS spectra picking up X-rays from nearby particles.....69

Figure 16. Scanning electron microscopy (SEM) backscattered electron images (BSE) of Cr, Ni, and Fe-rich spherical particulates in the dust collected throughout the mine. Corresponding energy dispersive spectroscopy (EDS) spectra for each of the grains showing the peak elemental counts are also presented. The particulates in 16A, 16C, and 16E were found in dust collected from the Main Pit (Site 3). The particles range from less than a micron 5 μm. Respective EDS spectra in 16B, 16D and 16F show intensity peaks in multiple elements including Cr, Ni, and Fe. The co-occurrence of these elements is commonly associated with stainless-steel alloys. However, these spectra also show high O peaks and the presence of other elements such as Si, Al, and K. This could be due to the EDS spectra picking up X-rays from nearby particles. The spherical morphology of these particulates is distinct and was commonly associated with Cr, Ni, and Fe. 70

Figure 17. Scanning electron microscopy (SEM) backscattered electron images (BSE) of Cr, Ni, and Fe-rich spherical particulates in the dust collected throughout the mine. Corresponding energy dispersive spectroscopy (EDS) spectra for each of the grains showing the peak elemental counts are also presented. The particulates in 17A, 17C, and 17E were found in dust collected from the Main Pit (Site 2). The particles are about 2.5 μm and have a distinct spherical morphology. Respective EDS spectra in 17B and 17D show intensity peaks in multiple elements including Cr, Ni, and Fe. The co-occurrence of these elements is commonly associated with stainless-steel alloys. However, these spectra also show high O peaks and the presence of other elements such as Si and Al. This could be due to the EDS spectra picking up X-rays from nearby particles. The spherical particulate in 17E is likely an iron-oxide as the corresponding EDS spectrum in 17F does not show Cr and Ni and other elements. The spherical morphology of these particulates is distinct and was commonly associated with Cr, Ni, and Fe. 71

Figure 18. Average concentration (mg/kg) of elements in dust collected at each of the five sites within the Jackpile-Paguate mine that are at or below their crustal averages. Total average concentrations for uranium (18A), vanadium (18B), and cerium (18C) are presented with their corresponding standard deviations, crustal average, and Bernalillo County, New Mexico, soil averages. The bars are representative of the average concentration at each site and the horizontal lines represent the crustal (orange) and soil average (blue). The site averages are consistently below the crustal and soil averages as represented by the bars being below the horizontal lines. 72

Figure 19. Histogram showing the average concentrations for uranium, vanadium, and cerium at each of the five sites. There is an enrichment in these ore-associated elements specifically at Site 3 which is in the Main Pit near an exposed U-bearing outcrop. The concentrations of U, V, and Ce are higher at Site 3 compared to the other sites. 73

Figure 20. Average concentration (mg/kg) of elements in dust collected at each of the five sites within the Jackpile-Paguate mine that are at or below their crustal averages. Total average concentrations for lead (20A), manganese (20B), iron (20C), cobalt (20D), and aluminum (20E) are presented with their corresponding standard deviation, crustal average, and Bernalillo County, New Mexico, soil average. Standard deviations that appear negative result from the dataset not being normally distributed. The larger the spread of data the longer the standard deviation bar. The histogram bars are representative of the average concentration at each site and the horizontal lines represent the crustal (orange) and soil average (blue). The site averages are consistently below the crustal and soil averages as represented by the bars being below the horizontal lines. 74

Figure 21. Average concentration (mg/kg) of elements in dust collected at each of the five sites within the Jackpile-Paguate mine that are above their crustal averages. Total average concentrations for molybdenum (21A), arsenic (21B), zinc (21C), and copper are presented with their corresponding standard deviation, crustal average, and Bernalillo County, New Mexico, soil average. Standard deviations that appear negative result from the dataset not being normally distributed. The larger the spread of data the longer the standard deviation bars. The histogram bars are representative of the average concentration at each site and the horizontal lines represent the crustal (orange) and soil average (blue). The site averages are consistently above the crustal and soil averages as represented by the bars being below the horizontal lines. 75

Figure 22. Average concentration (mg/kg) of elements in dust collected at each of the five sites within the Jackpile-Paguate mine that are above their crustal averages. Total average concentrations for chromium (22A), nickel (22B), cadmium (21C), and tin (21D) are presented with their corresponding standard deviation, crustal average, and Bernalillo County, New Mexico, soil average. Standard deviations that appear negative result from the dataset not being normally distributed. The larger the spread of data the longer the standard deviation bar. The histogram bars are representative of the average concentration at each site and the horizontal lines represent the crustal (orange) and soil average (blue). The site averages are consistently above the crustal and soil averages as represented by the bars being below the horizontal lines. 76

Figure 23. Raw logged concentration data (mg/kg) of elements in dust collected at each of the five sites within the Jackpile-Paguate mine that are generally at or below their crustal averages. The raw data for uranium (23A), vanadium (23B), and cerium (23C) are presented. The histogram bars are representative of the raw data at each site and the horizontal line (red) represents the crustal average. Data are also separated by settler (S) and windblown (WB) collector types. 77

Figure 24. Raw logged concentration data (mg/kg) of elements in dust collected at each of the five sites within the Jackpile-Paguate mine that are generally at or below their crustal averages. The raw data for lead (24A), manganese (24B), iron (24C), cobalt (24D), and aluminum (24E) are presented. The histogram bars are representative of the raw data at each site and the horizontal lines (red) represents the crustal average and Bernalillo County, NM, soil average (yellow). Data are also separated by settler (S) and windblown (WB) collector types. 78

Figure 25. Raw logged concentration data (mg/kg) of elements in dust collected at each of the five sites within the Jackpile-Paguate mine that are generally above their crustal averages. The raw data for molybdenum (25A), arsenic (25B), zinc (25C), and copper (25D) are presented. The histogram bars are representative of the raw data at each site and the horizontal lines (red) represent the crustal average and Bernalillo County, NM, soil average (yellow). Data are also separated by settler (S) and windblown (WB) collector types. ... 79

Figure 26. Raw concentration data (mg/kg) of elements in dust collected at each of the five sites within the Jackpile-Paguate mine that are generally above their crustal averages. The raw data for chromium (26A), nickel (26B), cadmium (26C), and zinc (26D) are presented. The histogram bars are representative of the raw data at each site and the horizontal lines (red) represent the crustal average and Bernalillo County, NM, soil average (yellow). Data are also separated by settler (S) and windblown (WB) collector types. 80

Figure 27. Average concentration (mg/kg) of elements in dust collected during each of the eight sampling periods that were primarily at or below the crustal average. Total average concentrations for uranium (27A), vanadium (27B), cerium (27C), and lead (28D) with their corresponding standard deviation, crustal average, and Bernalillo County, New Mexico, soil average. Standard deviations that appear negative result from the dataset not being normally distributed. The larger the spread of data the longer the standard deviation bar. The histogram bars are representative of the average concentration during each month and the horizontal lines represent the crustal (orange) and soil average (blue). Peak elemental concentrations occurred during the January through February sampling period. 81

Figure 28. Average concentration (mg/kg) of elements in dust collected during each of the eight sampling periods that were primarily at or below the crustal average. Total average concentrations for manganese (28A), iron (28B), cobalt (28C), and aluminum (28D) with their corresponding standard deviation, crustal average, and Bernalillo County, New Mexico, soil average. Standard deviations that appear negative result from the dataset not being normally distributed. The larger the spread of data the longer the standard deviation bar. The histogram bars are representative of the average concentration during each month and the horizontal lines represent the crustal (orange) and soil average (blue). Peak elemental concentrations occurred during the January through February sampling period.....82

Figure 29. Average concentration (mg/kg) of elements in dust collected during each of the eight sampling periods that were primarily above the crustal average. Total average concentrations for molybdenum (29A), zinc (29B), copper (29C), and nickel (29D) with their

corresponding standard deviation, crustal average, and Bernalillo County, New Mexico, soil average. Standard deviations that appear negative result from the dataset not being normally distributed. The larger the spread of data the longer the standard deviation bar. The histogram bars are representative of the average concentration during each month and the horizontal lines represent the crustal (orange) and soil average (blue). Peak elemental concentrations occurred during the January through February sampling period. 83

Figure 30. Average concentration (mg/kg) of elements in dust collected during each of the eight sampling periods that were primarily above the crustal average. Total average concentrations for arsenic (30A), chromium (30B), cadmium (30C), and tin (30D) are presented with their corresponding standard deviation, crustal average, and Bernalillo County, New Mexico, soil average. Standard deviations that appear negative result from the dataset not being normally distributed. The larger the spread of data the longer the standard deviation bar. The histogram bars are representative of the average concentration during each sampling period and the horizontal lines represent the crustal (orange) and soil average (blue). Sn, Co, and Al peak concentrations occurred during January through February. The peak Cd concentration occurred in the October through December sampling period as opposed to January and February.....84

Figure 31. Raw concentration data (mg/kg) of elements in dust collected during each of the 8 sampling periods that are generally at or below the crustal averages. The raw data for uranium (31A), vanadium (31B), cerium (31C), and lead (31D) are presented. The histogram bars are representative of the raw data at each site and the horizontal lines (red) represent the crustal average and Bernalillo County, NM, soil average (yellow). Data are also separated by settler (S) and windblown (WB) collector types.....85

Figure 32. Raw concentration data (mg/kg) of elements in dust collected during each of the 8 sampling periods that are generally at or below the crustal averages. The raw data for manganese (32A), iron (32B), cobalt (32C), and aluminum (32D) are presented. The histogram bars are representative of the raw data at each site and the horizontal lines (red) represent the crustal average and Bernalillo County, NM, soil average (yellow). Data are also separated by settler (S) and windblown (WB) collector types. 86

Figure 33. Raw concentration data (mg/kg) of elements in dust collected during each of the 8 sampling periods that are generally above the crustal averages. The raw data for molybdenum (33A), zinc (33B), copper (33C), and nickel (33D) are presented. The histogram bars are representative of the raw data at each site and the horizontal lines (red) represent the crustal average and Bernalillo County, NM, soil average (yellow). Data are also separated by settler (S) and windblown (WB) collector types. 87

Figure 34. Raw concentration data (mg/kg) of elements in dust collected during each of the 8 sampling periods that are generally above the crustal averages. The raw data for arsenic (34A), chromium (34B), cadmium (34C), and tin (34D) are presented. The histogram bars are representative of the raw data at each site and the horizontal lines (red) represent the crustal

average and Bernalillo County, NM, soil average (yellow). Data are also separated by settler (S) and windblown (WB) collector type. 88

Figure 35. Plot of the average settler masses vs. the monthly average relative humidity. Figure 36A shows the average relative humidity near Pueblo of Laguna graphed against the logged average settler masses that were collected during each sampling period. This scatterplot shows that during periods of higher relative humidity, specifically from October to February, the average mass collected was lower. The line of best fit (y=-3725.8x + 49.811) found when graphing relative humidity against mass in Figure 36B produced a negative linear regression coefficient. This suggests that as relative humidity increased airborne mass decreases. However, the low R^2 (0.2439) value shows that there no significant correlation between the variables in this dataset. 89

Figure 36. Plot of the average settler masses vs. the monthly average windspeed. Figure 37A shows the average windspeed near Pueblo of Laguna graphed against the logged average settler masses that were collected during each sampling period. Although the linear regression (y=172.3x + 3.5197) coefficient was positive, suggesting an increase in mass with average windspeed, the R^2 (0.0738) value produced from graphing the average windspeed by mass in Figure 37B show that there is no correlation between the variables. 90

Figure 37. Plot of the average settler masses vs. the peak monthly windspeed. Figure 38A shows the peak windspeed near Pueblo of Laguna graphed against the logged average settler masses that were collected during each sampling period. The linear regression (y=-17.419x + 19.011) coefficient and the low R^2 (0.127) value produced from graphing the peak monthly windspeed by mass in Figure 38B shows that there is no significant correlation between the variables. The changes seen in the amount of mass collected over the sampling periods are not correlated to monthly peak windspeed. 91

LIST OF TABLES

Table 1. Showing data for each of the 8 sampling periods. The sampling ran from August 2023 to May 2024. Deployment date is when new filters were placed in the collectors and the retrieval date is when they were taken back from the field. During the retrieval dates, new filters were also placed in the collectors. The sampling period is also defined by the number of days the filters were out in the field, which was used to normalize the mass data. 92

Table 2. Table showing the different samples that were analyzed using scanning electron microscopy (SEM). The Filter # is the identifier used when the samples were placed out in the field and are correlated to the site and sampling period that they are from. The SEM analysis spanned each of the 5 different sites as well as the 8 different sampling periods. The composition of the dust grains was qualitatively analyzed using energy dispersive spectroscopy (EDS). EDS results are present in the last column of the table and show the common elements found throughout the dust grains. 93

Table 3. Compilation of the average relative humidity, average windspeed, and peak windspeed close to Pueblo of Laguna, New Mexico, during each of the different sampling dust sampling periods. This data was collected from the National Weather Service. These different weather variables were examined to determine if there was a correlation between them and the collected mass. 94

Table 4. Compilation of the geographical information of each of the five sites. Each of the different “sites” are associated with one of the three major pits in the Jackpile Mine. The coordinates of those locations as well as the elevation are also present..... 95

1 INTRODUCTION:

There are thousands of abandoned uranium mines (AUM) located throughout the Four Corners region of the southwest United States that disproportionately affect Native American communities (USEPA, 2008). Among these communities, the Pueblo of Laguna (POL) located in north central New Mexico, has several villages situated at distances ranging from 0.5 to 8 miles from the Jackpile-Paguate abandoned uranium (U) mine. The Jackpile Mine, which operated from 1952-1982, was one of the largest open pit uranium mines in the world. During active mining at the site, blasting led to the release of large quantities of harmful dust as well as the exposure of ore-bearing outcrops. Although remediation of the mine site was conducted during 1989-1995, in 2013 the site was placed on the Superfund National Priorities List (NPL) after reevaluation of the condition of the previous remediation efforts. Primary site contaminants, as reported by the US Environmental Protection Agency (EPA) in their Hazard Ranking Report (EPA, 2013). Chronic inhalation of these metals through the respiration of particulate matter (PM), which is easily mobilized from sources such as mine waste piles in the arid and windy southwestern climate of New Mexico, can lead to health conditions such as cancer, hypertension, kidney disease, and lung disease (El Hayek et al., 2021; Hettiarachchi et al. 2019; Zychowski et al., 2018).

Particulate matter is a term used to describe material such as dust and dirt, which becomes suspended in the air. However, the EPA has distinguished certain size ranges of particulate matter that pose the highest threat to human health. These subdivisions include PM_{10} and $PM_{2.5}$. PM_{10} are particulates that are 10 microns or less in diameter while $PM_{2.5}$ are particulates 2.5 microns or less in diameter. These sizes are of major concern because of their ability to travel into the respiratory tract, through inhalation and respiration, and penetrate the

lungs. When these fine particulates contain toxic metals, the health risks associated with inhalation increases. As a result, exposure to windblown, toxic, metal-bearing particulate matter from the Jackpile Mine has become a major concern for the Pueblo of Laguna communities. However, it is unknown whether inhalation of windblown PM is or has been a significant exposure pathway for the communities living near the Jackpile mine. This is largely because environmental monitoring of airborne dust during active mining as well as in the present has not been thoroughly conducted.

Understanding the mineralogy of uranium and its potential co-occurrence with metals in the Jackpile Mine is important to understanding the characteristics of potential windblown PM that may be being produced at the site. Analysis of subsurface minerals at the site revealed U-bearing mineral phases such as uraninite, meta-autunite, tyuyamunite and coffinite (Moench & Schlee, 1967; Deditius et al., 2008). Crystals of coffinite have been precipitated with layers of organic matter and vanadium-rich mica in the sandstone associated with the Morrison Formation in the Grants Mining District (Deditius et al., 2008). Abandoned mine wastes, which have been exposed to decades of weathering and oxidation, have also been found to contain coffinite (Blake et al., 2017). Uranium and rare earth elements (REEs) are commonly incorporated into nano-scale crystals of secondary coffinite (Deditius et al., 2008). Although the Jackpile Mine was primarily a uranium mine, several other metals are associated with the uranium ores. Electron microprobe mapping of the uranium ore, some of which is still exposed at the mine, revealed that these deposits commonly co-occur with other elements such as potassium, phosphorus, sulfur, iron, and vanadium (Blake et al., 2017; Hettiarachchi et al., 2019). These phases (U-P-K) are generally encapsulated by organic carbon and co-exist with kaolinite, quartz, and microcline that are likely associated with the

sandstone formation in which the U is hosted (Avasarala et al., 2019). Similarly, uranyl vanadate, uranyl arsenate, uraninite, coffinite, and other U-bearing particles have been found in the soils and dust collected near the Jackpile Mine from Tisch High Volume Air Samplers and Big Spring Number Eight Dust Flux samplers (Hettiarachchi et al., 2018; LaRosa-LoPresti, 2021). The chances of suspension and transportation of uranium-bearing minerals from the mine to neighboring communities increase when the U occurs in nanoparticulate clusters that can disaggregate and attach to other grains (Schindler et al., 2017). This nanoparticulate form is concerning because the highest proportion of contaminated material from mine waste is usually present within the airborne respirable particulates (Martin et al., 2016). Smaller particles associated with mine waste and soils often contain higher amounts of metals and metalloids (Kim et al., 2011).

There are several studies that have shown that fugitive dust from active and abandoned mine sites in arid environments can lead to significant environmental health risks (Csavina et al., 2012, Brown et al., 2017, LaRosa-LoPresti et al., 2021). Heavy metal exposure via airborne dust inhalation at the Jackpile Mine has not been studied in any detail. Knowledge about the chemical composition and morphology of collected PM directly within the mine site is limited (Hettiarachchi et al., 2018; McLemore et al., 2021). There are only limited studies that explicitly focus on the identification of metals, metalloids, and minerals in airborne dust from the mine with many assessing contaminants present in soil and water (Brown et al., 2017, Hettiarachchi et al., 2018; LaRosa-LoPresti, 2021). Establishing if potentially hazardous material is present within the dust collected from the mine is essential for establishing if airborne PM represents an exposure pathway to the community. Such information about the dust is also critical to helping deduce potential sources of any

contaminants to inform potential exposure mitigation strategies. Airborne sampling associated with the Jackpile Mine has primarily focused on collection in the vicinity of the mine (Brown et al., 2017, Hettiarachchi et al., 2018; LaRosa-LoPresti, 2021) and not directly in each of the three major pits, one of which is directly below the village of Paguate. Furthermore, previous sampling efforts did not sample systematically over an extended period of time at set intervals. As a result, there is limited information on how the characteristics of airborne dust change temporally. This study, performed over a period of 8 months and sampling at ~1-month intervals directly addresses the concerns of the POL communities concerning the potential role of the mine as a current exposure pathway to U and other toxic metals.

The objective of this study is to investigate the bulk elemental composition of the dust and the characteristics of the particulate matter (size, shape, mineralogy) present in passively collected airborne dust from within the Jackpile Mine site, located on lands of the Pueblo of Laguna (POL), New Mexico. Scanning electron microscopy (SEM) and inductively coupled plasma mass spectrometry (ICP-MS) analyses were conducted to evaluate the mineralogy and trace element content of these windblown dust samples. A comparison and evaluation of samples collected at intervals of approximately 1 month from different locations within the mine was performed to determine if there are temporal variations in the elemental concentrations and/or mineralogical and chemical characteristics of the dust. Furthermore, two types of passive collectors were used at each site to analyze if the mechanisms of dust transport were different. This study aims to provide fundamental data on the concentration of toxic metals in particulate matter collected from the Jackpile-Paguate Mine that provide key risk exposure assessment for Native communities located in proximity to abandoned uranium

mines. Importantly, these results address specific concerns raised by community members of the Pueblo of Laguna and hence enable informed decisions to be made on how to mitigate health risks for those impacted, as well as potential remediation pathways to be taken by the EPA.

2 MATERIALS AND METHODS:

2.1 Airborne Dust Sampling. Samples of airborne particulate matter were collected at five sites distributed throughout the Jackpile mine, three in the Main pit, one in the North pit, and one in the South pit. The locations of these five sites are shown in Figure 1 and 2. The largest of these pits, and most heavily mined, was the Main pit, and therefore more samplers were placed there. The locations of the samplers included a mesa top, a former major access road to the mine, and a gully adjacent to an exposed U-bearing outcrop. Locating a sampler near an exposed U-ore bearing outcrop was also important for investigating the present-day characteristics of dust that is being mobilized by aeolian erosion of ore-bearing strata and hence is acting as a current source of U-bearing dust. This location acted as an optimum position to sample dust that may contain U-bearing minerals leading to a further understanding of the characteristics associated with the material being eroded off the outcrop. However, it is important to note that dust from point sources is diluted by input from many other distal sources. The sampler in the South Pit was placed on the floor of the pit that had previously been backfilled. This collector was located about 50 feet from strata that had been exposed during the removal of overburden during mining, to gain access to the deeper ore-bearing material. The sampler in the North pit was located directly below the village of Paguate. This sampler was located closest to the community and directly sampled particulate matter that the community is being exposed to. Information from this sampler was paramount for addressing the community's concerns about what they are currently being exposed to in the air. Particulate matter samples were collected at about 1-month intervals from August 2023-May 2024 to allow for a comprehensive study of seasonal variability. This 10-month period represents a sampling interval for each of the four seasons, including the Spring

season from March to June. This is typically the windiest time of year in New Mexico, as the jet stream moves northwards, when wind velocities can reach as high as 27 meters per second (Houghton, 1972). Collection of ambient airborne dust at these sites was facilitated using TISCH TE-200-PAS and TE-PAS-DD outdoor samplers that were raised to a height of 8 feet above the ground surface on aluminum tubes. Locating the samplers at a height close to the 3-6 ft EPA established breathing zones for humans was crucial for understanding particulate matter inhalation risks (EPA, 2024). The TE-200-PAS samplers collected windblown dust within the ambient air while TE-PAS-DD samplers collected dust that settled out of the air through direct deposition. The two types of collectors were co-located on the same aluminum pole, at the same height, but 180^{o} from one another. Particulate matter was collected on removable 5.5” diameter by 0.5” thick polyurethane (PU) foam collection substrates, TE-1014, that are specifically designed for these samplers. A total of 10 filters were collected each month (2 from each of the 5 sites), with a total of 81samples collected during 8 sampling trips.

2.2 Dust Extraction from Filters. Dust collected on the filters were extracted by sonicating the PU foam substrates in either acetone or distilled water. The collected samples were cut into eighths. Seven of the eight slices were placed in 15 ml conical centrifuge tubes, submerged in water or acetone and were then sonicated for 30 minutes. The ultrasonication uses high frequency sound waves to agitate and dislodge the particles contained within the PU foam filter material. This stimulated removal of the dust particles from the polyurethane filter. The filters were then removed from the centrifuge tubes and the particles were left to settle for about 24 hours. To ascertain whether this process was effective, SEM photos of the filters were taken before and after sonication. These images, as well as the concentration of

dust at the bottom of the tubes, indicated that the process was efficient at removing the dust from the filters. Samples were then centrifuged for 10 minutes at a speed of 500 revolutions per minute. This created a pellet of dust at the bottom of the centrifuge tube.

2.3 Determination of Dust Mass. Evaporation of the acetone/distilled water within the centrifuge tubes was performed under a laminar flow bench. The flow bench contained a high efficiency particulate air (HEPA) filter that removed contaminants such as dust, pollen, mold, bacteria, and airborne particles from the air it blows out. This provided a contamination-free environment when the tubes were open to the air for evaporation of the acetone or distilled water Once the samples were dry, the concentrated dust was then extracted from the centrifuge tubes and weighed on a high-precision balance. Normalizing the dust masses was done to account for the days that each of the samples were in the field (see Table 1). To calculate the average mass collected by each site, it was first necessary to group the masses into their respective locations. The individual masses were divided by the number of days they were in the field. These masses were then averaged with the rest of the corresponding weights for each site. This calculation, therefore, estimated the amount of dust collected each day at the different sites throughout the entire 10-month sampling period.

2.4 Acid Digestion of Dust. To measure the bulk concentrations of elements in each of the dust samples in the dust by inductively coupled plasma mass spectrometry (ICP-MS) acid digestion of the solid dust samples was performed. Digesting the samples kept the analytes of interest in a homogenized solution. The pre-weighed dust samples were digested using a 2:1 ratio of hydrochloric acid to nitric acid. The samples were then left to digest on a VWR standard heat block for 30 minutes to an hour. Following cooling of the solution, 10 ml of

deionized water was added to the samples to bring them to volume. The samples were then filtered to 0.45 microns to remove insoluble material and undissolved solids.

2.5 Inductively Coupled Mass Spectrometry (ICP-MS). Acid digested samples that contained the dust solution were measured using ICP-MS. A NexION 300D ICP-MS, with a detection limit of < 0.5 mg L^{-1} and 5-point calibration curve, was utilized to determine the elemental concentrations of metals in the dust. Dust samples were measured for As, Mn, Li, Zn, Pb, U, Se, Cu, V, Co, Ni, Cd, Mo, Ti, La, Ce, Ba, Sn, Fe, Al, Sr, and Cr. Elemental concentrations in mg/Kg (parts per million). were calculated using the mass that was measured for each of the dust samples collected from each filter. More information on measuring the elemental concentrations of the dust can be found in Appendix A.

2.6 Scanning Electron Microscopy (SEM). To understand the elemental composition, morphology, and size of the particulate matter, selected dust samples were analyzed by scanning electron microscopy. SEM imaging was performed on a FEI NanoLab 650 Dualbeam Field Emission Gun SEM/Focused Ion Beam instrument, equipped with Oxford Instruments AZtec microanalysis coupled to an Ultim Max 170 mm^2 SDD energy dispersive spectrometer (EDS). A Tescan Vega3 XMU SEM equipped with a LaB_6 electron gun for high-resolution imaging coupled with the Iridium Ultra EDS system was also used for imaging. Dust particulates were placed on a piece of carbon tape attached to an SEM stub. Analysis of the dust was conducted using secondary electron (SE) imaging, backscattered electron (BSE) imaging (BSE), and energy dispersive X-ray spectroscopy (EDS). Secondary electron images provided information about the surface characteristics, size, and morphology of the sample. Backscattered electron imaging was used to identify high-Z phases, such as metal-rich particulates in the dust. Energy dispersive X-ray spectroscopy was used to

determine the semi quantitative elemental composition of individual particulates. In addition, X-ray mapping was carried out using Oxford Instruments AZtec SmartMap software to acquire full spectral X-ray maps of regions that included 1000s of particles. The maps were acquired at an accelerating voltage of 15-20 kV, a beam current of 3.2 nA and a pixel resolution of ~ 2 microns.

3 RESULTS:

3.1 Locations and Monthly Trends for Dust Mass Collection.

The mass of dust collected from the filters at each of the sites and sampling periods are summarized both as raw data (Figures 3 & 4) and normalized to the number of days each filter was in the field (Figure 5 & 6). Dust samples were collected during 8 different sampling trips spanning August 2023 to May 2024. Information on each of these sampling periods can be found in Table 1. The variation in the number of days samples were left in the field was due to weather conditions and other factors that limited access to the field sites. For that reason, mass data was normalized to the number of days the filter was deployed to more accurately compare the average mass collected across the different sites and sampling periods.

The raw data presented in Figure 3 and 4 shows the spread of masses obtained for both the settler and windblown filters by site and sampling period. The mass collected by the settler filters ranged from 0.003 g to 0.097 grams and from 0 g to 0.053 g for the windblown filters. Almost double the amount of mass was obtained from the settler filter that collected the most mass (0.097 g) compared to the windblown filter that collected the most mass (0.053 g). The month that obtained the highest raw settler mass occurred during the February through March sampling while the highest raw windblown mass occurred during the August through September sampling period. Once these masses were normalized by the number of days they were in the field, it was discovered that the settler filters acquired more mass than the windblown filters at each of the eight sampling intervals. The average settler masses tend to be one to two orders of magnitude larger than the average windblown masses. This can be seen in Figure 6 where the average settler and windblown masses are grouped by month. The

sampling month that collected the largest average settler mass was September through October (0.0036 g/day) and the sampling month that collected the largest windblown mass was August through September (0.00045 g/day). There is an eight-fold difference between these masses.

The raw mass data in Figure 4 and the normalized average mass data in Figure 5 show similar results. The raw mass data collected by the settler filters tends to be an order of magnitude larger than the windblown filters at each of the five sites. The largest raw settler mass (0.097 g) was collected at Site 2 while the largest raw windblown mass (0.053 g) was collected at Site 4. Normalizing the mass data in Figure 5 further revealed that the settler filters at each of the five sites within the mine collected a larger average mass than the windblown filters. Collection of settler and windblown dust favored certain sites. The settler collectors obtained the largest average mass at Site 1 (0.00093 g/day) while the windblown collectors obtained the largest average mass at Site 2 (0.000067 g/day).

Another noticeable difference between the settler and windblown collectors is that the settler masses tend to be more variable while the windblown masses tend to remain more consistent. Different locations within the mine obtained varying masses for the different sampler types and certain locations resulted in higher mass collection than others. Out of the five locations where settler dust collectors were present, Site 1 (Main Pit) tended to collect the largest amount of dust each day (0.00093 g/day; range 0.0015 g to 0.0038 g). It is important to note that this site does have three sampling periods with the highest masses (September- October, February-March, March-April) coupled with a sampling period with the lowest mass (January-February) when compared to the other sites. On the other hand, Site 2 (Main Pit) tended to obtain larger average masses each day for the windblown collectors

(000067 g/day; range 0.0014 g to 0.005 g). Site 5 (South Pit) collected the smallest average mass over the entire sampling period for both the settler (0.00007 g/day; range 0.0015 g to 0.0038 g) and windblown filters (0.000027 g/day; range 0 g to 0.0025 g). The Main Pit tended to produce the largest masses per day while the South Pit tended to produce the lowest. These masses tend to remain similar across the five sites for the windblown filters but vary by site for the settler filters. For example, the largest settler mass (0.00093 g) at Site 1 is 13 times greater than the smallest settler mass at Site 5 (0.00007 g) while the largest windblown mass at Site 2 (0.000067 g) is only 2 times greater than the lowest windblown mass at Site 5 (0.000027 g)

The mass collected from the windblown and settler filters also differed by sampling period. September through October represented the largest average mass collected by the settler filters during the entire sampling period (0.0036 g/day; range 0.0038 g to 0.091 g). On the other hand, the largest average mass collected by the windblown filters occurred during the August through September sampling period (0.00045 g/day; range 0.0034 g to 0.0053 g). January through February was the sampling period when the lowest average settler mass was collected per day (0.0003 g/day; range 0.0008 g to 0.003 g). Conversely, February through March was the sampling period that had the lowest average windblown mass obtained per day (0.00008; range 0 g to 0.0014 g). The settler and windblown collectors had different time periods when the filters produced the highest and lowest masses.

The monthly trends between the settler and windblown masses were different. When looking at Figure 6, the settler masses by sampling period are bimodally distributed. There is a peak in the average mass of dust collected during the September through October (0.0036 g) sampling period. This is followed by a period of lower masses that remained almost

constant throughout October through December, December through January and January through February (range of 0.0003 to 0.0005 g). These masses are an order of magnitude lower than the rest of the sampling periods. Eventually, there is then another peak in the mass during March through April (0.0031 g). As a result, it appears that the dataset has two distinct maxima with average masses that range from 0.0003 to 0.0036 during the sampling period. These average masses vary by a factor of twelve. As previously mentioned, the windblown masses tend to be more consistent, even when looking at the data by sampling period. The average windblown masses range from 0.00008 to 0.00045. These average masses vary by a factor of about six which is two times less than the settler masses.

3.2 Particulate Matter Morphology and Elemental Composition.

A total of 17 dust samples spanning the five different sites and sampling periods were analyzed using SEM EDS. Table 2 shows the filter number, site location, and sampling period of each investigated sample. The table presents a comprehensive list of elements enriched in the dust that were identified via EDS analysis.

The dust collected from the mine ranges in size from less than a micron to 100s of microns. The dust is primarily composed of widespread, naturally occurring minerals that are consistent with the geological characteristics of the southwest region. As a result, common minerals present within sandstone were found. Sandstones are primarily composed of calcium and potassium feldspars, quartz, iron oxides, carbonates, and sulfates. These types of minerals were found at each of the five sampling sites. Figures 7 and 8 show an array of these naturally occurring minerals found within the dust. This included barium sulfate, calcium sulfate, iron sulfide, and an abundance of feldspars and other silicates. These

minerals were identified through point EDS spectra analysis and full spectral X-ray mapping of the dust samples.

In addition to the suite of naturally occurring minerals that constitute the dominant mineralogy of the dust, SEM-EDS analysis revealed the presence of particulates that contain a range of metals, including alloys, containing Cu, Ce, Fe, Mg, Ni, Cr, Zn, and Sn. Metals were identified based on qualitative EDS analysis of elemental X-ray intensity peaks. These particles have compositions that are not consistent with naturally occurring minerals. These metal-rich particulates exhibit a variety of different morphologies, sizes, and compositions. Many of the particulates have rough edges and irregular shapes while some are rounded, spherical, and have smooth surfaces. These metal-rich particulates vary in size from less than a micron to 10 microns.

Examples of BSE images and associated EDS spectra of particulate matter Cu metal can be found in Figure 9. These Cu-rich particulates are less than five microns and have irregular morphologies (Figures 9A & 9C). Qualitative analyses of the EDS spectra (Figures 9B & 9D) revealed high intensity Cu peaks coupled with low intensity O peaks. The low intensity O indicates that the particulates are metallic in nature. Cu-oxides and silicates rich in Cu were also found in the dust samples. Furthermore, Table 2 emphasizes that Cu was found at each of the five mine sites.

Other metal particulates found in the mine dust include Sn and Ni. Figures 10A and 10C show BSE images of Sn metal particulates that are less than five microns found in the dust collected from Site 3. The corresponding EDS spectrums in Figure 10B and 10D show low intensity O peaks coupled with high intensity Sn peaks. The difference in the sizes of the elemental peaks indicates that the particulate is metal. Similarly, Figure 11A shows a BSE

image of a Ni metal particulate found in the dust collected from Site 4 that is less than a micron. Analysis of the EDS spectra in 11B reveals a low intensity O peak with higher intensity Ni peaks. Once again, this is indicative of a metal-rich particulate.

Figure 12 displays examples of BSE images of Ce-rich grains and their associated EDS spectra found in the dust samples. The grains ranged in size from less than 1 micron (Figures 12A & 12C) to 10 microns (12E). Each of the grains are shaped irregularly. The EDS spectra in Figure 12B shows O and Ce peaks indicating that the particulate is a cerium oxide. Figure 12D has small Ce peaks coupled with a larger O and Si peak indicating the grain is a cerium-rich silicate. Figure 10F displays multiple elemental peaks including P, Ce, O, and La. The co-occurrence of these elements indicates that this is the mineral monazite $(Ce,La,Nd,Th)(PO_4,SiO_4)$, which is a phosphate commonly associated with the erosion of granite and metamorphic rocks. It is important to note that Ce-rich particulates were only found in the dust collected at Site 3.

The EDS spectra of some particles suggest that brass and stainless-steel metal alloys are present within the samples. The most common metals that co-occur within the particulate matter are Cu and Zn and Cr, Ni, and Fe. Brass alloys are commonly composed of 33% Zn and 67% Cu. Figure 13 displays examples of potential brass particulates found in dust collected from Site 2 and Site 3. The EDS spectra consistently show low intensity oxygen peaks with the Cu and Zn peaks being more intense. Furthermore, the intensity of the Cu peaks surpasses that of the Zn peaks, aligning with the expected elemental ratios in brass alloys. The shapes of these particulates are irregular and tend to have rough edges. The particulates ranged in size from 2.5 to 10 microns. Although these brass alloys were

specifically found in dust samples from Site 2 and Site 3, Cu and Zn were found in particulates at each of the mine sites (see Table 2).

Stainless steel alloys are commonly composed of an iron content greater than 50%, a Cr content of 17-27%, and a Ni content of 6-22%. Particulates containing Cr, Ni, and Fe were found at each of the 5 sites; examples are shown in Figures 14 and 15. The BSE images show that these particulates range in size from less than 2.5 microns to 5 microns and have irregular shapes with rough or sharp edges. Most of the particulates have more intense Fe peaks compared to Cr and Ni, consistent with the elemental characteristics of stainless steel. Some spectra also contain other elements such as Si, S, O and Co. Silicon and S are not commonly associated with stainless steel. However, Co is known to be an unintentional impurity of stainless steel that contains Ni (Wang et al., 2022). The oxygen present within the samples could be due to the ability of stainless steel to produce passive films, when exposed to air and water, that are composed of chromium oxide layers on the surface (Olsson & Landolt et al., 2003). The only particulate that does not appear to have an oxygen intensity peak is 12E. This sample also has very low intensity S and Si peaks. It is likely that an overlap of the electron beam is picking up Si, S, and O X-rays from adjacent silicates and sulfates that are below these smaller particulates. Further analysis of the other particulates should be conducted to verify if they are stainless steel.

In addition to the irregular and asymmetric morphologies, spherical particulates were prevalent in the dust samples. Figures 16 and 17 show BSE images of spherical particulates found in the collected dust from Site 2 and Site 3. The particulates ranged in size from less than a micron to 5 microns. Corresponding EDS spectra of these particulates show that they consistently contained Cr, Fe, and Ni. The presence of O, Si, and Al in the EDS spectrums

are likely due to the electron beam picking up X-rays from adjacent or overlapping particles. The composition of these grains is again similar to stainless steel alloys.

3.3 Identification of Metal Concentrations in Dust.

ICP-MS was conducted to determine the concentrations, in mg/kg, of metals present in the dust. Figures 17 and 18 show the average concentration of elements analyzed by ICP-MS in comparison with global upper crustal averages (Rudnick and Gao). The crustal averages represent the average natural abundance of elements occurring within the Earth's upper crust. ICP-MS results were also compared to the average concentrations of elements in soils in Bernalillo County, New Mexico, although not all elements analyzed in the Jackpile dust samples are reported in the USGS compilation. There are three major trends associated with this dataset—elements that are at or below the crustal average, elements that are higher than the crustal average, and elements that are enriched at Site 3 (Main Pit). Elemental data are presented in two different ways 1) as the entire raw data set for each site and month (see Figures 23-26 for site data and 31-34 for monthly data) and 2) as the data averaged for each site and sampling period (see Figures 18-22 for site data and 27-30 for monthly data). However, averages based on the raw data set for some elements need careful interpretation because of large variations that are a function of when they were collected.

Elements at or below the crustal average include U, V, and Ce. Figure 18 displays the average concentrations of these elements at each site and Figure 23 displays the raw data. The median concentration of U for the entire dataset is 1.2 mg/kg and the mean concentration is 2.2 mg/kg with values ranging from 0.0027 mg/kg to 24.3 mg/kg. The median concentration is 2 times less than the U crustal average of 2.8 mg/kg Both the mean and median concentrations of U are below the crustal average. However, the average

concentration for U at Site 3 is about 2 times greater than the crustal average. The average concentration at Site 3 is 4.49 mg/kg with values ranging from 0.039 mg/kg to 24.3 mg/kg. The average concentration of U by each site can be seen in Figure 18 A and the raw data in 23A. The median concentration of V for the entire dataset is 11.9 mg/kg and the mean is 21.7 mg/kg with values ranging from 0.00074 mg/kg to 232 mg/kg. The median concentration is about 10 times less than the crustal average of 120 mg/kg and the average is about 6 times less. Each of the site averages is below the crustal average. The site with the highest concentration of V was Site 3. The average concentration at Site 3 is 34 mg/kg with values ranging from 1.76 mg/kg to 232 mg/kg. This average concentration is about two times higher than the concentrations at each of the other sites. The average concentration of V by each site can be seen in Figure 18B and the raw data in Figure 23B. The median Ce concentration for the entire dataset is 17.7 mg/kg and the mean is 33.1 mg/kg with values ranging from 0.011 mg/kg to 385 mg/kg. The median is 3 times lower than the 60 mg/kg crustal average and the average is about 2 times lower. Similar to V, the concentration of Ce at each of the five sites is below the crustal average with Site 3 being enriched in Ce by a factor of two compared to the other sites. The average concentration at Site 3 is 54 mg/kg with values ranging from 3.14 mg/kg to 385 mg/kg. The average concentration of C by each site can be seen in Figure 18C and the raw data in 23C. Although average U, V, and Ce are below their crustal averages at Sites 1,2, 4 and 5, there is an enrichment in these elements, at Site 3 (Main Pit). This can be seen in Figure 19. The average elemental concentrations of these elements are higher at Site 3 than at each of the other sites.

As can be seen in Figure 20 the average Pb, Mn, Fe, Co, and Al are also at or below the crustal averages. The median concentration of Pb for the entire dataset is 13.3 mg/kg, just

below the crustal average of 14 mg/kg, with values ranging from 0.0048 mg/kg to 106 mg/kg. The median concentration is about 2 times lower than the Bernalillo Country soil average of 24 mg/kg. The average concentration of Pb is 18.9 mg/kg, about 5 mg/kg above the crustal average and 5 mg/kg below the soil average. When grouping the average Pb concentrations, sites 1, 2, 4, and 5 are slightly above the crustal average by 1-4 mg/kg but below the Bernalillo County Soil average by 5-9 mg/kg. Site 3 has the largest average concentration of Pb at 24.2 mg/kg, with values ranging from 3.33 mg/kg to 106 mg/kg. This average concentration is about 2 times higher than the crustal average and right at the Bernalillo County soil average. Average concentrations of Pb by site can be seen in Figures 20A with raw data in Figure 24A.

The median Mn concentration is 277 mg/kg and the mean concentration is 470 mg/kg with values ranging from 0.793 to 4,392 mg/kg. The median is 3 times lower than the crustal average of 950 mg/kg and the mean is 2 times lower. Average concentrations of Mn by site can be seen in Figures 20B with raw data in 24B. The median and average Mn concentrations are more similar to the Bernalillo County soil average of 481 mg/kg. The median concentration of Fe for the entire dataset is 9,451 mg/kg and the mean is 17, 515 mg/kg. The median is six times lower than the crustal average of 56, 300 mg/kg and 3 times lower than the Bernalillo County soil average of 28,700 mg/kg. The mean is 3 times lower than the crustal average and about 2 times lower than the soil average. Average concentrations of Fe by site can be seen in Figures 20C with raw data in 24C.The median concentration of Al for the entire dataset is 4,586 mg/kg which and the mean is 10,349. The median concentration is 18 times lower than the crustal average of 82,300 mg/kg and 10 times lower than the Bernalillo County soil average of 47, 600 mg/kg. The mean concentration is about 8 times

lower than the crustal average and about 5 times lower than the soil average. Average concentrations of Al by site can be seen in Figures 20E with raw data in 24E. Lastly, Co is also below the crustal average. The median Co concentration for the entire dataset is 8.6 mg/kg and the mean is 13.4 mg/kg with values ranging from 0.0022 mg/kg to 102 mg/kg. The mean is two times lower than the 15 mg/kg crustal average while the mean is 1.6 mg/kg less. Average concentrations of Co by site can be seen in Figures 20D with raw data in 24D.

The elements that are above their crustal averages include Mo, As, Zn, Cu, Cr, Ni, Cd, and Sn. The median concentration of Mo for the entire dataset is 4.8 mg/kg and the mean is 7.76 mg/kg with values ranging from 0.0009 mg/kg to 61.0 mg/kg. The median is 4 times higher than the crustal average of 1.2 mg/kg and the mean is about 7 times higher. The average and raw concentrations at each of the sites, as seen in Figures 21A and 25A, are above the crustal average. The average concentration at Site 1 is 8.63 mg/kg with values ranging from 0.001 mg/kg to 21.5 mg/kg. The average concentration at Site 2 is 6.50 mg/kg with values ranging from 0.768 mg/kg 17.9 mg/kg. The average concentration at Site 3 is 11.6 mg/kg with values ranging from 1.51 mg/kg to 61.0 mg/kg. The average concentration at Site 4 is 1.29 with values ranging from 19.3 mg./kg to 12.8 mg/kg. Lastly, the average concentration at Site 5 is 5.49 mg/kg with values ranging from 2.25 mg/kg to 12.8 mg/kg. The average concentrations of Mo at the five sampling sites ranged from 5 to 10 times above the crustal average.

Arsenic also tends to have concentrations above the crustal average. The median concentration of As for the entire dataset is 3.56 mg/kg and the mean concentration is 7.13 mg/kg with values ranging from 0.249 mg/kg to 46.8 mg/kg. The median is about two times higher than the crustal average of 1.8 mg/kg and the mean is about 4 times higher. The

median was about 1 mg/kg below the Bernalillo County soil average of 4.4 mg/kg while the mean was about 2 times larger. The average and raw concentrations of As at each of the sites, which can be seen in Figuress 21B and 25B, are above the crustal average. The average concentration at Site 1 is at 6.45 mg/kg with values ranging from 0.249 mg/kg to 20.7 mg/kg. The average concentration at Site 2 is 9.2 mg/kg with values ranging from 0.942 mg/kg to 44.7 mg/kg. The average concentration at Site 3 is 10.1mg/kg with values ranging from 0.901 mg/kg to 46.8 mg/kg. The average concentration at Site 4 is 5.69 mg/kg with values ranging from 0.488 mg/kg to 36.2 mg/kg. Lastly, the average concentration at Site 5 is and 3.61 mg/kg with values ranging from 0.837 mg/kg to 7.25 mg/kg. Site 5 was the only site that had an average concentration below the Bernalillo County soil average. The average concentration of As at the five sampling sites ranged from 2 to about 6 times the crustal average.

As can be seen in Figures 21C and 25C the concentrations of Zn at each of the five sites are also above the crustal average. The median for the entire data set is 354 mg/kg and the mean is 488 mg/kg with values ranging from 4.29 mg/kg to 2,819 mg/kg. The median is about 5 times higher than the crustal average of 75 mg/kg and 6 times higher than the Bernalillo County soil average of 58 mg/kg. The mean is about 7 times higher than the crustal average and 8 times higher than the soil average. The average concentration at Site 1 is 513 mg/kg with values ranging from 4.29 mg/kg to 1,354 mg/kg. The average concentration at Site 2 is 551 mg/kg with values ranging from 88.1mg/kg to 2,164 mg/kg. The average concentration at Site 3 is 619 mg/kg with values ranging from 88.9 mg/kg to 1043 mg/kg. The average concentration at Site 4 is 386 mg/kg with values ranging from 88.7 mg/kg to 1043 mg/g. Lastly, the average concentration at Site 5 is 391 mg/kg with values

ranging from 178 mg/kg to 668 mg/kg. The average concentrations of Zn ranges from 5 to 8 times above the crustal average and 7 to 11 times above the soil average.

The average concentration of Cu is also above the crustal average throughout the mine sites. The median Cu concentration for the entire dataset is 150 mg/kg and the mean is 266 mg/kg with values ranging from 0.863 mg/kg to 1,670 mg/kg. The median is 2 times higher than the crustal average of 63 mg/kg and 15 times higher than the Bernalillo County soil average of 10 mg/kg. The mean is 4 times higher than the crustal average and 27 times higher than the soil average. The average concentration at Site 1 is 330 mg/kg with values ranging from 0.864 mg/kg to 1,023 mg/kg. The average concentration at Site 2 is 322 mg/kg with values ranging from 20.0 mg/kg to 1,670 mg/kg. The average concentration at Site 3 is 299 mg/kg with values ranging from 56.7 mg/kg to 1459 mg/kg. The average concentration at Sie 4 is 171 mg/kg with values ranging from 52.8 to 456 mg/kg. Lastly, the average concentration at Site 5 is 210 mg/kg with values ranging from 61.8 mg/kg to 781 mg/kg. The average concentration of Cu varies from 3 to 5 times above the crustal average and 17 to 33 times the soil average. The average concentration of Cu at each of the sites can be seen in Figures 21D and the raw data in 25D.

At each of the five sites, the concentration of Cr is above the crustal average. This can be seen in Figures 22A and 26A. The median concentration of Cr for the entire dataset is 315 mg/kg and the mean is 521 mg/kg with values ranging from 1.27 mg/kg to 4,47 mg/kg. The median is 2 mg/kg above the crustal average of 140 mg/kg and the mean is about 4 times above. The average concentration of Cr at Site 1 is 526 mg/kg with values ranging from 1.27 mg/kg to 1,155 mg/kg. The average concentration at Site 2 is 1,440 mg/kg with values ranging from 90.5 mg/kg to 1,1155 mg/kg. The average concentration at Site 3 is 2, 892

mg/kg with values ranging from 55.5 mg/kg to 4,475 mg/kg. the average concentration at Site 4 is 3,459 mg/kg with values ranging from 58.3 mg/kg to 2,732 mg/kg. The average concentration at Site 5 is 253 mg/kg with values ranging from 60.0 mg/kg to 681 mg/kg. The average concentration of Cr varies from about 2 to 6 times above the crustal average.

As can be seen in Figures 22B and 26B The Ni concentrations at each site are also above the crustal average. The median Ni concentration for the entire dataset is 184 mg/kg and the mean is 330 mg/kg with values ranging from 1.25 mg/kg to 1,895 mg/kg. The median is 2 times higher than the 84 mg/kg crustal average and the mean is 4 times higher. The average concentration of Ni at Site 1 is 396 mg/kg with values ranging from 1.25 mg/kg to 1,373 mg/kg. The average concentration at Site 2 is 224 mg/kg with values ranging from 49.5 mg/kg to 709 mg/kg. The average concentration at Site 3 is 449 mg/kg with values ranging from 51.4 mg/kg to 1,895 mg/kg. The average concentration at Site 4 is 278 mg/kg with values ranging from 55.5 mg/kg to 1,484 mg/kg. Lastly, the average concentration at Site 5 is 177 mg/kg with values ranging from 43.2 mg/kg to 383 mg/kg. The average concentration of Ni varies from 2 to 5 times the crustal average by site.

Figure 22C and 26C shows the average Cd concentrations at each site being above the crustal average. The median concentration of Cd for the entire dataset is 15.6 mg/kg and the mean concentration is 336 mg/kg with values ranging from 0.0022 mg/kg to 4,671 mg/kg. The median 100 times higher than the crustal average of 0.15 mg/kg and the mean is 2,200 times higher. The average concentration of Cd at Site 1 is 535 mg/kg with values ranging from 0.002 mg/kg to 3,713 mg/kg. The average concentration at Site 2 is 675 mg/kg with values ranging from 3.01 mg/kg to 4,671 mg/kg. The concentration of Cd at Site 3 is 50.3 mg/kg with values ranging from 0.859 mg/kg to 374 mg/kg. The concentration of Cd at

Site 4 is 327 mg/kg with values ranging from 1.27 mg/kg to 19.3 mg/kg. Lastly, the concentration of Cd at Site 5 is 45.8 mg/kg with values ranging from 2.25 mg/kg to 12.8 mg/kg. The average concentration of Cd varies from 300 to 4,500 times larger than the crustal average.

Lastly, the Sn concentrations at each of the five sites are also above the crustal average. This can be seen in Figures 22D and 26D. The median concentration for the entire dataset is 212 mg/kg and the mean concentration is 391 mg/kg with values ranging from 2.08 mg/kg to 4,367 mg/kg. The median is about 22 times higher than the crustal average of 9.8 mg/kg and the mean is 40 times higher than the crustal average. The mean Sn concentration at Site 1 is 426 mg/kg with values ranging from 2.08 to 1,207 mg/kg. The average concentration at Site 2 is 276 mg/kg with values ranging from 16.1 to 1,206 mg/kg. The average concentration at Site 3 is 751 mg/kg with values ranging from 27.1 to 4,366 mg/kg. The average concentration at Site 4 is 190 mg/kg with values ranging from 58.0 to 504 mg/kg. The average concentration at Site 5 is 350 mg/kg with values ranging from 241 to 989 mg/kg. The average concentration of Sn varies from 19 to 77 times larger than the crustal average.

Some of the metals also have large variations in elemental concentrations in between dust samples collected at the same site at different sampling periods. The averaged and raw elemental concentrations are also plotted by each of the eight sampling periods. As seen in Figures 27- 28 (averaged) and 31-32 (raw), the U, V, Ce, Pb, Mn, Fe, Co, and Al concentrations tend to be at or below the crustal average for seven of the eight sampling periods but are generally higher or enriched during the January through February sampling

period. The sampling period that has the lowest average concentration of each element occurred during the March through April sampling period.

Similar to the site data, Mo, Zn, Cu, Ni, Cr, Cd, and Sn were consistently above their crustal averages during each sampling period. The raw and average Mo concentrations throughout the sampling periods can be found in Figure 30A and 33A. The average Mo concentration is 8.96 mg/kg for August through September with values ranging from 3.23 mg/kg to 15.8 mg/kg. The average concentration for September through October is 5.05 mg/kg with values ranging from 0.0009 mg/kg to 12.9 mg/kg. The average concentration for October through December is 5.93 with values ranging from 2.74 mg/kg to 11.2 mg/kg. The average concentration for December through January is 7.62 mg/kg with values ranging from 3.56 to 21.3 mg/kg. The average concentration of January through February is 18.2 mg/kg with values ranging from 2.51 mg/kg to 61.0 mg/kg. The average concentration for February through March is 7.74 mg/kg with values ranging from 4.04 mg/kg to 34.8 mg/kg. The average concentration for March through April is 2.16 mg/kg with values ranging from 0.03 to 4.02 mg/kg. Lastly, the average concentration for April to May is 4.23 mg/kg with values ranging from 7.0 mg/kg to 2.64 mg/kg. The average concentrations vary from 2 to 15 times higher than the crustal average throughout the entire sampling period. January through February has the highest average concentration while March through April has the lowest average concentration.

The Zn concentrations for each sampling period can be seen in Figure 30B and 33B. The average concentration of Zn for August through September is 372 mg/kg with values ranging from 110 mg/kg to 237 ppm. The average concentration for September through October is 372 mg/kg with values ranging from 88.1 mg/kg to 1,056 mg/kg. The average

concentration for October through December is 314 mg/kg with values ranging from 201 mg/kg to 816 mg/kg. The average concentration for December through January is 394 mg/kg with values ranging from 192 mg/kg to 668 mg/kg, The average concentration for January through February is 422 mg/kg with values ranging from 171 mg/kg to 2,298 mg/kg. The average concentration for February through March is 325 mg/kg with values ranging from 91.0 mg/kg to 2,819 mg/kg. The average concentration for March through April is 47.3 with values ranging from 4.29 mg/kg to 313 mg/kg. Lastly, the average concentration for March through April is 330 mg/kg with values ranging from 229 mg/kg to 487 mg/kg. The average concentrations vary by 2 to 14 times the crustal average and 2 to 18 times the soil average. January through February has the highest Zn concentration and March through April has the lowest concentration.

The average Cu concentrations by sampling period can be found in Figure 30C and 33C.The average concentration for August through September is 391 mg/kg with values ranging from 58.3 mg/kg to 1,024 mg/kg. The average concentration for September through October is 323 mg/kg with values ranging from 30.3 mg/kg to 1,670 mg/kg. The average concentration for October through December is 290 mg/kg with values ranging from 96.4 to 781 mg/kg. The average concentration for December through January is 211 mg/kg with values ranging from 98.3 mg/kg to 662 mg/kg. The average concentration for January through February is 468 mg/kg with values ranging from 52.8 mg/kg to 1,459 mg/kg. The average concentration for February through March is 147 mg/kg with values ranging from 20.0 mg/kg to 666 mg/kg. The average concentration for March through April is 69 mg/kg with values ranging from 0.86 to 146 mg/kg. Lastly, the average concentration for April to May is 147 mg/kg with values ranging from 61.8 mg/kg to 261 mg/kg. Average monthly

concentrations ranged from a few mg/kg above the crustal average to 7 times higher than the crustal average. In terms of the Bernalillo County soil average, the monthly averages are 6 to 47 times higher. January through February has the highest Cu average while March through April has the lowest.

The Ni concentrations by sampling period can be found in Figure 30D and 33D. The average Ni concentration for August through September is 418 mg/kg with values ranging from 110 mg/kg to 1,373 mg/kg. The average concentration for September through October is 201 mg/kg with values ranging from 51.3 to 471 mg/kg. The average concentration for October through December is 205 mg/kg with values ranging from 98.0 mg/kg to 411 mg/g. The average concentration for December through January is 296 mg/kg with values ranging from 103 mg/kg to 838 mg/kg. The average concentration for January through February is 589 mg/kg with values ranging from 98 mg/kg to 1,483 mg/kg. The average concentration for February through March is 511 mg/kg with values ranging from 51.7 mg/kg to 1,895 mg/kg. The average concentration for March through April is 83 mg/kg with values ranging from 1.25 mg/kg to 164 mg/kg. Lastly, the average concentration for April through May is 98 mg/kg with values ranging from 41.2 mg/kg to 200 mg/kg. Ni concentrations range from 1 mg/kg below the crustal average in March through April to 7 times the crustal average in January through February.

The average Cr concentrations for each sampling period can be found in Figure 31B and 34B. The average Cr concentration for August through September is 489 mg/kg with values ranging from 175 mg/kg to 980 mg/kg. The average concentration for September through October is mg/kg with values ranging from 90.5 mg/kg to 612 mg/kg. The average concentration for October through December is 277 mg/kg with values ranging from 88.7

mg/kg to 777 mg/kg. The average concentration for December through January is 392 mg/kg with values ranging from 124 mg/kg to 880 mg/kg. The average concentration for January through February is 1,333 mg/kg with values ranging from 81.7 mg/kg to 4,475 mg/kg. The average concentration for February through March is 874 mg/kg with values ranging from 132 mg/kg to 2,119 mg/kg. The average concentration for March through April is 76.3 mg/kg with values ranging from 1.27 mg/kg to 162 mg/kg. Lastly, the average concentration for April through May is 190 mg/kg with values ranging from 60.0 mg/kg 394 mg/kg. January through February has the highest Cr average and is about 10 times higher than the crustal average. March through April has the lowest concentration of Cr and is about 2 times lower than the crustal average.

Cd concentrations by sampling period can be found in Figure 31C and 34 Cl. The average Cd concentration for August through September is 565 mg/kg with values ranging from 2.25 mg/kg to 2,319 mg/kg. The average concentration for September through October is 27.9 mg/kg with values ranging from 0.0022 mg/kg to 215 mg/kg. The average concentration for October through December is 892 mg/kg with values ranging from 10.8 mg/kg to 4,671 mg/kg. The average concentration from December through January is 337 mg/kg with values ranging from 9.66 mg/kg to 2,616 mg/kg. The average concentration for January through February is 656 mg/kg with values ranging from 4.42 mg/kg to 4,382 mg/kg. The average concentration for February through March is 25.6 mg/kg with values ranging from 2.37 mg/kg to 126 mg/kg. The average concentration for March through April is 36.5 mg/kg with values ranging from 0.0268 mg/kg to 166 mg/kg. The average concentration for April through May is 29 mg/kg with values ranging from 0.859 mg/kg to 140mg/kg. October through December has the highest Cd average and is about 6,000 times higher than the

crustal average. February through March has the lowest Cd average and is about 173 times higher than the crustal average.

Lastly, the Sn average Sn concentrations by sampling period can be found in Figure 31D and 34D. The average Sn concentration for August through September is 345 mg/kg with values ranging from 111 mg/kg to 923 mg/kg. The average concentration for September through October is 139 mg/kg with values ranging from 14.7 mg/kg to 565 mg/kg. The average concentration for October through December is 397 mg/kg with values ranging from 103 mg/kg to 1,271 mg/kg. The average concentration for December through January is 304 mg/kg with values ranging from 130 mg/kg to 562 mg/kg. The average concentration for January through February is 910 mg/kg with values ranging from 62.3 mg/kg to 4,367 mg/kg. The average concentration for February through March is 411 mg/kg with values ranging from 18.6 mg/kg to 2,334 mg/kg. The average concentration for March through April is 89.7 mg/kg with values ranging from 2.08 mg/kg to 142 mg/kg. The average concentration for April through May is 396 mg/kg with values ranging from 86.2 mg/kg to 1,207 mg/kg. Average monthly Sn concentrations vary from 9 to 93 times higher than the crustal average.

4. DISCUSSION:

4.1. Temporal and Topographical Considerations on Dust Collection:

Analysis of the mass data suggests that the sampler type, time-period of collection, and location within the mine all influence the amount of dust collected.

4.1.1 Collection Type:

There is a notable difference in the masses collected by the settler and windblown filters. The settler filters collected dust suspended in the ambient air while the windblown collectors gathered aeolian dust. As a result, the settler filter constantly collects material that stayed lofted and suspended in the air by consistent periods of low velocity winds. The monthly average windspeeds throughout the 8 sampling periods ranged from 2.7 m/s to 4.8 m/s (see Table 3). The steadiness of these low velocity winds could have allowed dust particulates to remain in suspension and be consistently collected by the settler filters. On the other hand, collection of windblown dust is more dependent on higher wind velocities and the ability of those winds to produce saltation events that lift, suspend, and break up larger soil particles (Kok et al., 2012). When these events take place, small clouds of smaller dust particles can be lofted and collected by the windblown filters (Kok et al., 2012). While the settler filters were able to consistently collect dust out of the ambient air, the windblown filters relied on environmental conditions reaching certain threshold values that would allow for dust transport and collection. As a result, the settler filters were overall able to collect more dust than the windblown filters.

The differences in the settling and windblown collection mechanisms, and their associated masses, may also have implications for human health. The settling filters act as a

proxy for the type of ambient material that may be respired during a normal day while the windblown filters are more representative of dust that would be inhaled during a windy day. Although windier days could be more hazardous in terms of the amount of mass being lofted, the low velocity winds are able to keep smaller particles suspended for extended periods of time. Mass data from the settler filters suggest that the continued suspension of particles was induced by low velocity. Consistent low velocity winds appear to result in higher potential suspension of dust into the atmosphere by mass than windblown dust that requires higher velocities.

4.1.2 Temporal Variations:

Previous studies conducted at the Jackpile Mine have indicated that seasonal variations influence the concentration of airborne particulate matter (Brown et al., 2017, LaRosa-LoPresti et al., 2021). The changes in mass collected each month indicate that seasonal changes could also be influencing the mass of dust collected. As previously mentioned, the largest amount of windblown dust was collected from August through September and during September through October for the settling dust. High levels of PM have previously been recorded during these months at Pueblo of Laguna (LaRosa-LoPresti et al., 2021). LaRosa-LoPresti (2021) collected Dustrak data from January through November 2019 and recorded daily average particulate matter concentrations at the Village of Paguate, located above the North Pit of the Jackpile Mine. Of the six days that exceeded the National Ambient Air Quality Standards (NAAQS), one occurred from August to September and two occurred from September to October. The highest overall concentration of PM occurred in September ($77\ \mu g/m^3$).

When comparing the meteorological conditions associated with these days with elevated dust concentrations to normal days, LaRosa -LoPresti (2021) determined that a low relative humidity was the major factor influencing PM concentrations. Low relative humidity could also have been a factor that contributed to variations in dust mass collected in this study. During August-October 2023, when the windblown and settler dust masses were highest, New Mexico was experiencing drought conditions. The National Weather Service reported that it was the fourth hottest August on record and the hottest September on record. This made the typically wet monsoon season exceptionally hot and dry (National Weather Service, 2023). The August 2023 precipitation was 0.69" which was 0.62" below the normal amount (National Weather Service, 2023). These drought conditions resulted in a low relative humidity. Low amounts of precipitation also meant that wet deposition of dust was infrequent allowing for dust particulates to remain suspended in the air. Furthermore, the average wind speed in August was 2.7m/s, one of the higher recorded averages during this sampling period (see Table 3). According to the National Oceanic and Atmospheric Administration (NOAA) climatological monthly report, the average relative humidity for both August and September was 41%. This represented the third lowest average relative humidity during the 10-month collection period. This lack of moisture in the atmosphere coupled with limited precipitation and a relatively high average wind speed could have allowed for dust particulates to remain in suspension during this sampling period and continuously be collected by the settler filters.

As previously mentioned, this monthly dataset represents a bimodal distribution for the settler masses. Apart from May, April was the only other month that had a lower relative humidity than August and September. The relative humidity in April was 35%. Along with this low relative humidity was an increase in wind speeds during the March through April

sampling period (see Table 3) (NOAA Online Weather Data). The windiest time of year in New Mexico occurs in the Spring, from March to June, because of regional scale high-wind events associated with the passage of cold fronts (Cooke et al., 2001). A study conducted in Dona Ana County, New Mexico by the Air Quality Bureau found that exceedances of 24-hour PM_{10} concentrations occurred on multiple days between April and June and were correlated with high wind speeds (Cooke et al., 2001). The maximum hourly PM concentration tended to occur within the same hour as the maximum wind speed. When looking at wind speeds reported by NOAA for this dataset's sampling period, March represented the month that had the peak windspeed of 21.5 m/s. This is approximately 6 m/s greater than the lowest reported maximum windspeed during dust collection, which occurred in November 2023. Both March and April represented two of the months with the highest average windspeed at 4.4 m/s and 4.7 m/s, respectively. However, as seen in Figures 35-37. when graphing the relative humidity and windspeed data with mass there was little to no correlation with these variables and mass collection. The high wind speeds coupled with the low relative humidity seen during March through April did not result in any enhanced transport of particulate matter during this period.

The lowest average settler and windblown masses were associated with similar seasonal weather variations. Average masses decrease from October to February. These months were associated with higher relative humidities coupled with colder temperatures and lower average wind speeds. Lower wind speeds limit the ability for soil particulates to be suspended into the air (Kof et al., 2012). Previous particulate matter studies of the Jackpile Mine area report similar findings. These studies indicated that winter sampling periods correspond with the lowest vapor pressure and relative humidities along with the smallest

mass flux and concentration of particulate matter (Brown et al., 2017, LaRosa-LoPresti, 2021). Furthermore, a similar seasonal trend to these data was found in another study conducted within the Jackpile Mine that reported dust flux in the winter showed a marked decrease compared to the other three seasons (McLemore et al., 2021). Although there is insufficient data to suggest that seasonal variations are impacting the mass of dust collected in this study, similar trends were reported in previous studies.

4.1.3 Geomorphic Differences:

Results show that there are also differences in the mass collected based on the locations of the samplers within the mine. Sites within the Main Pit collected the largest settling and windblown masses. Filters collected from Site 1 have the largest recorded settling masses. Site 1 was located on a highly exposed mesa top in the Main Pit, distant from any rock walls and is also the site at the highest elevation (1867 m) compared to all the other sites. Site 1 was about 30 meters higher than the other sites. (see Table 4). As a result, Site 1 has 360 ^{o} exposure to the environment with limited topographic constraints impacting dust transport as opposed to some of the other sites (see Figure 1). A previous study conducted at the Jackpile Mine found that topographically higher locations were more susceptible to higher winds which led to increasing dust flux (Brown et al., 2017). Similarly, another study conducted within the Jackpile Mine found that location was the most important factor in determining mining dust flux and that more exposed areas were associated with higher dust flux (McLemore et al., 2021). This was also found in this study when looking at Site 1 compared to the other sites. The higher elevation coupled with a more exposed area that can allow for more extensive wind exposure explains why Site 1, and the Main Pit in general, had a larger mass flux.

Comparatively, the samplers located within the South Pit (Site 5) collected both the lowest settling and windblown dust masses. Site 5 is much more sheltered compared to the other sites and is surrounded by high rock walls formed by the opencast mining. The topography is more characteristic of a partially enclosed bowl constricting wind flow and dust transport. These topographically lower locations within the mine tend to experience lower wind speeds and therefore less dust transport (Brown et al., 2017). Furthermore, dust flux in valleys within the mine compared to mesa tops was previously found to be a factor of two lower (Brown et al., 2017). In conclusion, lower wind speeds coupled with more topographical constraints explains the lowest average dust masses collected in the South Pit.

4.2. Implications of Particulate Composition & Morphology:

Data characteristics of the dust such as size, morphology, and mineralogical composition are important to further understand potential impacts to human health and attempting to identify active sources of particulate matter. However, identifying direct sources can be challenging because fine-grained particulates can be suspended in the air for weeks at a time and be transported thousands of miles (Kof et al., 2012).

The collected dust is comprised of naturally occurring minerals commonly found in airborne particulates in arid desert regions such as the Southwest United States. These minerals, such as silicates, carbonates, and sulfates, are abundant in the soils and rocks across the southwestern region. The presence of these minerals as the major constituents of the dust suggests a combination of long-distance regional transport of similar geologically sourced minerals mixed with locally derived sources. Minerals collected in the dust also have the potential to be derived from the Jackpile Mine. However, apart from enrichments in U, V, and Ce at Site 3—a known source of ore-bearing minerals—there is no evidence to suggest that

the mine is releasing hazardous minerals becoming airborne. Uranium-bearing minerals were not found during SEM analysis of the dust samples from any of sites further implying that the current impact of the mine as a source of potentially hazardous material from exposed ore bodies and waste piles is extremely low. The data more notably suggests that the collected dust contains a variety of different particles that do not have compositions or morphologies consistent with naturally occurring minerals. This implies that anthropogenic activities are likely contributing specific types of metal-rich particles to the aeolian dust, as discussed below.

Scanning electron microscopy observations reveal that airborne dust collected from the mine sites contained $PM_{2.5}$ and PM_{10}. These size categories are designated as harmful to human health by the EPA because of their ability to penetrate deep into the lungs. Ultrafine particles, which are smaller than 0.1 microns in diameter, were also located in the dust samples. This is of concern because a significant body of research shows that the finer a particulate, the deeper it can travel into the respiratory tract and the less likely it is to be expelled from the body (Kim et al, 2015; Li et al. 2022; Hettiarachchi et al., 2018). Additionally, the presence of a variety of metal-rich grains was found within the particulate matter. Continued exposure to metal-bearing particulate matter can lead to health problems such as irregular heartbeat, asthma, decreased lung function, and prolonged respiratory issues (Kim e al., 2015). This has previously been documented within indigenous populations who were especially susceptible to heavy metal-rich PM exposure because of their proximity to abandoned mines (El Hayek et al, 2021). Documented health problems within these communities associated with the continued inhalation of metal-bearing PM include kidney and cardiovascular diseases along with hypertension (El Hayek et al., 2021).

However, the metal-bearing particulate matter found within the dust is likely due to anthropogenic activities and not sourced from the mine. There is a distinct spherical morphology associated with some of the metal-bearing particulate matter that suggests certain anthropogenic processes. Geogenic particles, such as soils, tend to contain distinct minerals, aggregated forms, and irregular shapes and sizes (Zeb et al., 2018). These types of morphologies are consistent with the identified mineral grains found within the dust collected from the mine. On the other hand, particulates that are anthropogenically emitted, through processes such as fossil fuel combustion, smelting, and transportation, tend to be rounded and smooth with a spherical shape (Zajzon et al., 2013, Zeb et al., 2018). Similarly, particulates associated with metallurgical processing tend to exhibit nearly perfect sphericity (Lanteigne et al; 2014, Zeb et al., 2018). Spherical particles associated with smelting and combustion activities tend to be comprised of Fe oxides such as magnetite, or silica (Zajzon et al., 2013, Zeb et al., 2018). An abundance of spherical particulates with these compositions was found within the mine dust. This indicates that the samplers were collecting anthropogenically sourced material that was transported throughout the mine. The presence of busy highways, the Four Corners coal-fired power plant, and metallurgy industries in the vicinity to the mine could be contributing to anthropogenically sourced particulates found in the dust.

4.3 Potential Metal Sources:

Analysis of elemental concentrations that are at or below the crustal average reveals an enrichment of ore-bearing elements, including U, V, and C, at Site 3. The average concentration of U The average elemental data produced at each site reveals an enrichment of ore-bearing elements at Site 3. The average concentration of U at Site 3 is two to four times greater than the averages at the other sites. The average concentration of V and Ce at Site 3

are about two times greater than the averages at the other sites. Since Site 3 is in the Main Pit and located about 30 meters away from an exposed ore outcrop, it can be said that these enrichments are likely associated with the mine. This can only be said of Site 3 because of where the collectors were positioned in the mine. The higher concentrations of U, V, and Ce seen at Site 3 demonstrate a clear correlation to a known source within the mine that is producing dust enriched in these ore-related metals. Enrichments of some of these metals relative to crustal averages have been observed in previous studies conducted at Pueblo of Laguna and the Jackpile Mine (Brown et al., 2017, LaRosa-LoPresti et al., 2021).

With the exception of U at Site 3, the concentrations of U, V, and Ce in the dust samples are consistently below their crustal averages and show no evidence of enrichment. The median U concentration for the entire dataset is 1.2 mg/kg which is 2 times lower than the crustal average of 2.8 mg/kg. These new measurements are consistent with multiple other studies including LaRosa-LoPresti et al., 2021, Natoli & Brearley, unpublished and Haley et al., unpublished. These studies focused on determining the concentration of ore-bearing metals in actively collected dust in Pueblo of Laguna and in soil samples from the Village of Paguate and inside the Jackpile Mine. The concentrations of U and V observed in the bulk soil concentrations in previous samples are also typically at or below the crustal average with the exception of the fine-grained fractions exhibiting slightly elevated concentrations.

Although U and other ore-bearing metals are not elevated in comparison to their crustal averages, high concentrations of multiple toxic metals were discovered within the dust samples compared to crustal and New Mexico soil averages. These levels could be associated with both anthropogenic activities and/or geogenic origins associated with the surrounding geology and mine. Elements that were consistently above their crustal averages

in the analyzed dust samples across temporal and geographical variations included Mo, As, Zn, Cu, Ni, Cr, Sn, and Cd. Anthropogenic input from industrial processes and transportation are likely the dominant mechanisms for the elevated metals concentrations seen in this study. Potential sources contributing to elevated concentrations of metals within the mine dust are discussed below.

4.3.1 Molybdenum:

Mo values are consistently above the crustal average of 1.2 mg/kg. The median value for the entire Mo dataset is 4.80 mg/kg and the total average of all the samples is 7.75 mg/kg (range 0.0009 mg/kg to 61.0 mg/kg), 4 times and 6 times higher than the crustal average, respectively. There are only four out of seventy samples in this dataset where the Mo concentrations are below the crustal average.

Minor contributions to a higher overall crustal average could be due to the mineralogy of the mine. Elevated levels of Mo were previously found in active dust samples collected around Pueblo of Laguna (La Rosa-LoPresti et al., 2021). Although Mo minerals have been found within the Jackpile Sandstone (Schilling, 1965, Adams et al., 1978) it does not appear to be associated with any particulate component of the ore at the mine (Moench and Schlee, 1967). A study of minor elements in ore material from the Jackpile Mine, conducted by Moench and Schlee, revealed that Mo was overall not concentrated in ores from the Jackpile deposits.

The consistent average concentrations of Mo, by site and sampling period, have enrichment factors as much as15 times the crustal average suggesting inputs from anthropogenic processes. Combustion of coal, industrial operations, and municipal sewage

sludge can all lead to the release of Mo in the atmosphere. Locations in the vicinity of combusted fossil fuels produce substantially higher concentrations of Mo (Barceloux, 1999). The Four Corners coal-burning power plant in New Mexico could be contributing to Mo in the atmosphere. Another common source of Mo comes from metallurgical applications. Molybdenum is commonly added to stainless steel and iron alloys to improve the strength and thermal resistance of the product (Barceloux, 1999). Waste products associated with these processes, such as fly ash, therefore contain Mo and can become airborne. The high frequency of these industrial practices, and the ability for particulates to travel long distances and remain suspended in the air for long periods of time, suggest the elevated concentration of Mo are more likely associated with anthropogenic processes and not from ore minerals associated with the mine.

4.3.2 Arsenic:

Arsenic levels throughout the southwest tend to be higher than the national soil average due to increased groundwater withdrawals for irrigation and drinking water that have increased movement of contaminants (Diawara et al., 2006, USGS, 2015). As a result, it was important to compare the As concentrations to the Bernalillo County soil average for a background more consistent with the geology of New Mexico. The crustal average for As is 1.8 mg/kg while the Bernalillo County soil average for New Mexico is 4.43 ± 0.762 mg/kg. The average As concentration for this dataset is 7.13 mg/kg with values ranging from 0.249 mg/kg to 46.8 mg/kg. This is about 4 times higher than the crustal average and 2 times higher than the soil average. However, the median concentration is 3.56 mg/kg which is below the soil average but 2 times the crustal average. Concentrations of As above the crustal average have previously been reported in dust collected at Pueblo of Laguna and surrounding mine

areas (LaRosa-LoPresti et al., 2021, Natoli & Brearley, unpublished). However, these studies reported elemental ratios, not absolute concentrations.

Enrichment in As compared to the crustal average could be associated with the continued erosion of exposed ore and mine waste at the Jackpile Mine. Arsenic is associated with the shale-sandstone interfaces in the lower units of the Jackpile Sandstone and as a component of uraniferous organic matter (Moench and Schlee, 1967, Pearce, et al., 2020, McLemore et al., 2021). The dissolution of arsenic from uraniferous organic matter within the Jackpile sandstone ores has previously been reported (Pearce et al., 2020). Arsenic can be released through sulfide oxidation and attenuated by adsorption and co-precipitation with Fe-bearing minerals, clays, and organic matter (Bowell et al., 2014). Furthermore, the New Mexico Bureau of Geology and Mineral Resources has also reported As concentrations as high as several hundreds of mg/kg in organic-rich shale and silica-rich volcanic rocks. This implies that continued weathering and erosion at and around the mine could be releasing arsenic into the surrounding environment.

However, it is possible that elevated arsenic levels are also associated with the by-products of coal burning and smelting metals (Zajon et al., 2013, Goa, 2020, Zhou et al., 2021). For example, the Four Corners coal-fired power plant, located in New Mexico (200 miles away from Pueblo of Laguna), is a polluter known to produce fly ash containing arsenic (Cannon & Swanson, 1975). Arsenic can be associated with the organic matter of coals and with the presence of sulfur and iron bearing minerals, such as pyrite. When coal is burned, As-bearing micromineral phases escape into the gaseous and particulate phase and become released into the atmosphere (Yudovich & Ketris, 2004). The U.S. Geological Survey reports that the average arsenic concentration for U.S. coal is about 24 mg/kg.

However, the arsenic content of coal ash is enriched and can be as high as 50 ± 5 mg/kg (Yudovich & Ketris, 2004). The continuous burning of coal can therefore lead to increased levels of As in the environment. Another likely contributor to elevated arsenic levels is from the smelting of Cu. Copper metallurgy produces dust that contains arsenic due to arsenic-bearing minerals such as tennantite ($Cu_{12}As_{14}S_{13}$) and enargite (Cu_3AsS_4) that are commonly present in Cu ore. When copper is smelted, arsenic is oxidized to the vapor phase creating arsenic-containing flue gas that can be transported in the air (Yao et al., 2021, Montenegro et al., 2010).

4.3.3 Copper & Zinc:

Both the copper and zinc metal concentrations were above the crustal average and NM soil averages. The crustal average of Cu is 63 mg/kg and the soil average in Bernalillo New Mexico is 10.2 ± 3.25 mg/kg. Cu concentrations were consistently above 100 mg/kg. Only nine out of the sixty-nine samples were below the Cu crustal average. The median concentration for the entire dataset is 150 mg/kg, two times greater than the crustal average of Cu and 15 times greater than the soil average. The total average for the dataset is 266 mg/kg (range 0.863 mg/kg to 1,670 mg/kg) which is 4 times higher than the crustal average and more than 26 times higher than the soil average.

Zn also commonly had concentrations above the crustal average. The crustal average of Zn is 75 mg/kg and the Bernalillo County, New Mexico, soil average is 58.2 ± 14.6. mg/kg. The Zn concentrations at each of the sites were consistently 3-6 times higher than the crustal and soil averages. Only one of the sixty-nine samples was below the crustal and soil average. The median concentration for the entire dataset is 354 mg/kg, almost five times higher than the crustal average and six times higher than the soil average. The total average

for the dataset is 488 mg/kg (range 4.29 mg/kg to 2,819 mg/kg) which is more than 6 times the crustal average and 8 times the soil average.

Cu and Zn were consistently found to co-occur within the dust particulates collected at the mine, a correlation that could be indicative brass alloys in the air. Brass alloys are not formed naturally in the environment, they are manmade. Brass is a common friction modifier used in engine oils and automatic transmission fluids (Burlakova et al., 2020). If extreme wear or damage is done to the engine bearings, build-up of these brass shavings can occur in the oils. Combustion processes and resulting exhaust gases can then release some of the very fine brass residue into the air. Moreover, brass can be found in the tanks, tubes, and radiator cores of cars (Thin Metals Sales, 2023). It is also a popular additive in brake pads (Straffelini et al., 2015). As a result, road dust tends to contain elevated levels of Cu and Zn (Adameic et al., 2016, Jeong et al., 2022). The presence of co-occurring Cu & Zn in the collected dust could therefore be due to busy highways and vehicular traffic.

The association of Cu and Zn particulates is also commonly associated with smelting and other forms of metallurgy. The volatilization and oxidation of metals at high temperatures can lead to the enrichment of Cu and Zn in smelting dust that can be transported throughout the atmosphere (Zhou et al., 2021). Smelting copper can produce zinc vapors and metallic copper droplets that are released into the air (Zhou et al., 2021). Excess levels of Cu and Zn have been found in people and areas near copper smelters (Zhou et al., 2021). Elevated levels of Cu and Zn has also been found in particulate matter collected close to the Four Corners Power Plant in Shiprock, New Mexico (Gonzalez-Maddux et al., 2014). Although these enrichments were not directly linked to the power plant, principal component

analysis revealed that the Cu and Zn levels were indicative of anthropogenic activities (Gonzalez-Maddux et al., 2014).

There were a few instances where copper and zinc were found independent of each other in the form of oxides. A potential cause of the copper oxide particulate matter could be from the high-rolled steel likely used on railways. Copper can also be present in brake linings and brake pads used in vehicles (Straffelini et al., 2015). These materials are already attracting concern due to the contribution of wear products to particulate matter emissions (Straffelini et al., 2015).

The presence of particulate matter Zn may also be related to automobiles. Zinc accounts for about 1% of the weight of tire tread material (Councell et al., 2004). Furthermore, zinc is added to tires in the form of zinc oxide during the process of repair from cracks or punctures (Councell et al., 2004). This means that as the tire wears, it can release zinc to the environment. It is also possible that zinc, and other metal oxides, are being produced from the burning of trash in neighboring communities. Zinc is commonly added to plastic products to enhance polymer properties and prolong life (Hahladakis et al., 2017). As a result, the combustion of plastic films, such as sandwich bags, could be releasing zinc into the atmosphere.

In conclusion, there are multiple common sources that can result in the release of Cu, Zn, and brass particles into the environment and appear to be the best explanation for the presence of particles with these compositions in airborne dust. We conclude that such sources are most likely to be the major cause of the elevated Cu and Zn concentrations in the PM collected within the Jackpile mine and hence indicative of externally derived anthropogenic materials

4.3.4 Chromium & Nickel:

Both the Ni and Cr concentrations are higher than their crustal averages. The crustal average of Cr is 140 mg/kg. Only sixteen of the sixty-nine samples were at or below this crustal average with 53 being above. The average concentration of Cr for the entire dataset is 521 mg/kg (range from 1.27 mg/kg to 4.47 mg/kg) and the median concentration is 315 mg/kg. These concentrations are about 4 and 2 times the crustal average, respectively. Levels of Cr above the crustal average have previously been reported at the Pueblo of Laguna and the surrounding mine area (Brown et al., 2017, LaRosa-LoPresti, 2021).

Ni also had higher concentrations than the 84 mg/kg crustal average. Out of sixty-nine samples tested for Ni, nine were below the crustal average while 60 were above the crustal average. The median for the entire dataset is 184 mg/kg, 2 times greater than the crustal average. The total average for the dataset is 310 mg/kg (range 1.25 mg/kg to 1,895 mg/kg) almost four times higher than the crustal average.

Ni and Cr consistently co-occurred in spherules within the dust particulates collected at the mine. These spherical morphologies are commonly associated with metals that are heated above their melting point during industrial processes (Zeb et al., 2018, Cediel-Ulloa et al., 2021). The smelting of stainless steel can lead to Cr and Ni particulates in smelting dust. Dust enriched in Cr and Ni could also be coming from industrial businesses that weld metallic material. The proximity of the POL to steel plants, located about 30 miles upwind and downwind of POL, and the Four Corners Power Plant could also be contributing to these elevated levels. This implies that metallurgical activities could be contributing to the Cr and Ni spherules found in the dust samples.

Apart from industrial processes, the Cr and Ni bearing PM could also be associated with vehicular exhaust and brake lining of automobiles (Adameic et al., 2016). The exhaust systems and brake linings in cars and trucks are commonly composed of stainless steel. As a result, Cr and Ni are common metals found in fine road dusts (Jeong et al., 2022). Therefore, the anthropogenic usage of cars could also explain the prevalence of Cr and Ni in the dust.

4.3.5 Tin & Cadmium:

Sn and Cd concentrations both displayed concentrations higher than the crustal average. Sn and Cd have previously been discovered in dust collected from Pueblo of Laguna (LaRosa-LoPresti., 2021). The crustal average of Cd is 0.15 mg/kg. There were only two samples throughout this dataset that were below the crustal average. The median Cd concentration is 15.6 mg/kg, 100 times higher than the crustal average. The total average for the dataset is 336 mg/kg (range 0.0022 mg/kg to 4,671 mg/kg) over 2,000 times the crustal average. Large variations in Cd are seen throughout the entire sampling period (see Figures 31C and 34C) which is likely due to anthropogenic events.

Similar trends were observed when looking at the average Sn concentrations. The crustal average of Sn is 9.8 mg/kg. The median Sn concentration for the dataset is 212 mg/kg, about 22 times the crustal average. The total average is 391 mg/kg (range 2.08 mg/kg to 212 mg/kg) about 40 times the crustal average. Only one of the seventy samples analyzed for Sn is below the crustal average.

Contributions of Cd could be associated with the mineralogy of the mine. Enrichment of Cd can be found in organic-rich clays such as shales (Liu et al., 2017). Anthropogenic activities, such as mining, can accelerate the release of Cd from these shales into the environment (Liu et al., 2017). There is evidence of shale-sandstone interfaces in lower

regions of the Jackpile sandstone within the mine (McLemore et al., 2021). Shales tend to be composed of organic matter, iron sulfides, and carbonates. Sulfide minerals are the primary source of geogenic Cd (Liu et al., 2017). Cadmium tends to be present in sulfide minerals or bound to organic material within shales (Kubier et al., 2019). The oxidation of organic matter and sulfides can enhance the mobility of Cd in the environment (Liu et al., 2017). The continued erosion of shale at the mine could be contributing to the elevated levels of Cd found in the dust. However, the exceedingly high Cd concentrations and significant variations by sampling period point towards anthropogenic activities.

Elevated concentrations of both Sn and Cd can result from municipal waste disposal. Studies have shown that heavy metals, such as Sn and Cd, are typically released when waste is incinerated (Zhang et al., 2001, Abanades et al., 2002). Incineration is one of the most common disposal methods of sewage, trash, and food scraps. (Zhang et al., 2001). Sn and Cd are metal additives commonly found in everyday use plastic material, including food packaging, because they act as stabilizers (Turner & Filella, 2021). As a result, when municipal waste is burned Cd and Sn can be released through gas dusts and fumes (ASTDR, 2005). The volatized metals produced from burning waste condense to form metal fumes or deposits on available surfaces (Zhang et al., 2001). The proximity of Pueblo of Laguna and the mine to waste incineration sites could be contributing to these high levels of Cd and Sn in the collected dust. Furthermore, the smelting and refining processes as well as the burning of fossil fuels can increase Cd and Sn into the atmosphere (ASTDR, 2005).

Coal is enriched in Sn, and when combusted can release enriched dust into the atmosphere. Previous $PM_{2.5}$ sampling conducted in Shiprock, New Mexico, found enriched concentrations of Sn that were associated with coal burning at the nearby Four Corners

Power Plant and San Juan Generating Station (Gonzalez-Maddux et al., 2014). Principal component analysis found that coal combustion was a factor in enriched concentrations of Sn in the particulate matter. This suggests that coal-burning and the ability of particulates to travel from power plant sources could be influencing the concentration of Sn in dust collected from the mine.

Another anthropogenic source of elevated Cd levels and Cd dust could be from pottery production. Artists use paints, such as yellow ochre, that tend to be pigmented with Cd to produce vibrant colors of yellow and orange (Cepria et al., 2005). Cadmium pigments are not only used by potters for their vibrant colors, but also because they tend to resist high processing temperatures (Cepria et al., 2005). As a result, Cd is also found within ceramic glazes because they can be fired in kilns. Previous studies of metal exposure from kilns have found elevated concentrations of cadmium in their emissions (Douglas, 1996). This indicates that ceramic making could be releasing Cd into the atmosphere.

Wastewater is also known to contain higher amounts of heavy metals like cadmium (Ibrahem et al., 2020). Old sewage lagoons (effluent disposal ponds) can also release hazardous substances into the atmosphere. The accumulation and movement of heavy metals in soils, including Cd, has been reported at sewage lagoons (Lund et al., 1976, Li et al., 2009). Old wastewater systems could be adding Cd into the soil that can then become windblown.

5 CONCLUSIONS:

Prior to this study, there had not been a thorough, systematic investigation of dust from the Jackpile-Paguate Mine collected using a passive mechanism over an extended sampling period. Additionally, a comprehensive analysis of the dust, focusing on its mineralogy, morphology, and elemental concentration—was lacking. Consequently, this dataset offers crucial insights into these aspects and provides a deeper understanding of the abandoned Jackpile-Paguate Mine's potential impact on the Pueblo of Laguna community.

Insights into the transport of dust throughout the Jackpile Mine were made as a result of new sampling techniques and the careful placement of these collectors throughout the mine. The consistently larger masses collected by the settler filters highlights the significance of low-velocity winds in continually suspending particulate matter. This implies that the settling dust is more representative of typical daily conditions. The windblown filters more accurately represented conditions on high-velocity wind days. Although the different conditions throughout each of the sampling periods, including relative humidity, peak windspeed, and average windspeed did not show a correlation with dust production, the different topography throughout the mine did. The sampler that was the most exposed to the open environment on a mesa top and at the highest elevation collected the largest dust masses. The sampler that was surrounded by rock walls and located in more of a valley collected the smallest dust mass. These results exemplify the importance of topography in influencing dust transport.

The dust that these windblown and settler filters collected also provided information for potential metals exposure. An exposed U-bearing ore outcrop in the main Jackpile pit is producing dust that is enriched in U, V, and Ce. However, these enrichments are only

observed in dust collected at the location within the Main Pit (Site 3) near the exposed outcrop and is clearly a highly localized phenomenon. The other sites show no evidence of any enrichments in these elements demonstrating that mine was not producing toxic windblown dust during the entire 10-month sampling period The concentration of these elements within the dust, at each of the other sites, remained at or below the crustal average, showing that the transport of windblown ore-bearing metals is not a major concern to the Pueblo of Laguna community. This assumption is furthered when looking at the bulk mineralogy of the dust collected at the mine, which is primarily composed of naturally occurring minerals expected to be found aeolian dust within the desert SW USA, with no evidence of U- or V-bearing particulates.

However, increased concentrations of certain metals and the identification of metal-bearing particulate matter (PM_{10} and $PM_{2.5}$) in the dust was found. Metals that consistently have elevated concentrations compared to crustal and soil averages include Mo, As, Cu, Zn, Cr, Ni, Sn, and Cd. These are metals not likely to be associated with the mine. Furthermore, the enrichments of these metals coupled with variability throughout the sites and seasons indicates anthropogenic inputs. These metals are associated with a range of anthropogenic processes including metallurgy, industry, transportation, and fossil-fuel burning. The ability of fine-grained particulate matter to remain suspended for extended periods and travel long distances increases the likelihood that the dust collected at the mine is linked to these anthropogenic sources. The findings from this study indicate that airborne dust from the mine does not currently pose a significant concern to the Pueblo of Laguna community and that the elevated metal levels are due to human anthropogenic factors. Continued collection and analysis of the dust should be conducted to further affirm these results.

Finally, this study developed a novel methodology for dust collection, effectively tackling the significant challenge of gathering and extracting ample dust quantities for thorough analyses. Using the TISCH TE-200 PAS and TE-PAS-DD passive air samplers at a height of ~2.4 m and leaving the filters in the field for extended periods of time proved to be successful. Extraction methods involving sonication and centrifugation proved effective in recovering masses from the filters sufficient for ICP-MS and SEM analysis while minimizing residual particulates left over on the filters. Consequently, the replication of this methodology in future studies is strongly encouraged.

6 FUTURE DIRECTIONS

To validate assumptions made in this dataset, transmission electron microscopy (TEM) of the dust and statistical analyses of the ICP-MS results should be conducted. TEM analysis would reveal if pure metal and metal alloys are present within the dust samples. This was difficult to determine by SEM EDS analysis alone due to the presence of oxygen within the samples and overlap of the electron beam with adjacent oxygen-bearing minerals such as oxides and silicates. Furthermore, principal component analysis should be performed on dust metal concentration data to better understand correlations and variations within the data. This may allow for the detection of more patterns within the data. Statistical analysis could also be used to determine if the metals are coming from the same sources.

Continued collection of samples at the mine with subsequent investigations of dust and soil should also be performed. Analyzing previously collected soil samples from the mine is necessary to determine if similar mineralogical and morphological characteristics are present in the bulk soil material. Furthermore, apart from the mine site, dust samplers should also be placed in and around the villages at Pueblo of Laguna. Similarly, dust should be sampled at a control site to provide a baseline for comparison with the samples from the mine and the village. It may also be beneficial to leave the samplers in the field for a longer period to gather more mass, thereby enabling additional analyses such as U isotope studies.

After conducting further statistical analyses, we will report the results back to the Pueblo of Laguna community. Participation in listening sessions, practice presentations with community members, and working with the University of New Mexico Metals Exposure and Toxicity Assessment on Tribal Lands in the Southwest (UNM METALS) translation core to

create an appropriate report back presentation centered on community knowledge will be carried out.

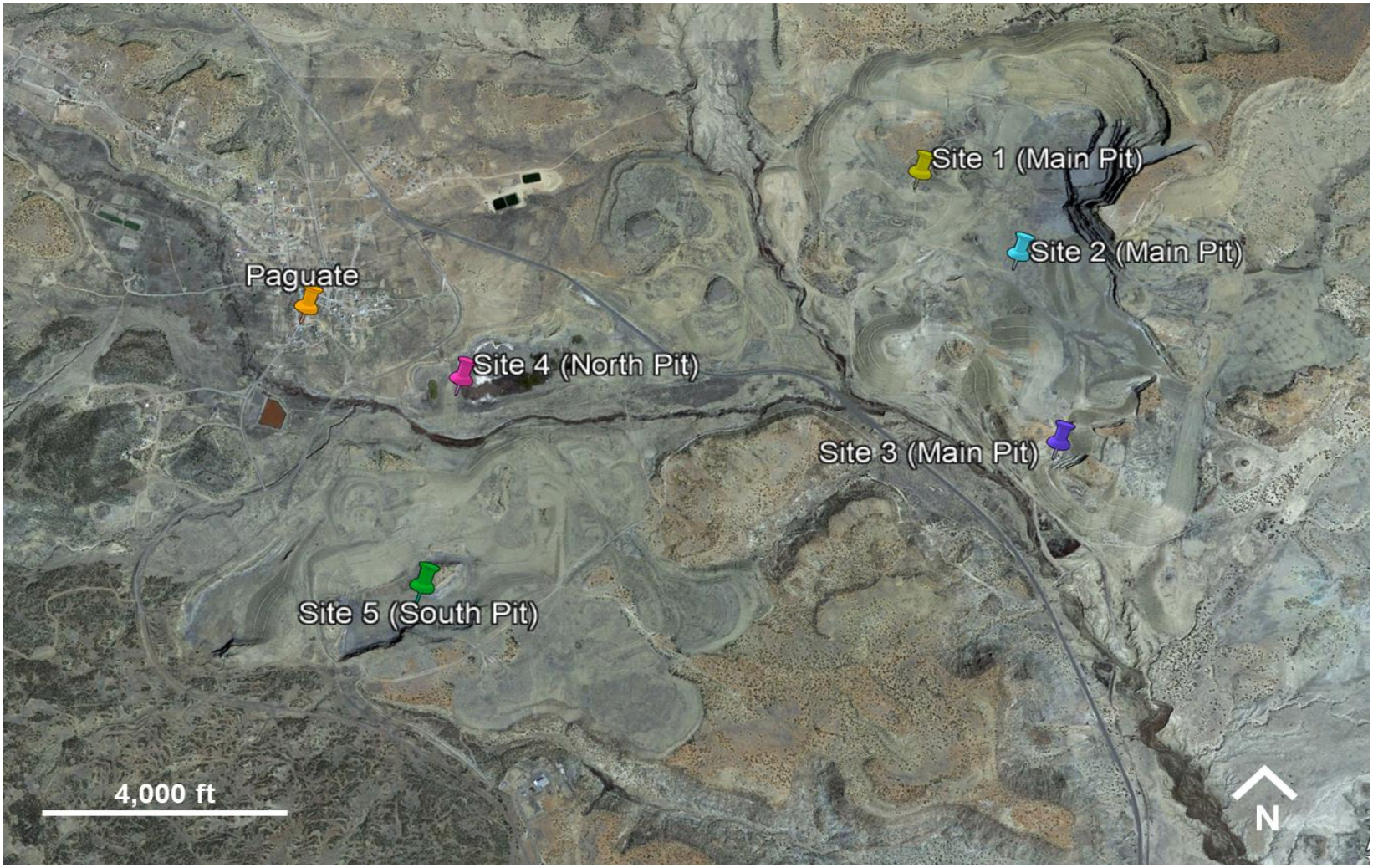

Figure 1. Aerial map, taken from Google Earth, of the five different sampling locations from where dust was collected throughout the Jackpile-Paguate Mine. Three dust samplers were placed in the Main Pit (Sites 1-3), one in the North Pit (Site 4), and one in the South Pit (Site 5). Proximity of the samplers to the Village of Paguate can also be seen on this map.

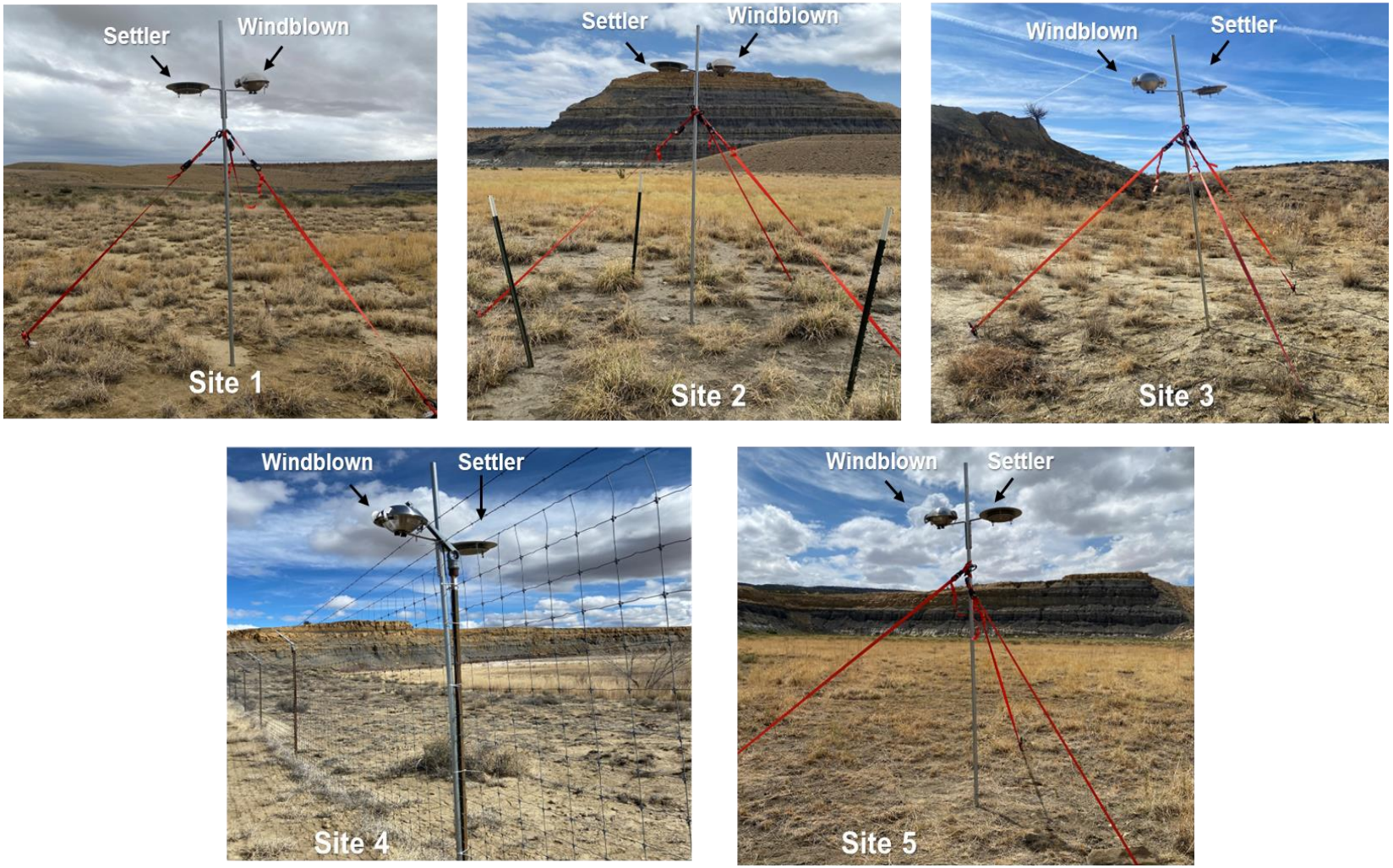

Figure 2. Ground-level images of each of the five sampling sites within the Jackpile-Paguate Mine and their surrounding topography. Site 1, in the Main Pit, was the most exposed out of all the samplers and located on a mesa top while Site 5 (South Pit) was the least exposed of all the samplers and located in a bowl-shaped depression surrounded by large sandstone cliffs.

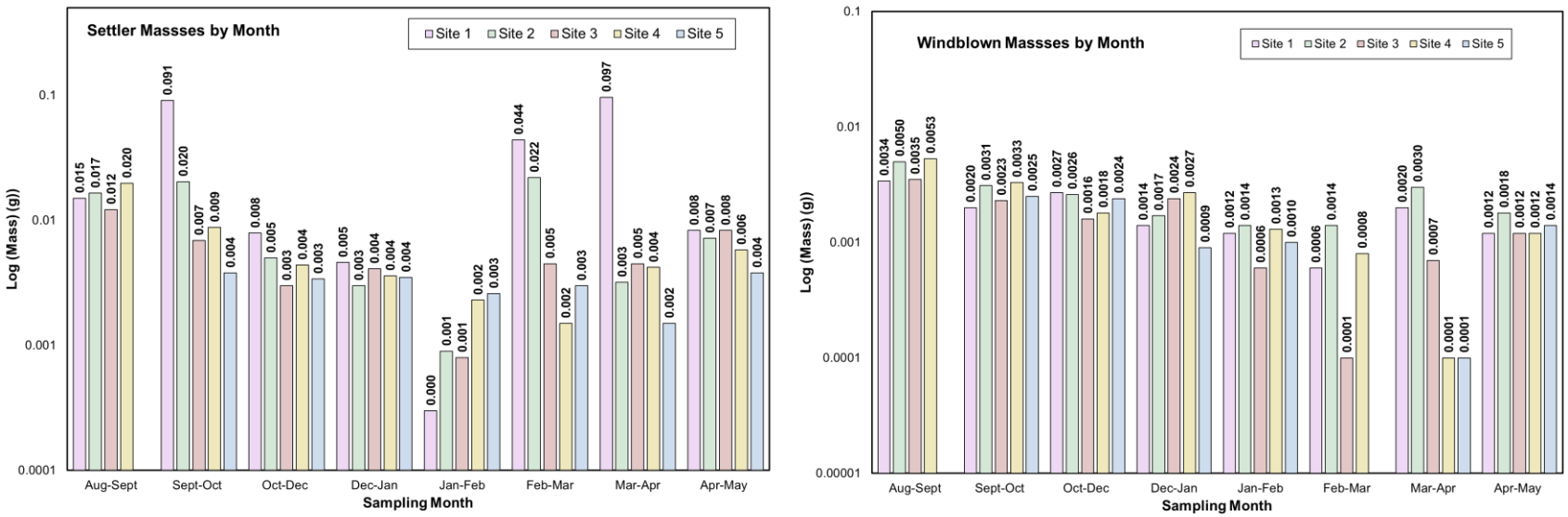

Figure 3. Bar graphs showing the raw, logged, mass data by sampling period and filter type. Graph 3A shows the masses collected by the settler samplers throughout the 8 sampling periods. The highest settler masses occurred during September through October, February through March, and March through April and all at Site 1. The lowest settler mass occurred at Site 1 from January through February. October through December, January through December, and January through February tended to have smaller masses compared to the other sampling periods. Graph 3B shows the masses collected by the windblown samplers throughout the 8 sampling periods. Apart from a slight decreasing trend and a few outliers, the windblown masses remain similar throughout the sampling periods and at each of the sites. In general, when comparing graph 3A to 3B the settler masses are more variable when compared to the windblown masses by sampling period.

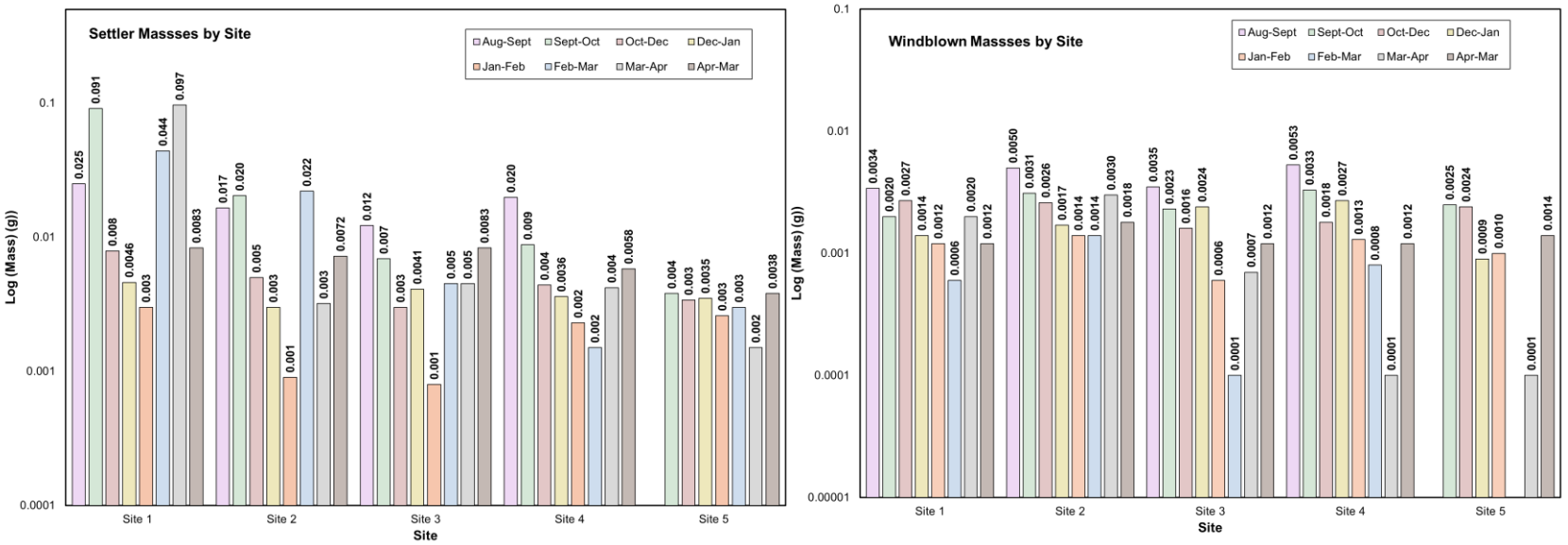

Figure 4. Bar graphs showing the raw, logged, mass data by site and filter type. Graph 4A shows the masses collected by the settler samplers at each of the 5 sites. Site 1 tended to collect the largest masses while Site 5 collected the smallest masses. The largest mass collected at Site 1 occurred during the March through April sampling period. The settler masses collected at Site 5 were consistent throughout the sampling period but varied for the other sites depending on the sampling month. Graph 4B shows the masses collected by the windblown samplers at each of the 5 sites. Apart from a few outliers, the windblown masses remained similar at each site during the different sampling periods. In general, when comparing graph 4A to 4B, the settler masses are more variable when compared to the windblown masses by site.

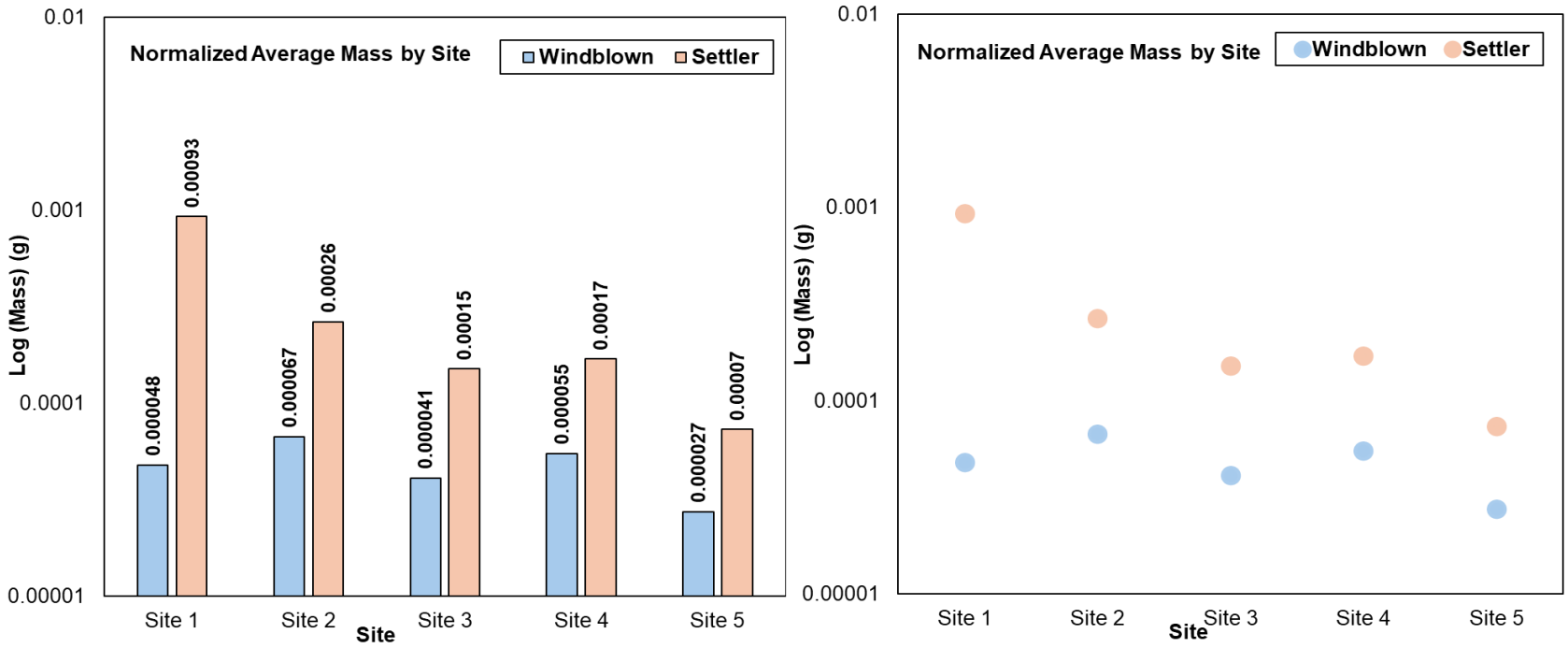

Figure 5. Bar and scatterplot showing the normalized average mass collected, on a logarithmic scale, by each site during the entire 10-month sampling period. These graphs show that the settler filters collected a larger mass than the windblown filters at each of the five sites. The settler masses varied more, sometimes by a whole order of magnitude, by site when compared to the windblown masses which stayed more consistent. The graphs also show that Site 1 collected the largest average settler mass while Site 5 collected the smallest average settler mass.

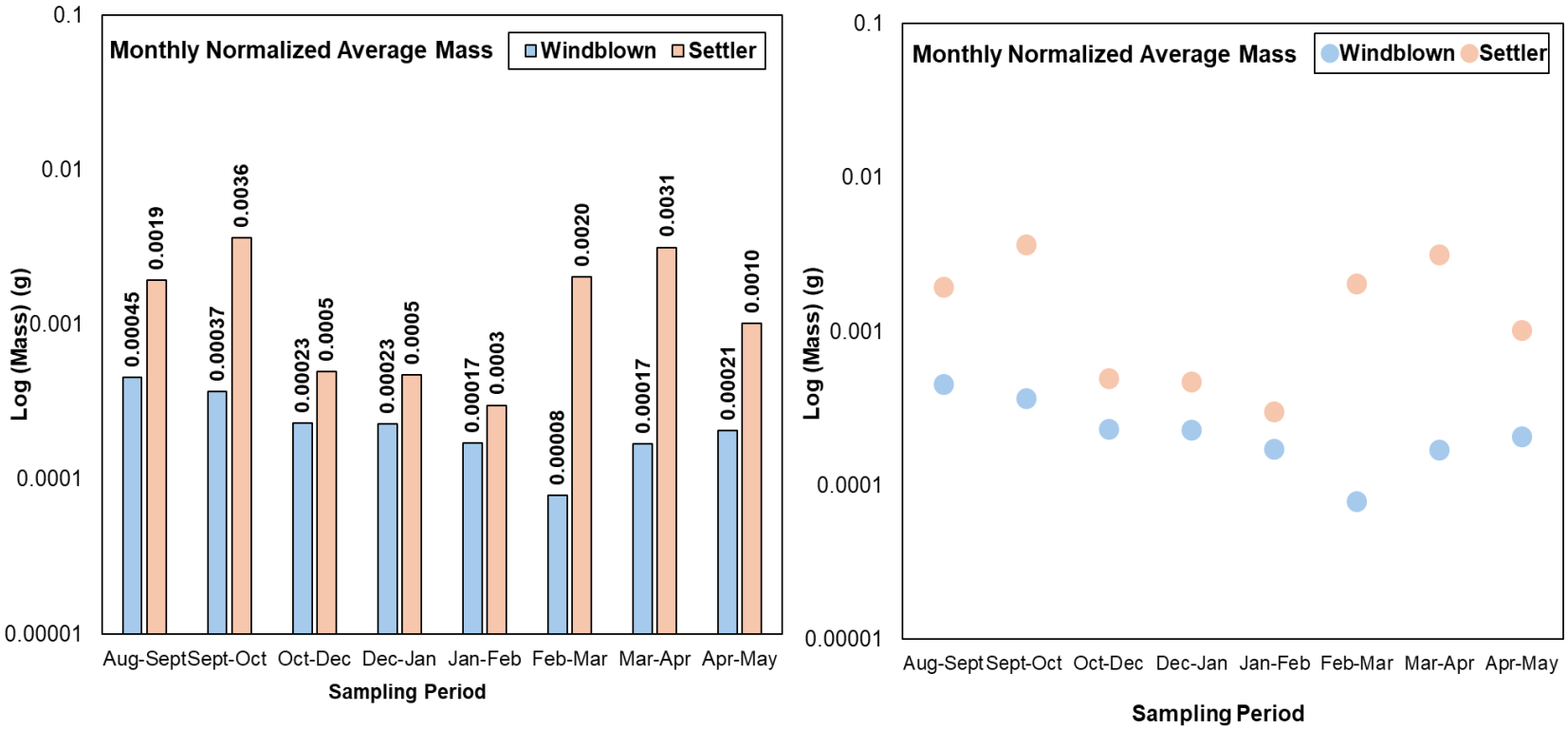

Figure 6. Bar and scatterplot showing the normalized average mass collected, on a logarithmic scale, by each sampling period. These graphs show that the settler filters collected a larger mass than the windblown filters during each sampling period. The graphs show a bimodal distribution of masses. The peak mass occurred during September through October, followed by a general decrease in mass from October through December, and another peak mass in March through April.

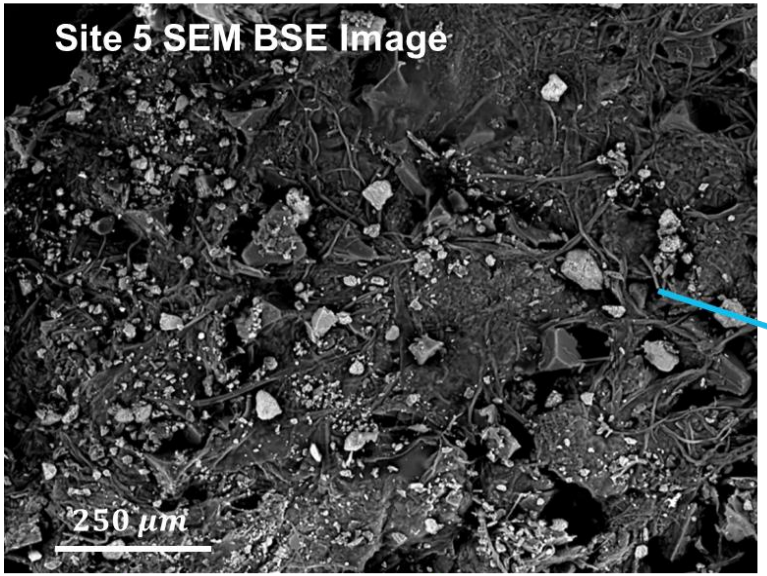

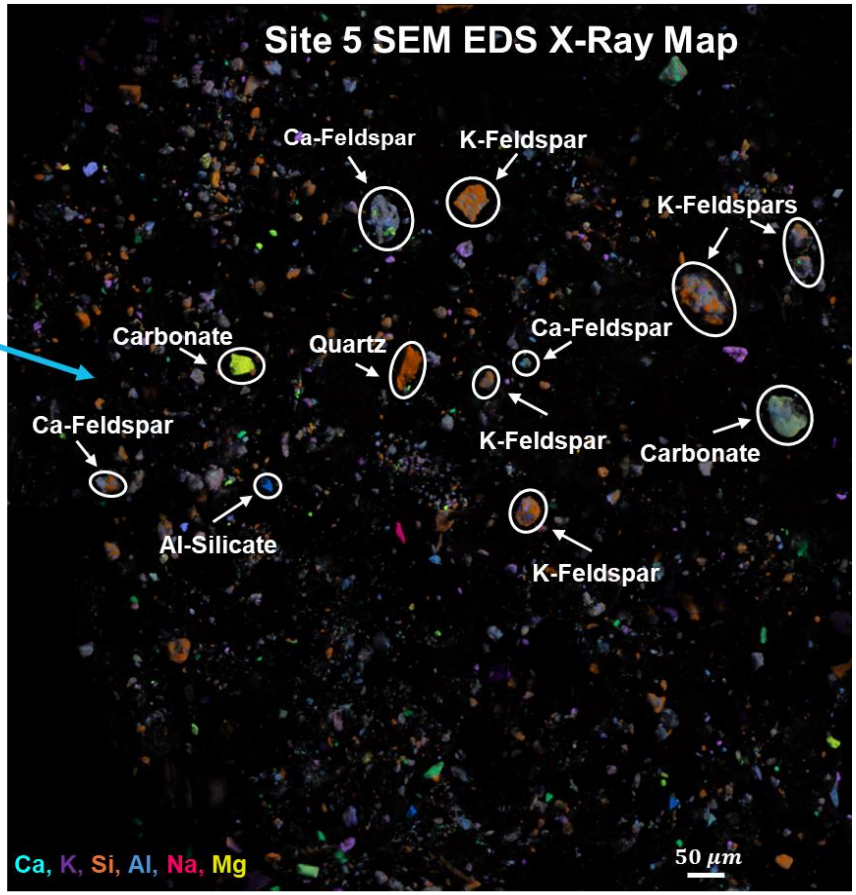

Minerals	Formula
Quartz	SiO_2
Feldspars (Silicates)	$(Na, Ca, K)AlSi_3O_8$
Sulfates	XSO_4
Carbonates	XCO_3
Oxides	X_mO_n

Figure 7. Scanning electron microscopy (SEM) backscattered electron image (BSE) and corresponding montaged energy dispersive spectroscopy (EDS) X-ray map of dust grains collected in Filter 10 located at Site 5. Overlaying different colors for each element produces a semi-qualitative understanding of the composition of dust grains. For example, if Si is assigned the color orange, a quartz grain would show up as orange. If mixes of elements are present, there will be a combination of colors (see feldspar grains that contain both Si and K and/or Ca). This elemental X-ray map shows the bulk mineralogy of dust collected at the Jackpile-Paguate Mine. Silicates, such as quartz and feldspars, sulfates, carbonates, and oxides are common within the dust samples. These minerals are consistent with regional geology, especially sandstone bodies. The table shows the chemical formula of common minerals found within the dust.

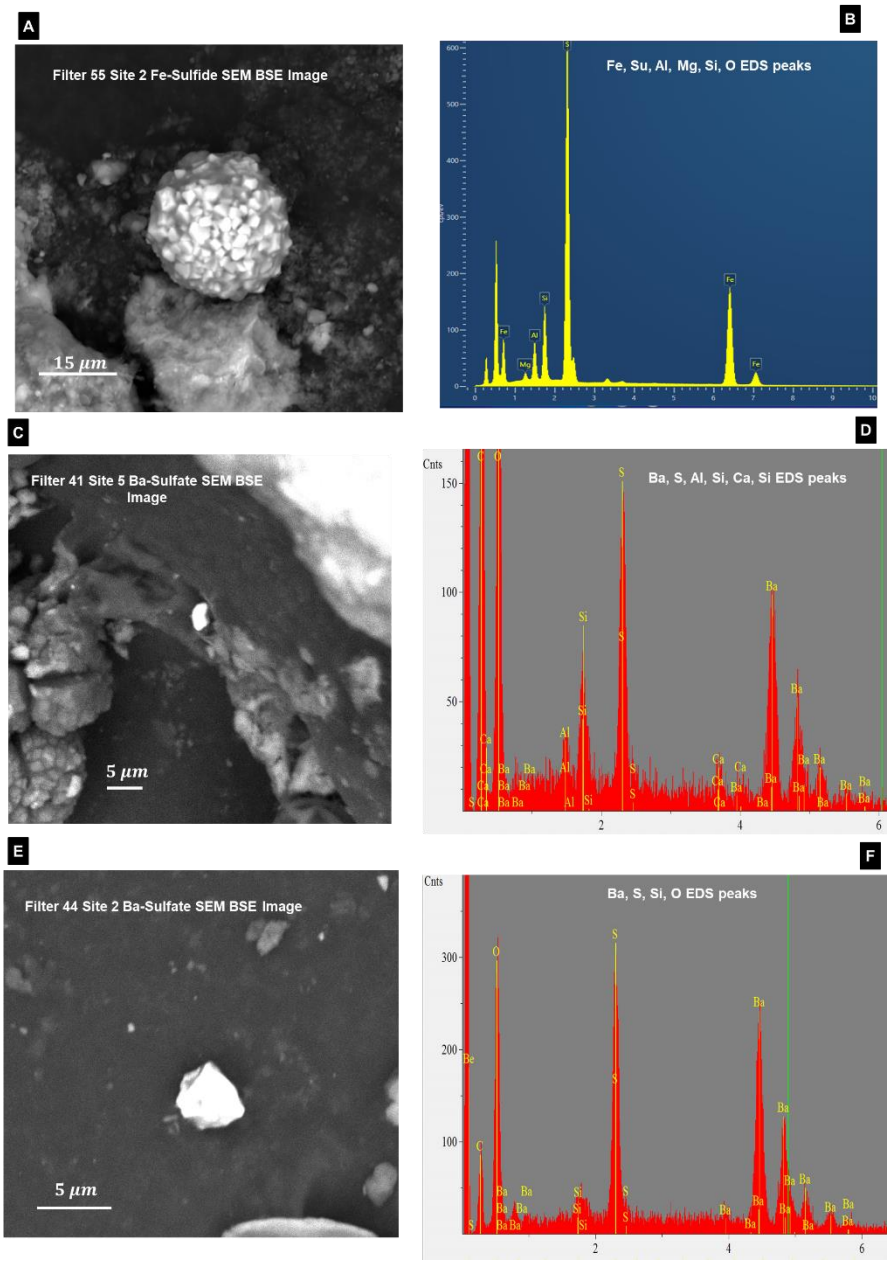

Figure 8. Scanning electron microscopy (SEM) backscattered electron (BSE) images of naturally occurring minerals found within the dust collected throughout the mine. Corresponding energy dispersive spectroscopy (EDS) spectra for each of the grains showing the peak elemental counts are also presented. Figure 8A shows an iron sulfide mineral found in the dust collected in the Main Pit that is about 15 μm. The spectrum in 8B shows high Fe and S intensity peaks indicating that the particulate is likely an iron-sulfide. Figure 8C and Figure 8E show barium-sulfate grains collected from the Main and South pit that are less than 5 μm. The spectrum in 8D and 8F shows high Ba and S intensity peaks indicating that the particulates are likely barium sulfate

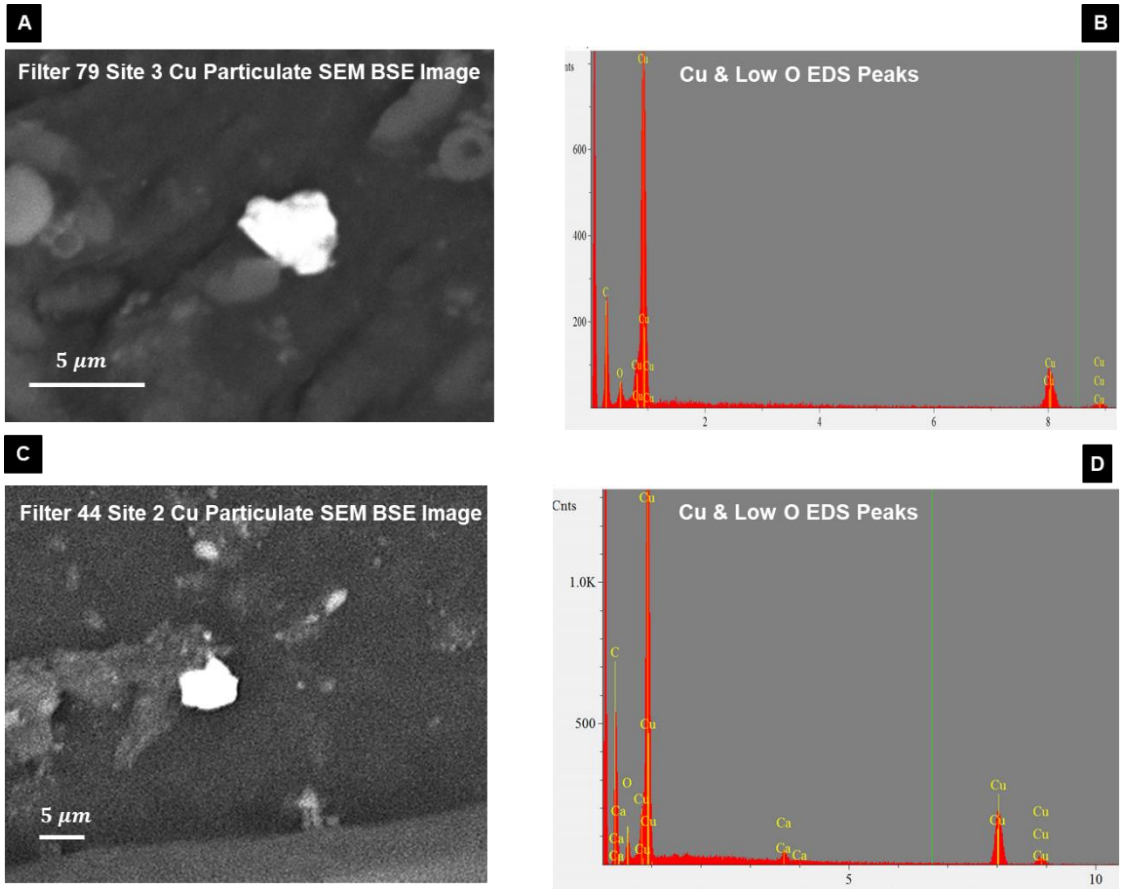

Figure 9. Scanning electron microscopy (SEM) backscattered electron (BSE) images of copper metal particulates in the dust collected throughout the mine. Corresponding energy dispersive spectroscopy (EDS) spectraa for each of the grains showing the peak elemental counts are also presented. Figure 9A and 9C show Cu metal particulates found in dust collected from the Main Pit (Site 2 & 3) and are both less than 5 μm. Both spectra in Figure 9B and 9D show low oxygen intensity peaks but high Cu peaks indicating that the particulates are likely metal.

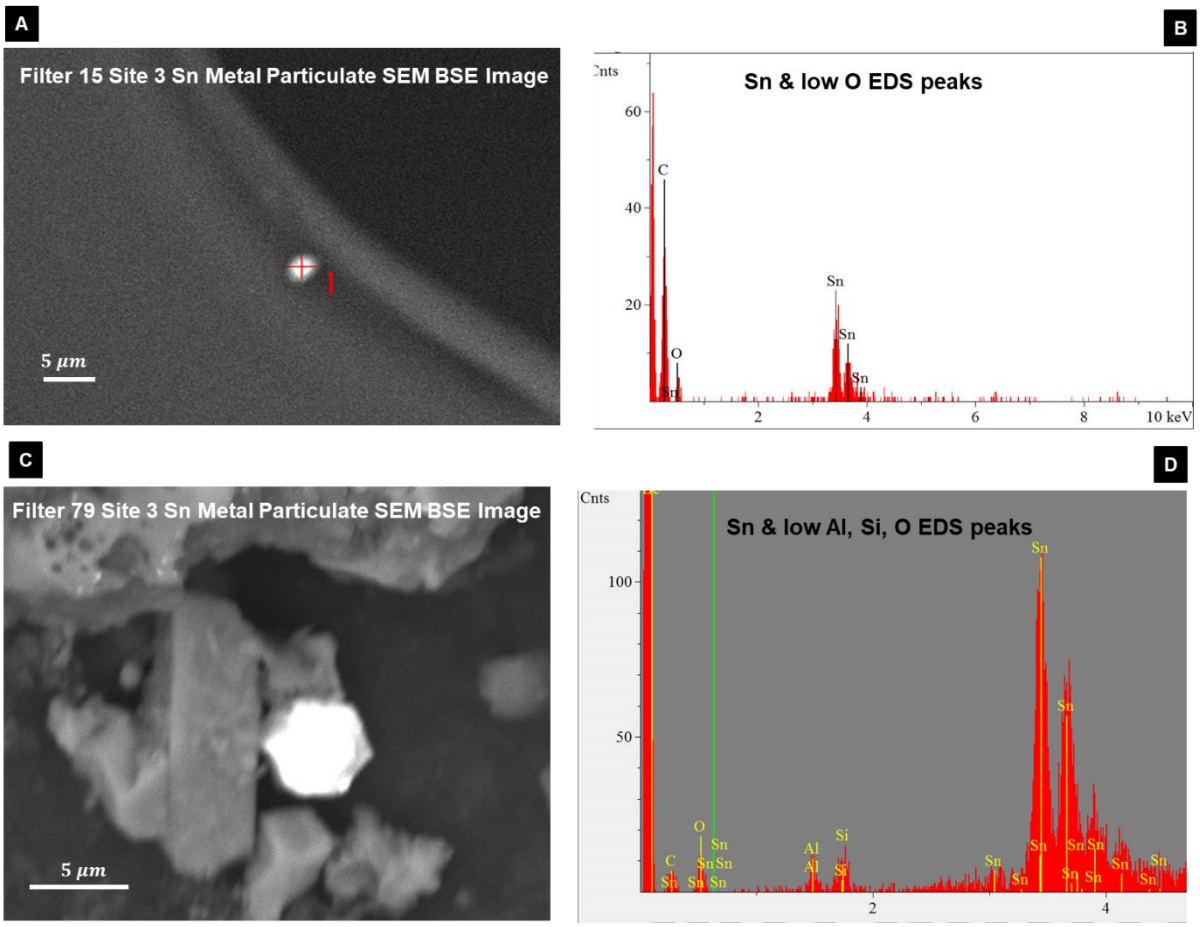

Figure 10. Scanning electron microscopy (SEM) backscattered electron (BSE) images of tin metal particulates in the dust collected throughout the mine. Corresponding energy dispersive spectroscopy (EDS) spectra for each of the grains showing the peak elemental counts are also presented. The Sn particulate in 10A and 10C were both collected in dust from the Main Pit (Site 3). The particulates in 10A and 10C are both less than 5 μm and have irregular morphologies. The spectrum in 10B, which corresponds to the particulate in 10A, shows low oxygen intensity peaks compared to higher intensity Sn peaks. The spectrum in 10D, which corresponds to the particulate in 10C, has multiple different elements present such as Al, Si, and O. However, since the Sn intensity peaks are larger, the EDS is likely picking up X-rays from other surrounding grains. The high intensity Sn peaks when compared to the other elements present in spectra 10B and spectra 10D indicate that the grains in 10A and 10C are likely tin metal.

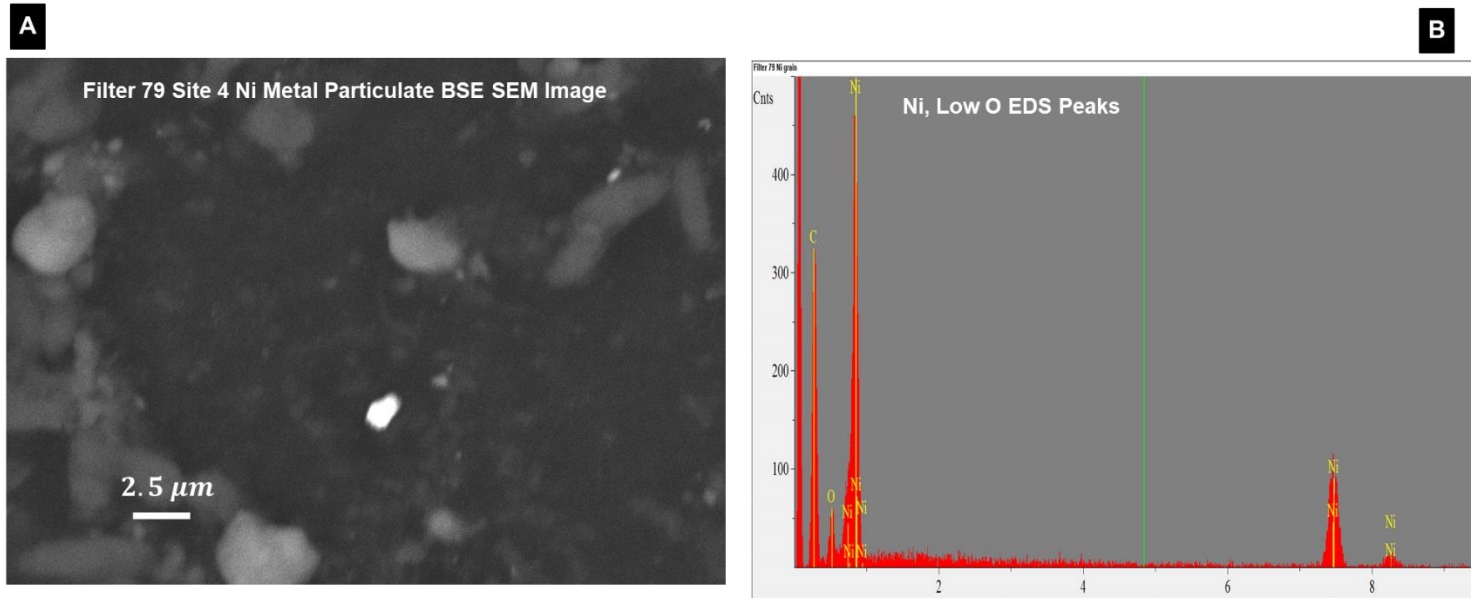

Figure 11. Scanning electron microscopy (SEM) backscattered electron image (BSE) of nickel metal particulate in the dust collected throughout the mine with corresponding energy dispersive spectroscopy (EDS) spectrra showing the peak elemental counts. The particulate in 11A was found in dust collected from the North Pit (Site 5). The Ni particulate is less than 2.5 μm and has an irregular morphology. The spectrum in 11B shows high intensity Ni peaks with a low intensity oxygen peak indicating that the particulate is likely a metal.

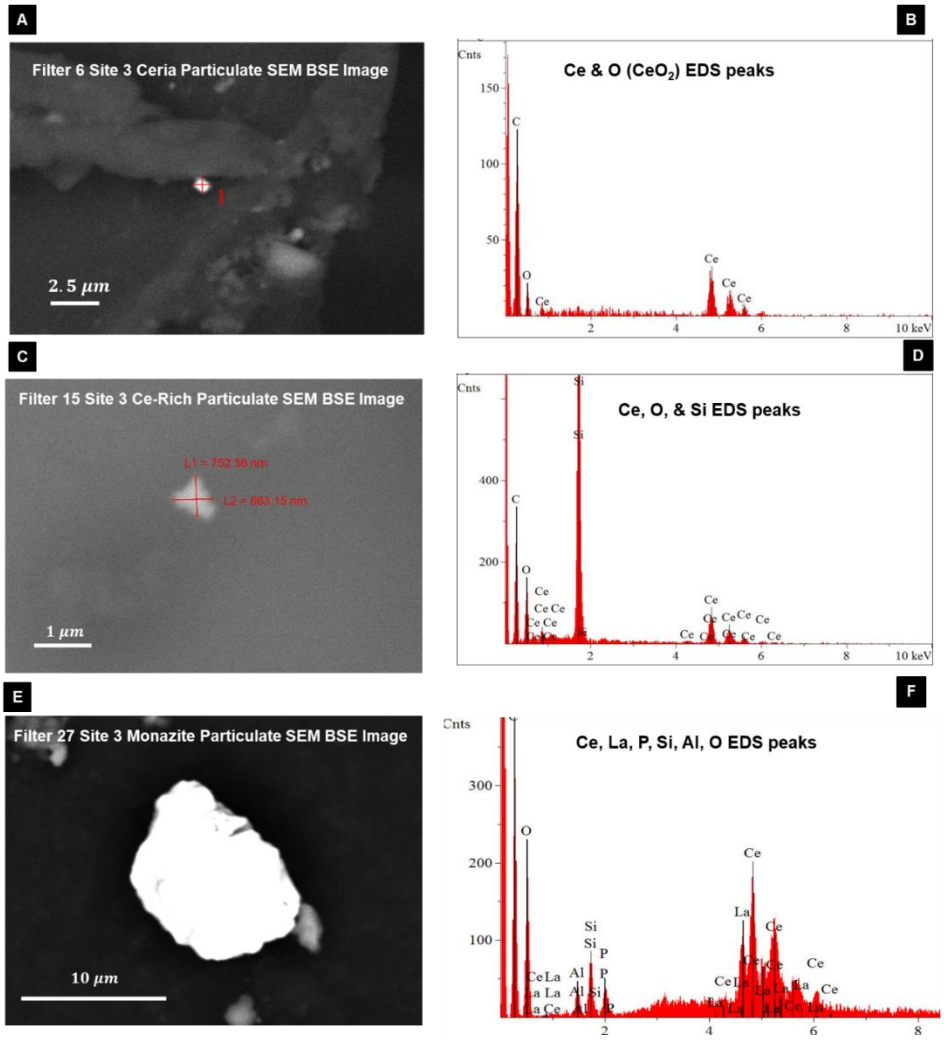

Figure 12. Scanning electron microscopy (SEM) backscattered electron images (BSE) of cerium-rich particulates in the dust collected throughout the mine. Corresponding energy dispersive spectroscopy (EDS) spectra for each of the grains showing the peak elemental counts are also present. The Ce-rich particulates in 12A, 12C, and 12E were all found in dust collected from the Main Pit (Site 3) located near the exposed U-bearing outcrop. Figure 12A shows a particulate that is less than 2.5 μm. The corresponding EDS spectrum in 12B shows Ce and O intensity peaks indicating that the particulate is likely ceria. Figure 12C shows a particulate that is less than a micron. The corresponding EDS spectrum in 12D shows a high Si intensity peak coupled with smaller Ce and O peaks indicating that the particulate is likely a Ce-rich silicate. Figure 12E shows a 10 μm particulate. The EDS spectrum in 12F reveals the presence of Ce and La, a rare earth element. There are also smaller intensity Al, Si, and P peaks. This composition is indicative of a monazite grain.

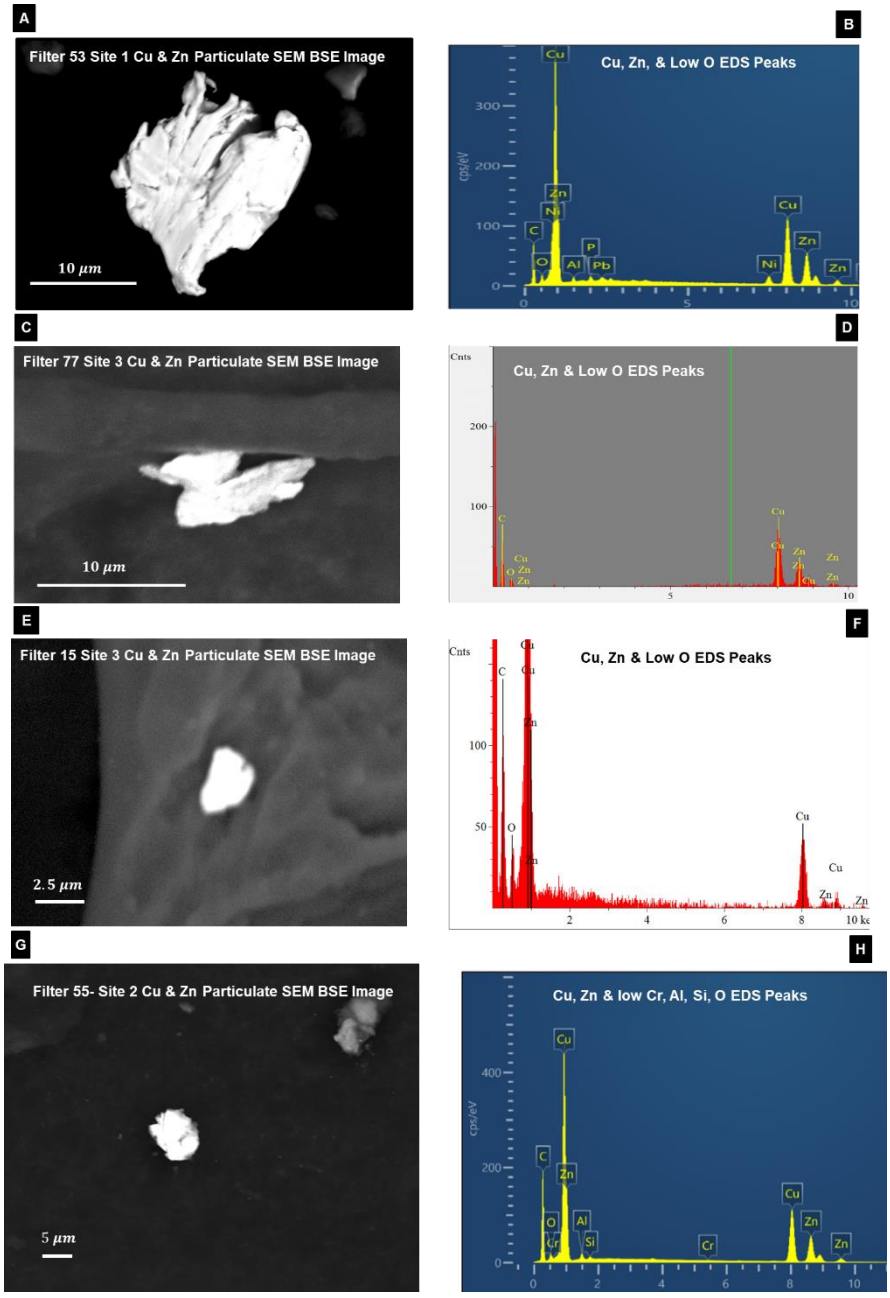

Figure 13. Scanning electron microscopy (SEM) backscattered electron images (BSE) of Cu & Zn-rich particulates in the dust collected throughout the mine. Corresponding energy dispersive spectroscopy (EDS) spectra for each of the grains showing the peak elemental counts are also presented. The particulates in 13A, 13C, 13E, and 13G, were all found in dust collected from the three sites within the Main Pit and range in size from 2.5 μm to 10 μm. The respective EDS spectra in 13B, 13D, 13F, and 13H show high intensity Cu and Zn peaks with low O peaks. This indicates that the particulates could be metal and associated with brass alloys.

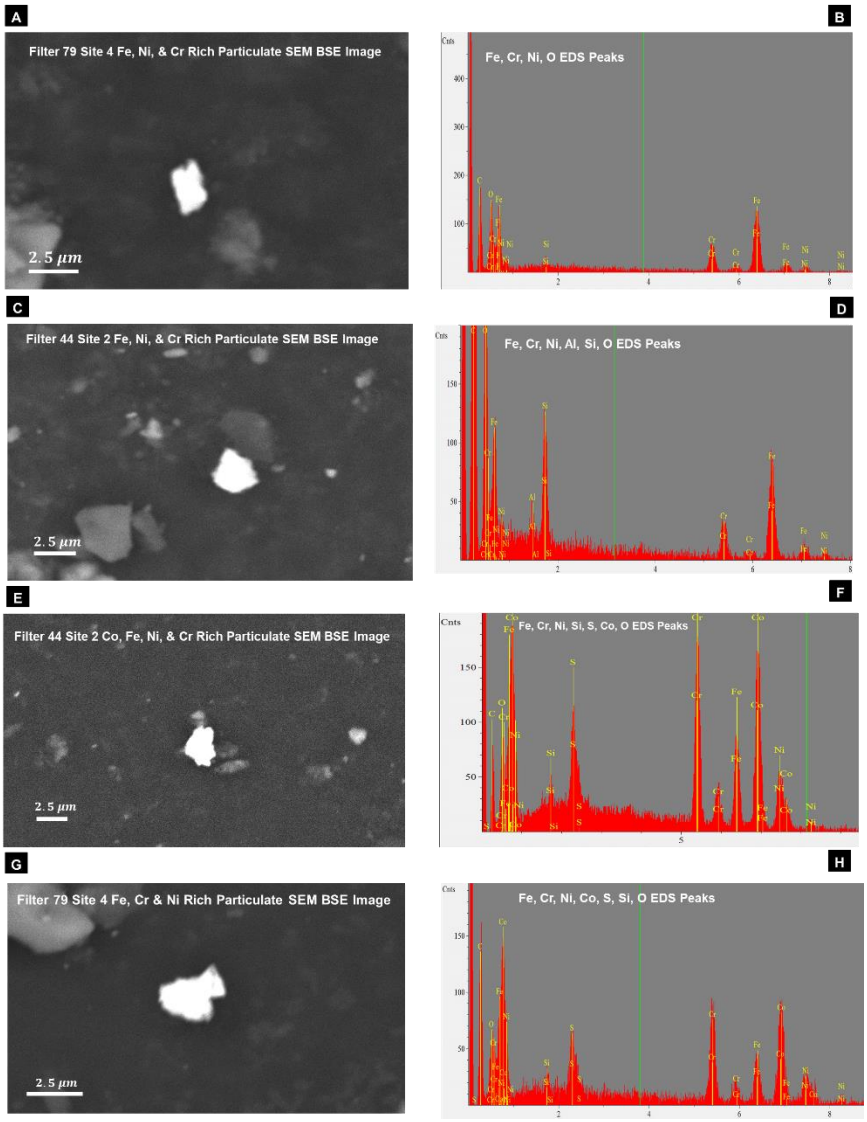

Figure 14. Scanning electron microscopy (SEM) backscattered electron images (BSE) of Cr, Ni, and Fe-rich particulates in the dust collected throughout the mine. Corresponding energy dispersive spectroscopy (EDS) spectra for each of the grains showing the peak elemental counts are also present. The particulates in 14A, 14C, 14E, and 14G were found in dust collected from the Main Pit (Site 2) and the North Pit (Site 4). Each of the particulates are 2.5 μm or less (14A). Respective EDS spectra in 14B, 14D, 14F, and 14H show intensity peaks in multiple elements including Cr, Ni, and Fe. The co-occurrence of these elements is commonly associated with stainless-steel alloys. However, these spectra also show high O peaks and the presence of other elements such as Si, S, Al, and Co. This could be due to the EDS spectra picking up X-rays from nearby particles.

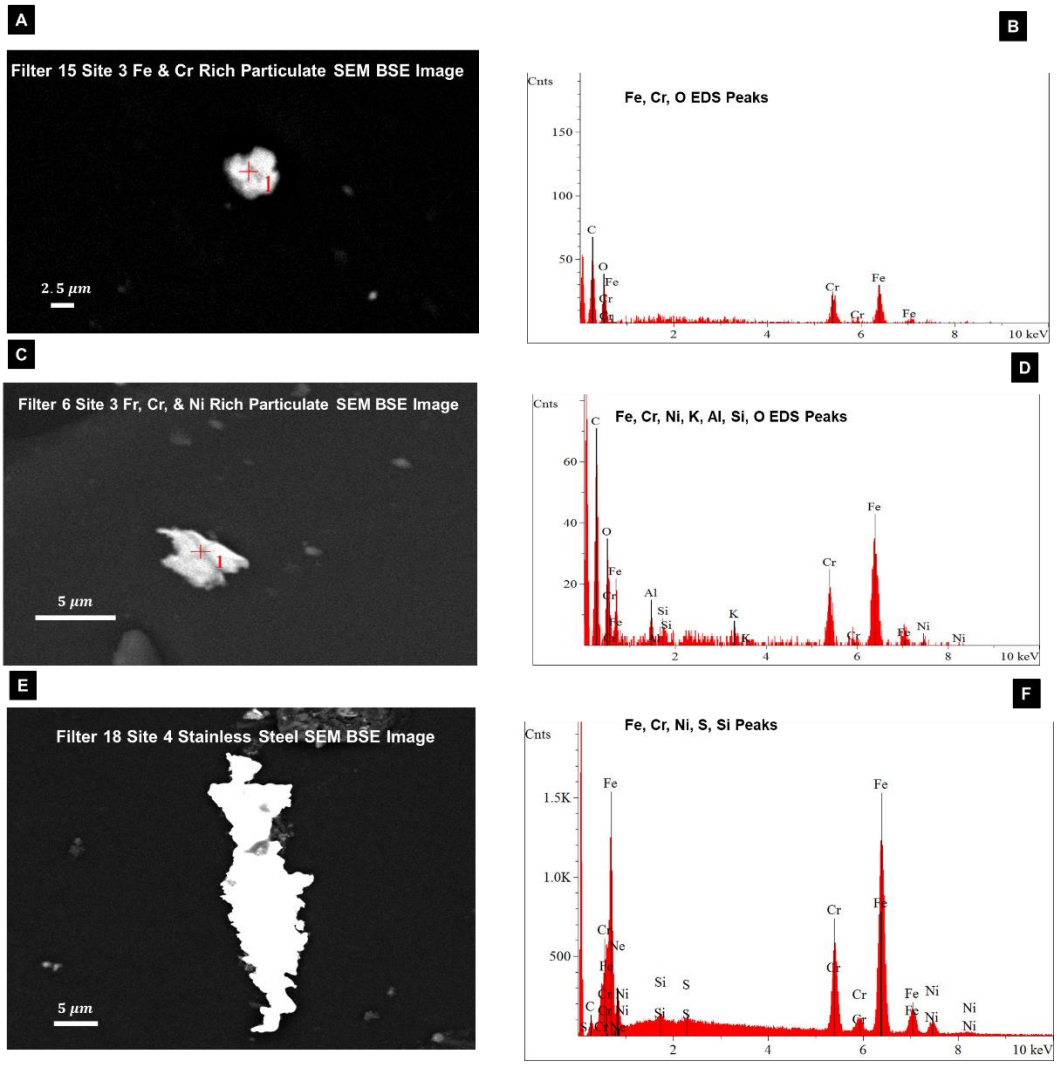

Figure 15. Scanning electron microscopy (SEM) backscattered electron images (BSE) of Cr, Ni, and Fe-rich particulates in the dust collected throughout the mine. Corresponding energy dispersive spectroscopy (EDS) spectra for each of the grains showing the peak elemental counts are also presented. The particulates in 15A, 15C, and 15E were found in dust collected from the Main Pit (Site 3) and the North Pit (Site 4). The particles range from 2.5 μm to 5 μm. Respective EDS spectra in 15B, 15D and 15F show intensity peaks in multiple elements including Cr, Ni, and Fe. The co-occurrence of these elements is commonly associated with stainless-steel alloys. However, these spectra also show high O peaks and the presence of other elements such as Si, S, Al, and Co. This could be due to the EDS spectra picking up X-rays from nearby particles.

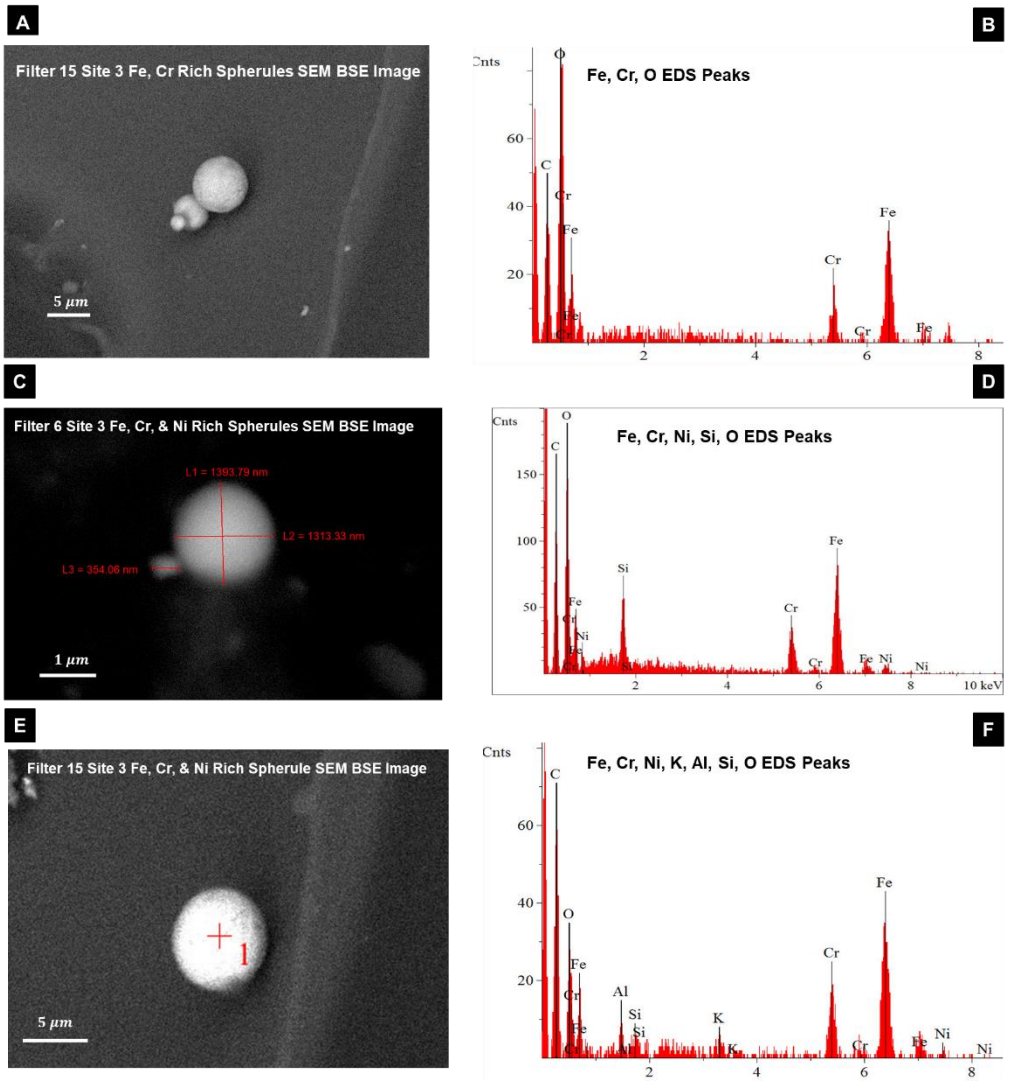

Figure 16. Scanning electron microscopy (SEM) backscattered electron images (BSE) of Cr, Ni, and Fe-rich spherical particulates in the dust collected throughout the mine. Corresponding energy dispersive spectroscopy (EDS) spectra for each of the grains showing the peak elemental counts are also presented. The particulates in 16A, 16C, and 16E were found in dust collected from the Main Pit (Site 3). The particles range from less than a micron 5 μm. Respective EDS spectra in 16B, 16D and 16F show intensity peaks in multiple elements including Cr, Ni, and Fe. The co-occurrence of these elements is commonly associated with stainless-steel alloys. However, these spectra also show high O peaks and the presence of other elements such as Si, Al, and K. This could be due to the EDS spectra picking up X-rays from nearby particles. The spherical morphology of these particulates is distinct and was commonly associated with Cr, Ni, and Fe.

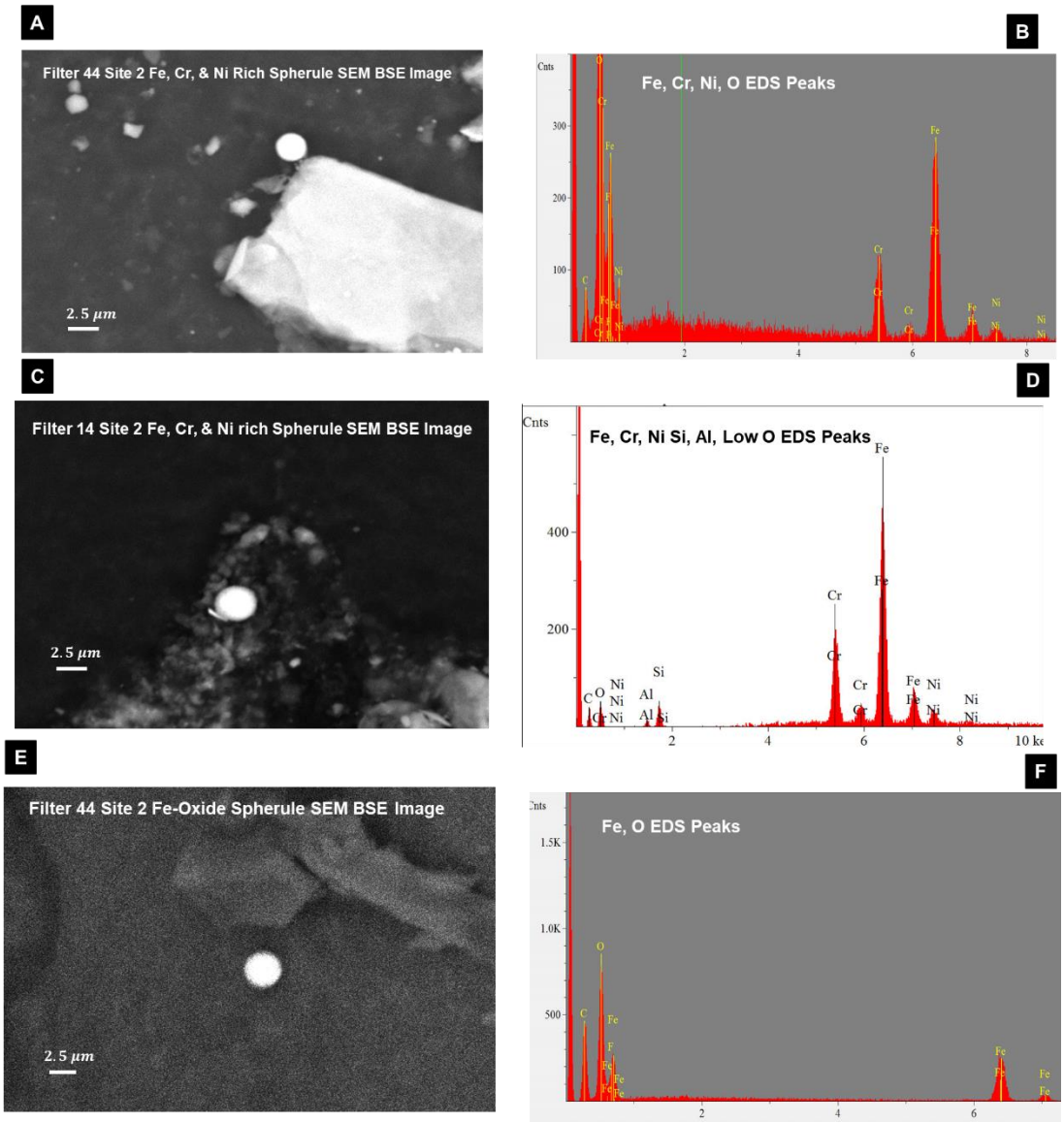

Figure 17. Scanning electron microscopy (SEM) backscattered electron images (BSE) of Cr, Ni, and Fe-rich spherical particulates in the dust collected throughout the mine. Corresponding energy dispersive spectroscopy (EDS) spectra for each of the grains showing the peak elemental counts are also presented. The particulates in 17A, 17C, and 17E were found in dust collected from the Main Pit (Site 2). The particles are about 2.5 μm and have a distinct spherical morphology. Respective EDS spectra in 17B and 17D show intensity peaks in multiple elements including Cr, Ni, and Fe. The co-occurrence of these elements is commonly associated with stainless-steel alloys. However, these spectra also show high O peaks and the presence of other elements such as Si and Al. This could be due to the EDS spectra picking up X-rays from nearby particles. The spherical particulate in 17E is likely an iron-oxide as the corresponding EDS spectrum in 17F does not show Cr and Ni and other elements. The spherical morphology of these particulates is distinct and was commonly associated with Cr, Ni, and Fe.

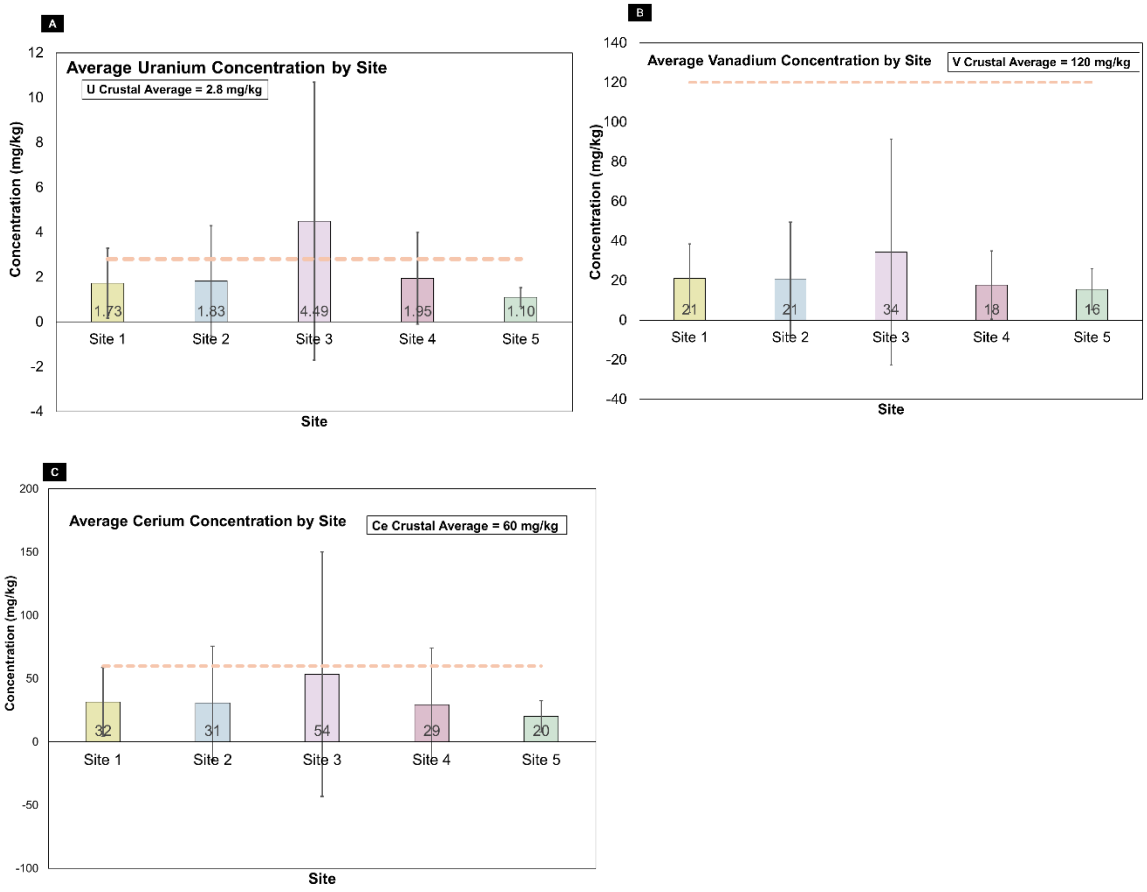

Figure 18. Average concentration (mg/kg) of elements in dust collected at each of the five sites within the Jackpile-Paguate mine that are at or below their crustal averages. Total average concentrations for uranium (18A), vanadium (18B), and cerium (18C) are presented with their corresponding standard deviations, crustal average, and Bernalillo County, New Mexico, soil averages. The bars are representative of the average concentration at each site and the horizontal lines represent the crustal (orange) and soil average (blue). The site averages are consistently below the crustal and soil averages as represented by the bars being below the horizontal lines.

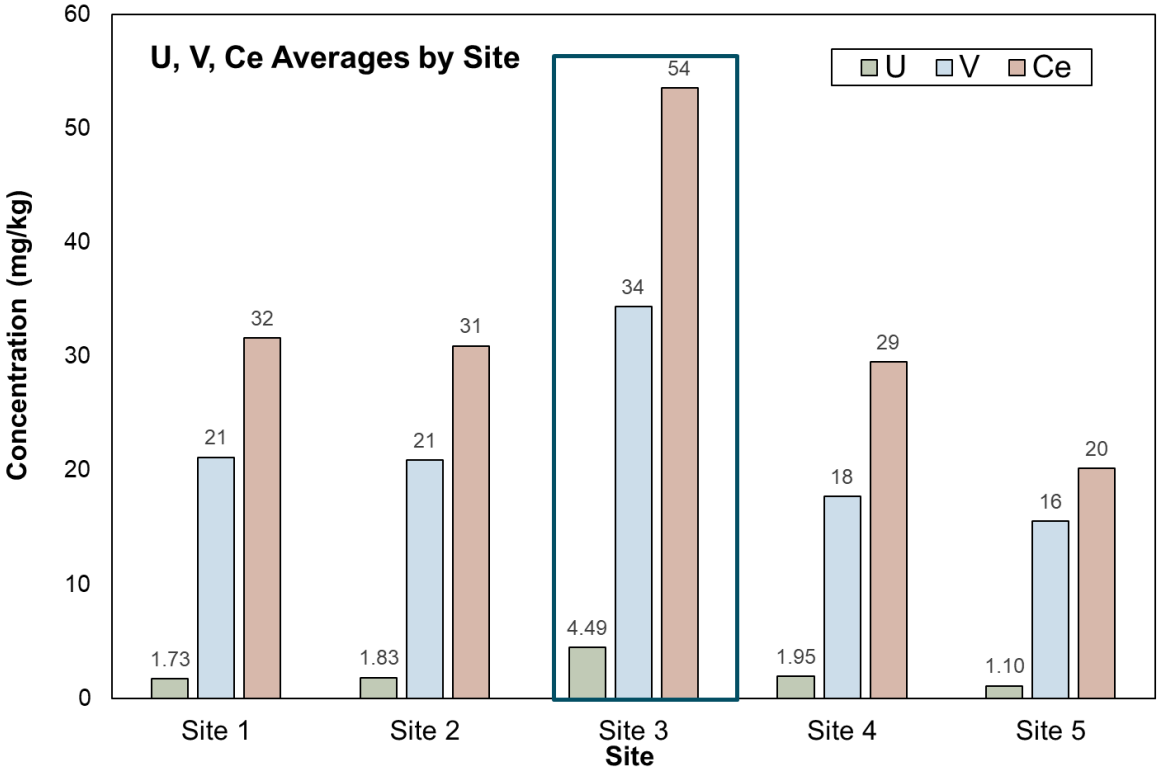

Figure 19. Histogram showing the average concentrations for uranium, vanadium, and cerium at each of the five sites. There is an enrichment in these ore-associated elements specifically at Site 3 which is in the Main Pit near an exposed U-bearing outcrop. The concentrations of U, V, and Ce are higher at Site 3 compared to the other sites.

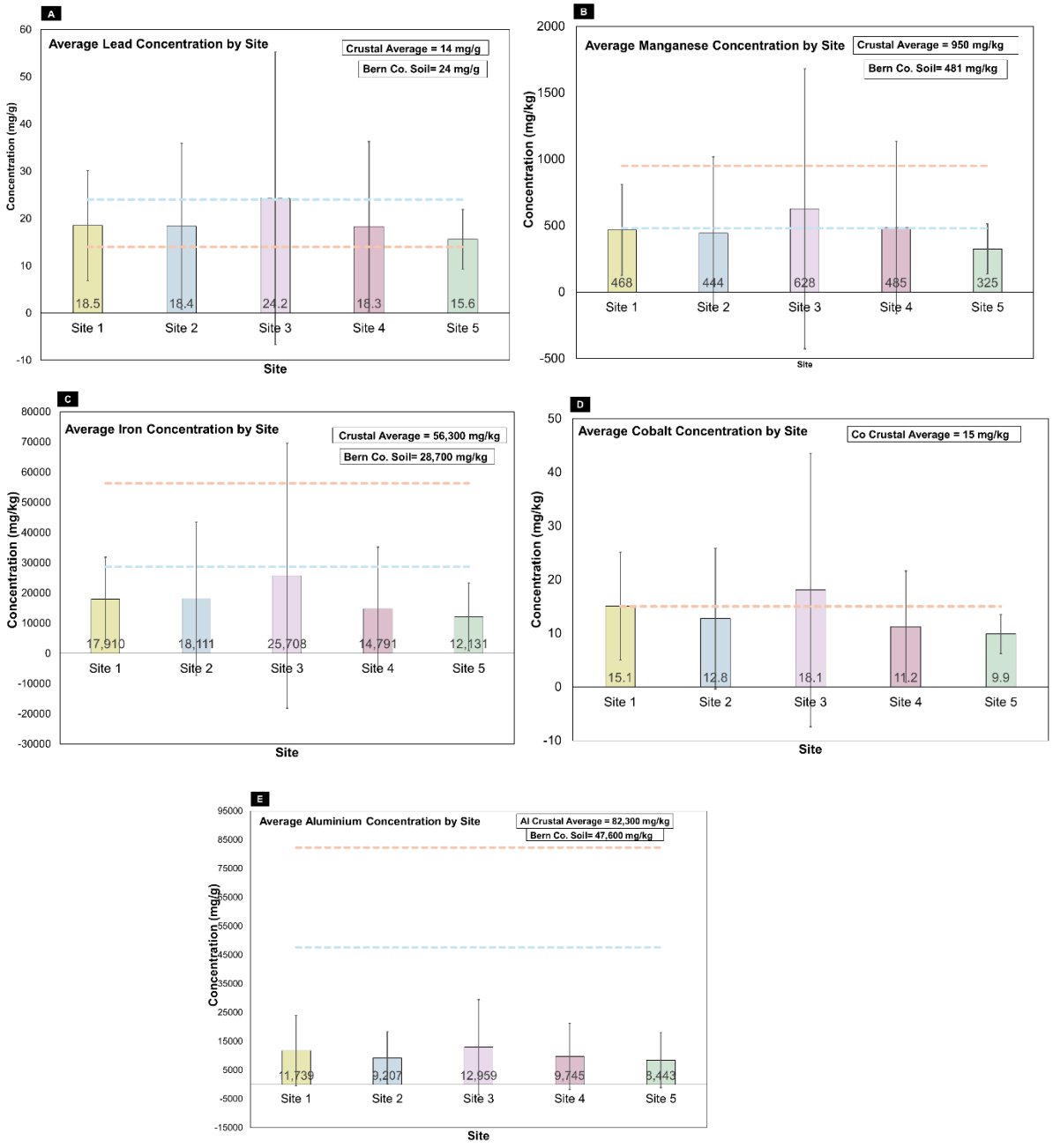

Figure 20. Average concentration (mg/kg) of elements in dust collected at each of the five sites within the Jackpile-Paguate mine that are at or below their crustal averages. Total average concentrations for lead (20A), manganese (20B), iron (20C), cobalt (20D), and aluminum (20E) are presented with their corresponding standard deviation, crustal average, and Bernalillo County, New Mexico, soil average. Standard deviations that appear negative result from the dataset not being normally distributed. The larger the spread of data the longer the standard deviation bar. The histogram bars are representative of the average concentration at each site and the horizontal lines represent the crustal (orange) and soil average (blue). The site averages are consistently below the crustal and soil averages as represented by the bars being below the horizontal lines.

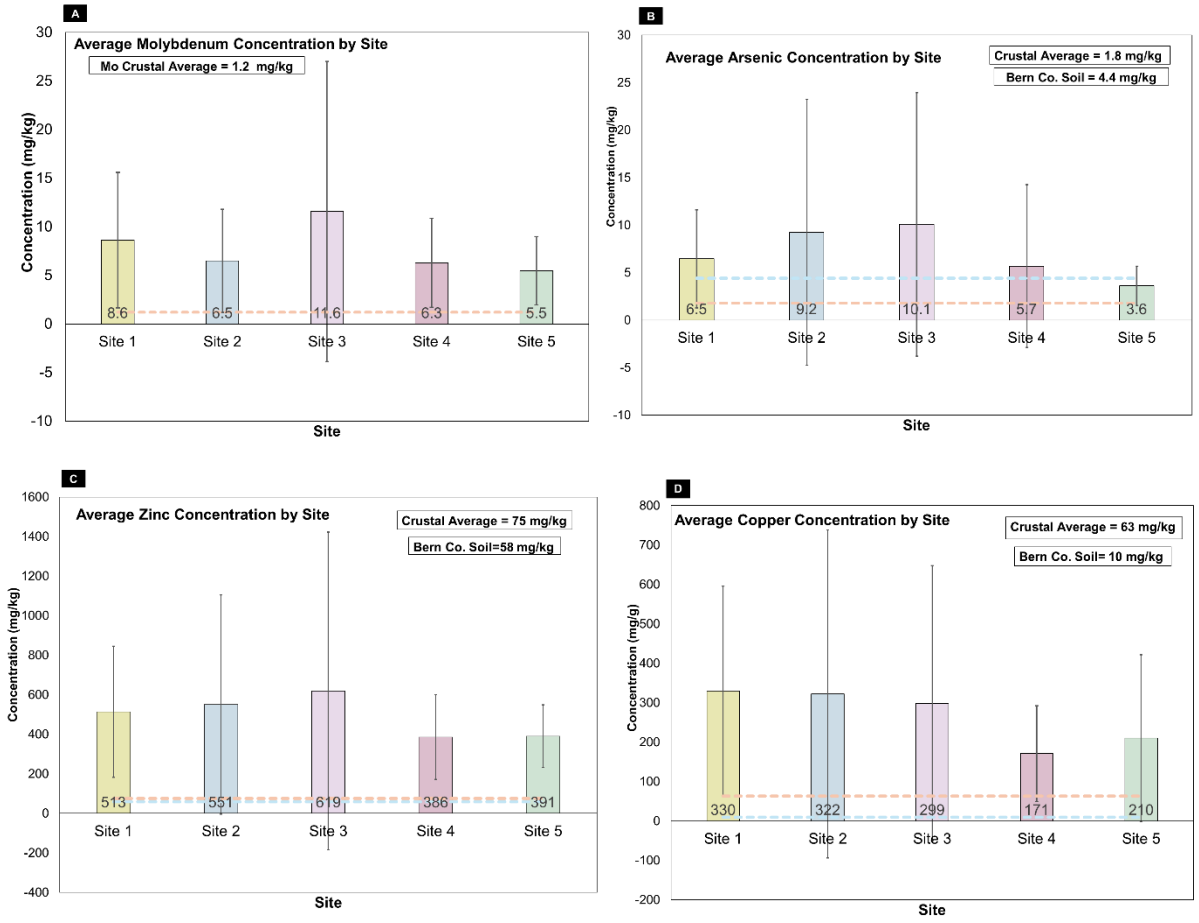

Figure 21. Average concentration (mg/kg) of elements in dust collected at each of the five sites within the Jackpile-Paguate mine that are above their crustal averages. Total average concentrations for molybdenum (21A), arsenic (21B), zinc (21C), and copper are presented with their corresponding standard deviation, crustal average, and Bernalillo County, New Mexico, soil average. Standard deviations that appear negative result from the dataset not being normally distributed. The larger the spread of data the longer the standard deviation bars. The histogram bars are representative of the average concentration at each site and the horizontal lines represent the crustal (orange) and soil average (blue). The site averages are consistently above the crustal and soil averages as represented by the bars being below the horizontal lines.

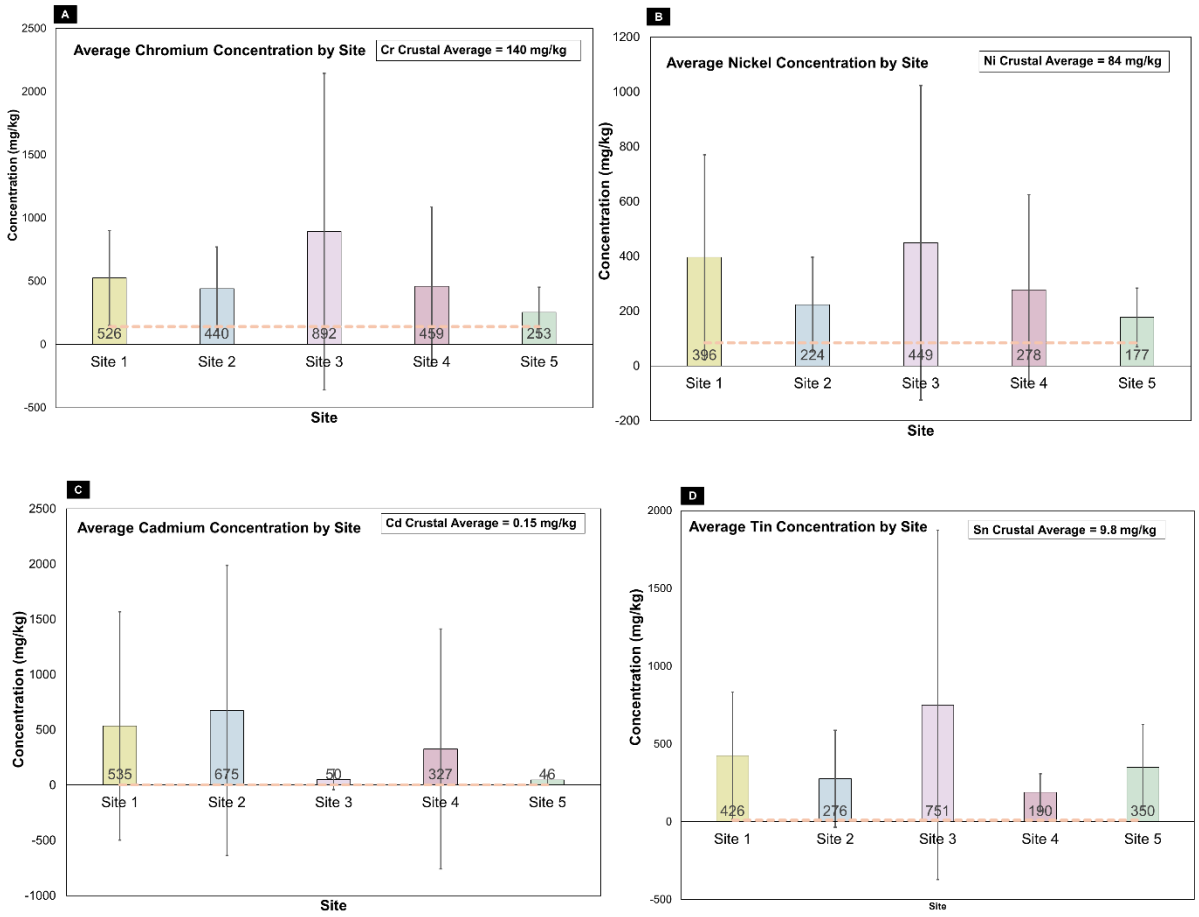

Figure 22. Average concentration (mg/kg) of elements in dust collected at each of the five sites within the Jackpile-Paguate mine that are above their crustal averages. Total average concentrations for chromium (22A), nickel (22B), cadmium (21C), and tin (21D) are presented with their corresponding standard deviation, crustal average, and Bernalillo County, New Mexico, soil average. Standard deviations that appear negative result from the dataset not being normally distributed. The larger the spread of data the longer the standard deviation bar. The histogram bars are representative of the average concentration at each site and the horizontal lines represent the crustal (orange) and soil average (blue). The site averages are consistently above the crustal and soil averages as represented by the bars being below the horizontal lines.

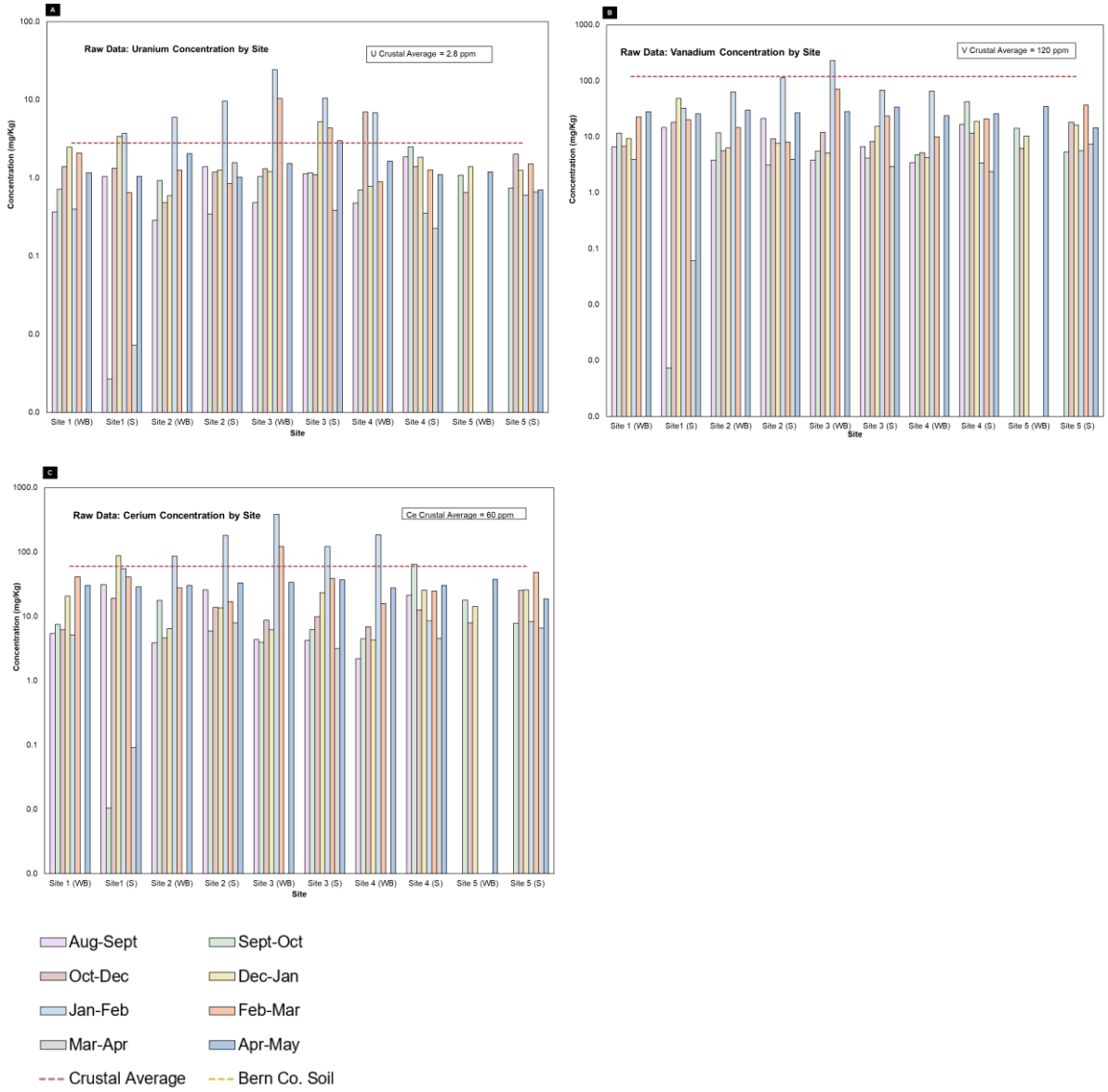

Figure 23. Raw logged concentration data (mg/kg) of elements in dust collected at each of the five sites within the Jackpile-Paguate mine that are generally at or below their crustal averages. The raw data for uranium (23A), vanadium (23B), and cerium (23C) are presented. The histogram bars are representative of the raw data at each site and the horizontal line (red) represents the crustal average. Data are also separated by settler (S) and windblown (WB) collector types.

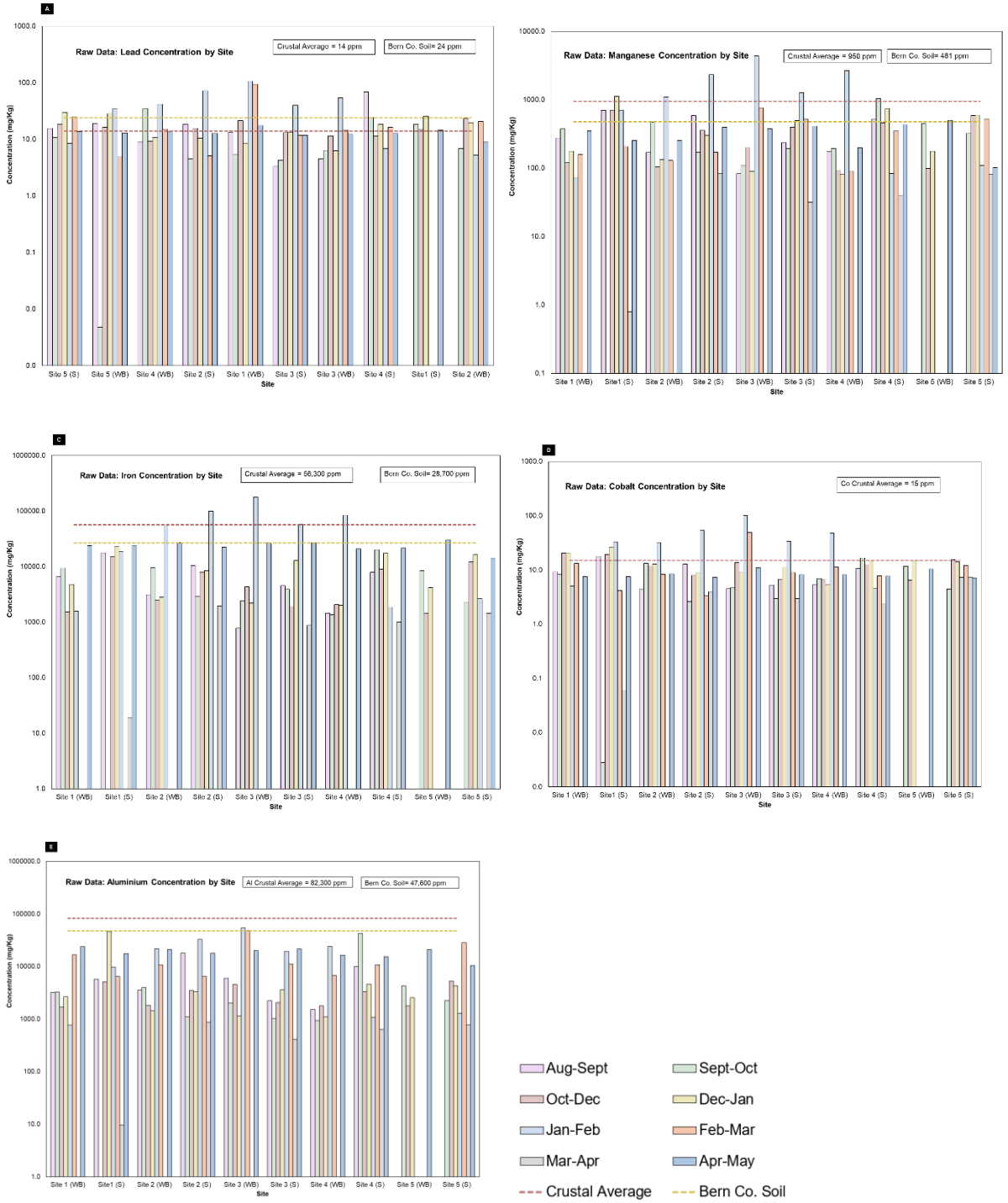

Figure 24. Raw logged concentration data (mg/kg) of elements in dust collected at each of the five sites within the Jackpile-Paguate mine that are generally at or below their crustal averages. The raw data for lead (24A), manganese (24B), iron (24C), cobalt (24D), and aluminum (24E) are presented. The histogram bars are representative of the raw data at each site and the horizontal lines (red) represents the crustal average and Bernalillo County, NM, soil average (yellow). Data are also separated by settler (S) and windblown (WB) collector types.

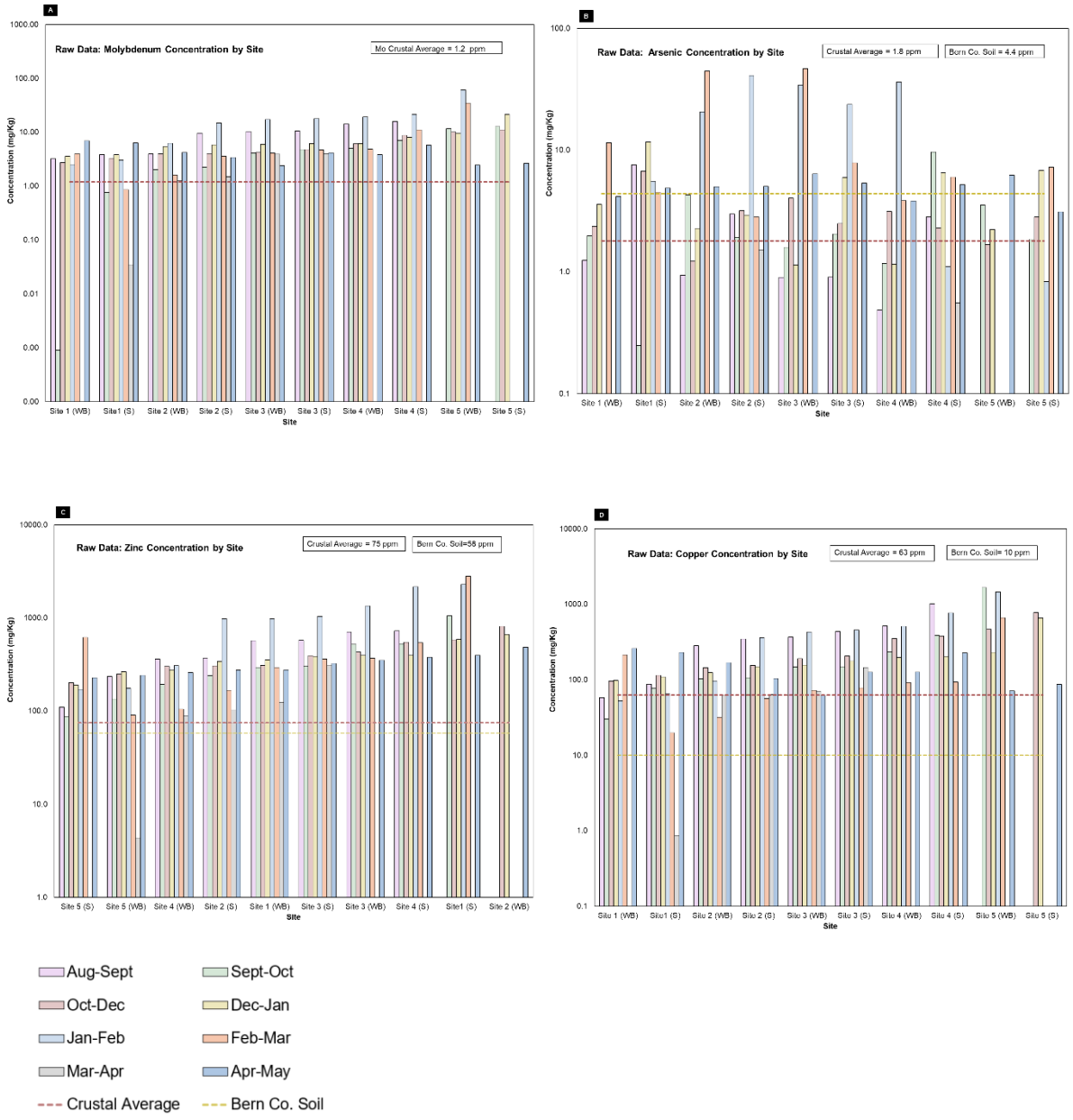

Figure 25. Raw logged concentration data (mg/kg) of elements in dust collected at each of the five sites within the Jackpile-Paguate mine that are generally above their crustal averages. The raw data for molybdenum (25A), arsenic (25B), zinc (25C), and copper (25D) are presented. The histogram bars are representative of the raw data at each site and the horizontal lines (red) represent the crustal average and Bernalillo County, NM, soil average (yellow). Data are also separated by settler (S) and windblown (WB) collector types.

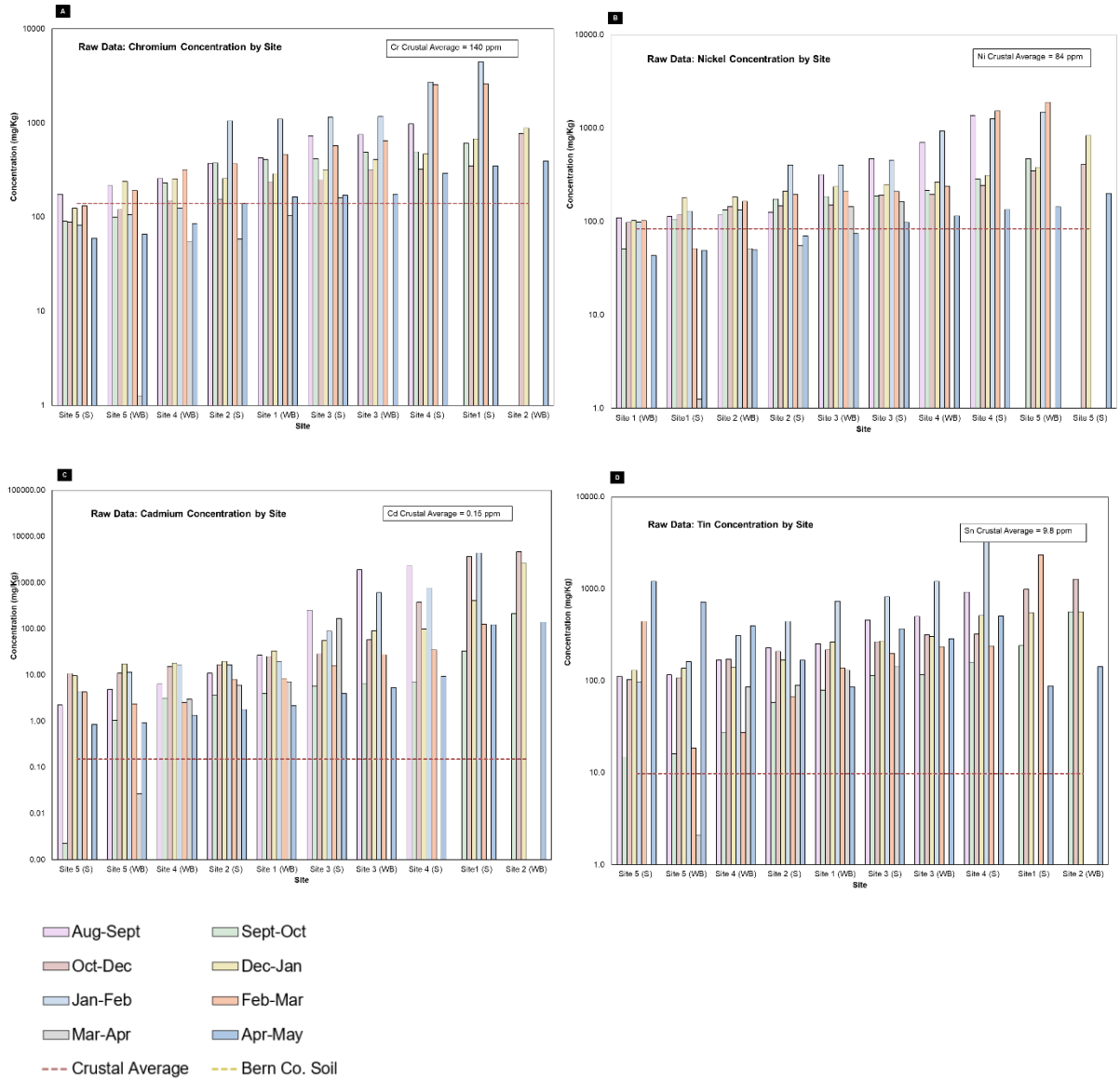

Figure 26. Raw concentration data (mg/kg) of elements in dust collected at each of the five sites within the Jackpile-Paguate mine that are generally above their crustal averages. The raw data for chromium (26A), nickel (26B), cadmium (26C), and zinc (26D) are presented. The histogram bars are representative of the raw data at each site and the horizontal lines (red) represent the crustal average and Bernalillo County, NM, soil average (yellow). Data are also separated by settler (S) and windblown (WB) collector types.

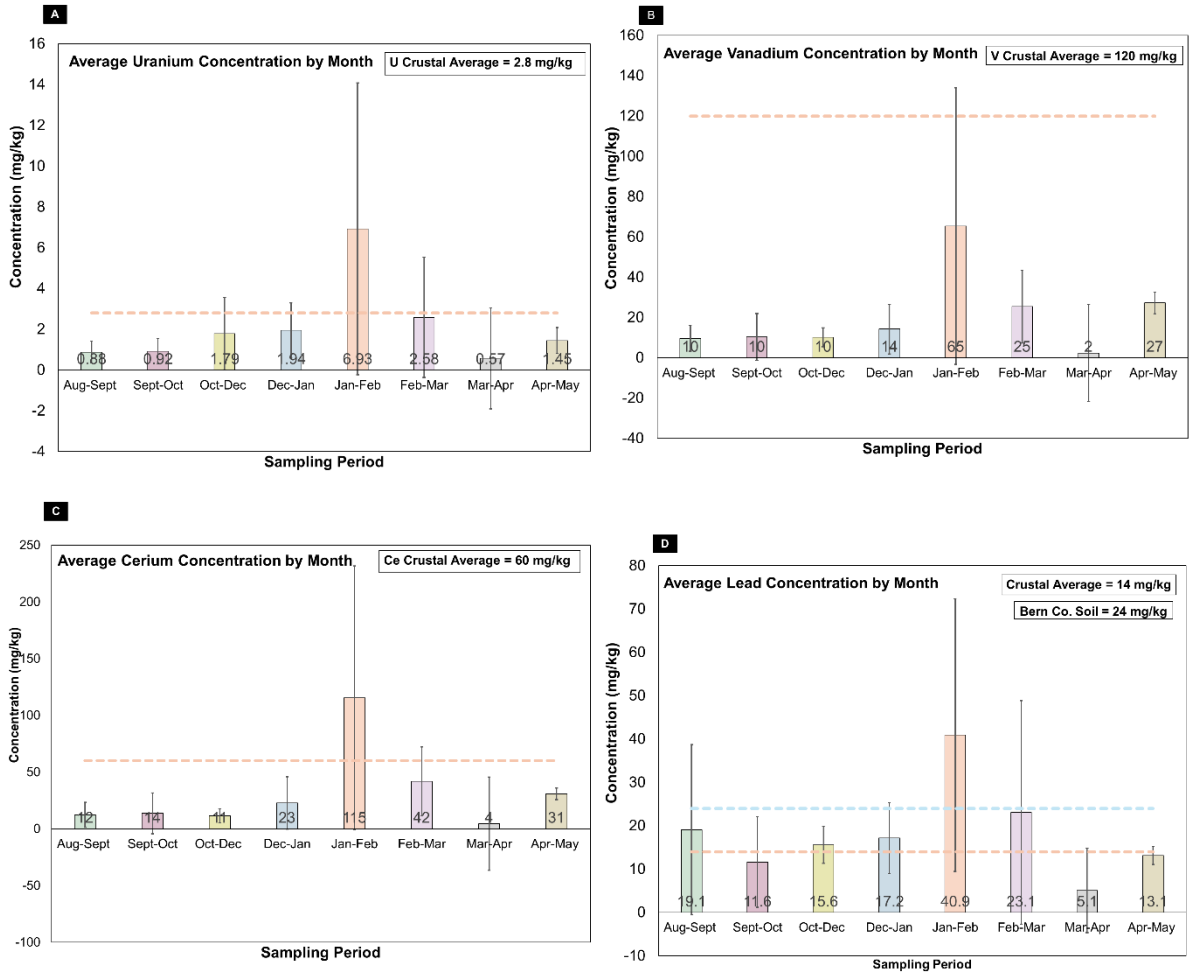

Figure 27. Average concentration (mg/kg) of elements in dust collected during each of the eight sampling periods that were primarily at or below the crustal average. Total average concentrations for uranium (27A), vanadium (27B), cerium (27C), and lead (28D) with their corresponding standard deviation, crustal average, and Bernalillo County, New Mexico, soil average. Standard deviations that appear negative result from the dataset not being normally distributed. The larger the spread of data the longer the standard deviation bar. The histogram bars are representative of the average concentration during each month and the horizontal lines represent the crustal (orange) and soil average (blue). Peak elemental concentrations occurred during the January through February sampling period.

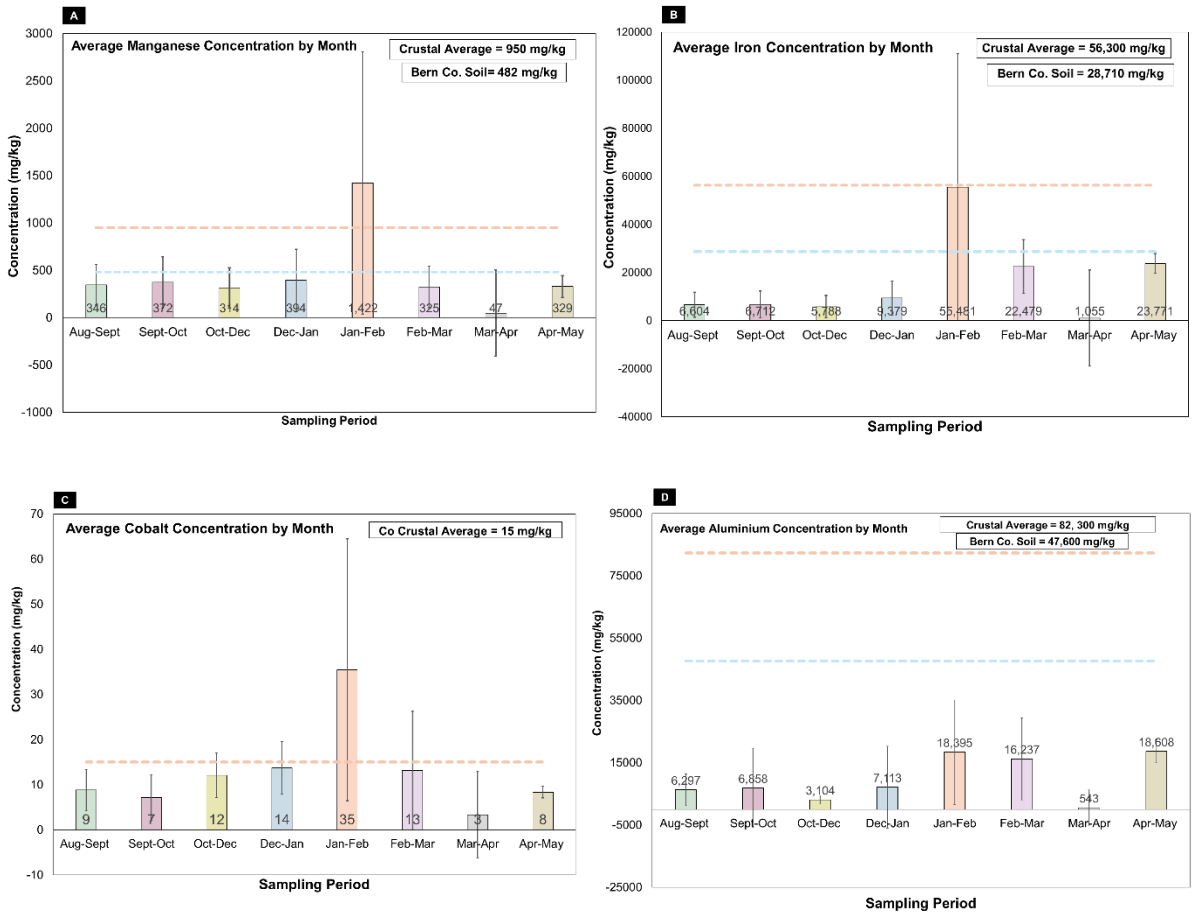

Figure 28. Average concentration (mg/kg) of elements in dust collected during each of the eight sampling periods that were primarily at or below the crustal average. Total average concentrations for manganese (28A), iron (28B), cobalt (28C), and aluminum (28D) with their corresponding standard deviation, crustal average, and Bernalillo County, New Mexico, soil average. Standard deviations that appear negative result from the dataset not being normally distributed. The larger the spread of data the longer the standard deviation bar. The histogram bars are representative of the average concentration during each month and the horizontal lines represent the crustal (orange) and soil average (blue). Peak elemental concentrations occurred during the January through February sampling period.

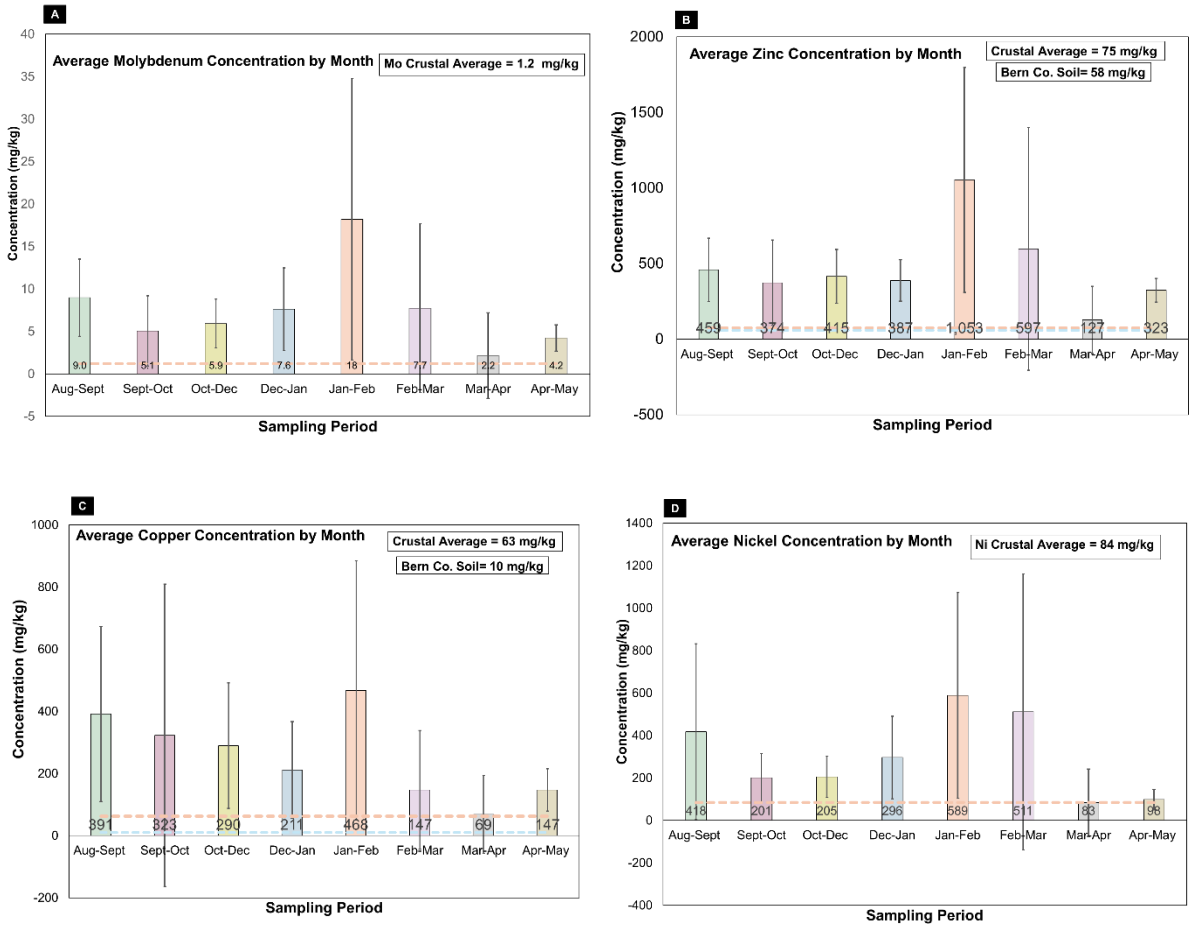

Figure 29. Average concentration (mg/kg) of elements in dust collected during each of the eight sampling periods that were primarily above the crustal average. Total average concentrations for molybdenum (29A), zinc (29B), copper (29C), and nickel (29D) with their corresponding standard deviation, crustal average, and Bernalillo County, New Mexico, soil average. Standard deviations that appear negative result from the dataset not being normally distributed. The larger the spread of data the longer the standard deviation bar. The histogram bars are representative of the average concentration during each month and the horizontal lines represent the crustal (orange) and soil average (blue). Peak elemental concentrations occurred during the January through February sampling period.

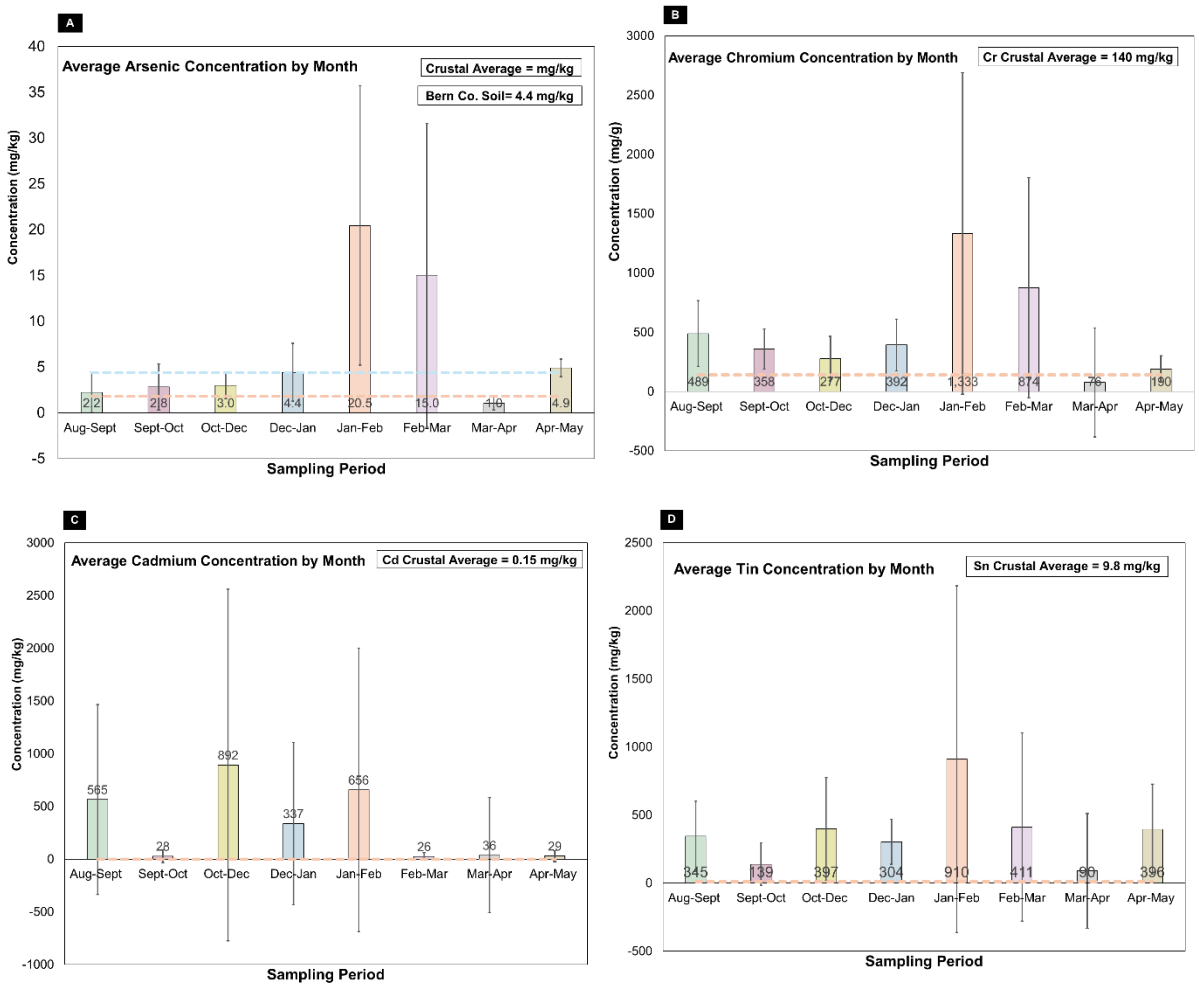

Figure 30. Average concentration (mg/kg) of elements in dust collected during each of the eight sampling periods that were primarily above the crustal average. Total average concentrations for arsenic (30A), chromium (30B), cadmium (30C), and tin (30D) are presented with their corresponding standard deviation, crustal average, and Bernalillo County, New Mexico, soil average. Standard deviations that appear negative result from the dataset not being normally distributed. The larger the spread of data the longer the standard deviation bar. The histogram bars are representative of the average concentration during each sampling period and the horizontal lines represent the crustal (orange) and soil average (blue). Sn, Co, and Al peak concentrations occurred during January through February. The peak Cd concentration occurred in the October through December sampling period as opposed to January and February.

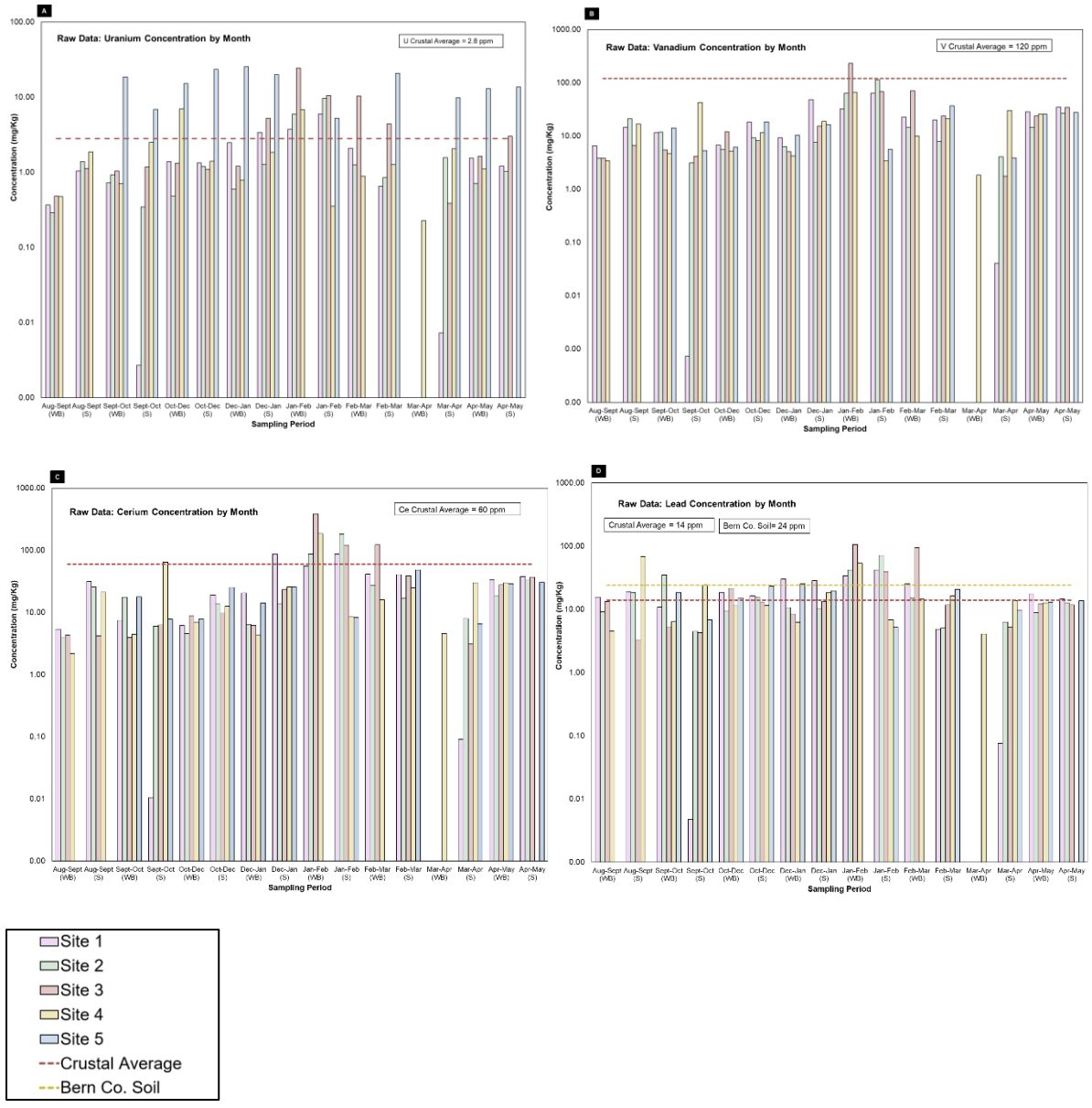

Figure 31. Raw concentration data (mg/kg) of elements in dust collected during each of the 8 sampling periods that are generally at or below the crustal averages. The raw data for uranium (31A), vanadium (31B), cerium (31C), and lead (31D) are presented. The histogram bars are representative of the raw data at each site and the horizontal lines (red) represent the crustal average and Bernalillo County, NM, soil average (yellow). Data are also separated by settler (S) and windblown (WB) collector types.

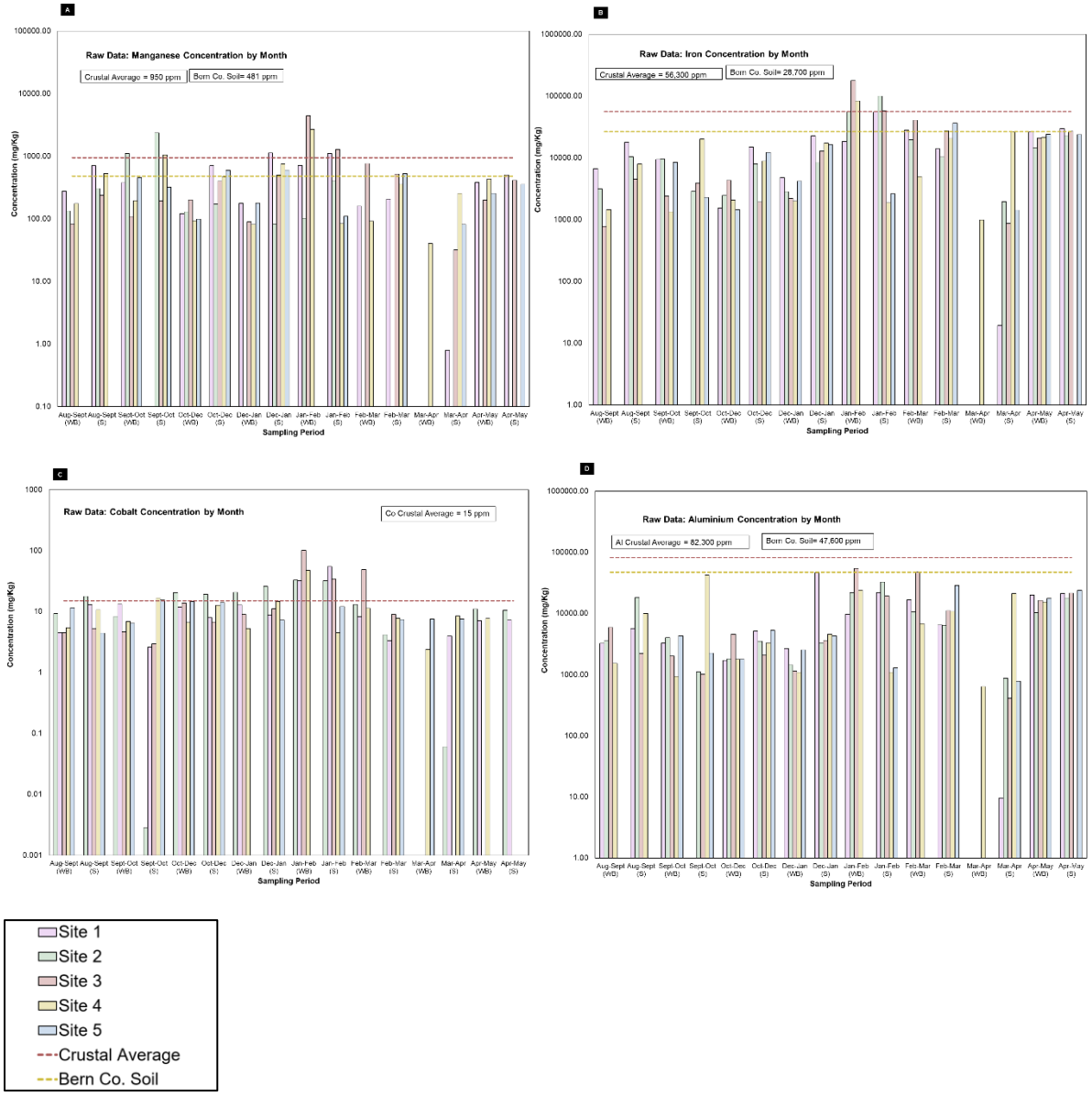

Figure 32. Raw concentration data (mg/kg) of elements in dust collected during each of the 8 sampling periods that are generally at or below the crustal averages. The raw data for manganese (32A), iron (32B), cobalt (32C), and aluminum (32D) are presented. The histogram bars are representative of the raw data at each site and the horizontal lines (red) represent the crustal average and Bernalillo County, NM, soil average (yellow). Data are also separated by settler (S) and windblown (WB) collector types.

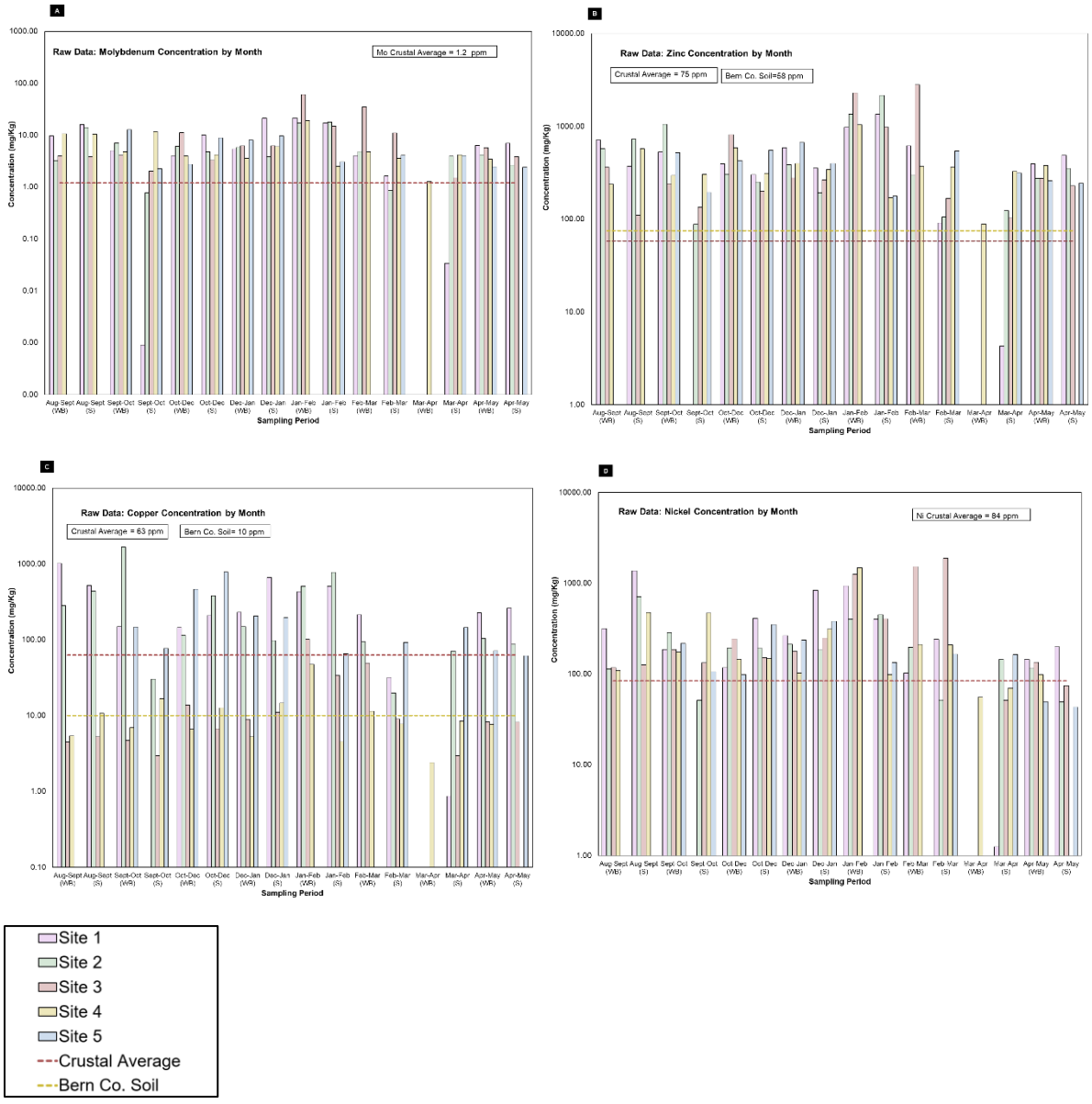

Figure 33. Raw concentration data (mg/kg) of elements in dust collected during each of the 8 sampling periods that are generally above the crustal averages. The raw data for molybdenum (33A), zinc (33B), copper (33C), and nickel (33D) are presented. The histogram bars are representative of the raw data at each site and the horizontal lines (red) represent the crustal average and Bernalillo County, NM, soil average (yellow). Data are also separated by settler (S) and windblown (WB) collector types.

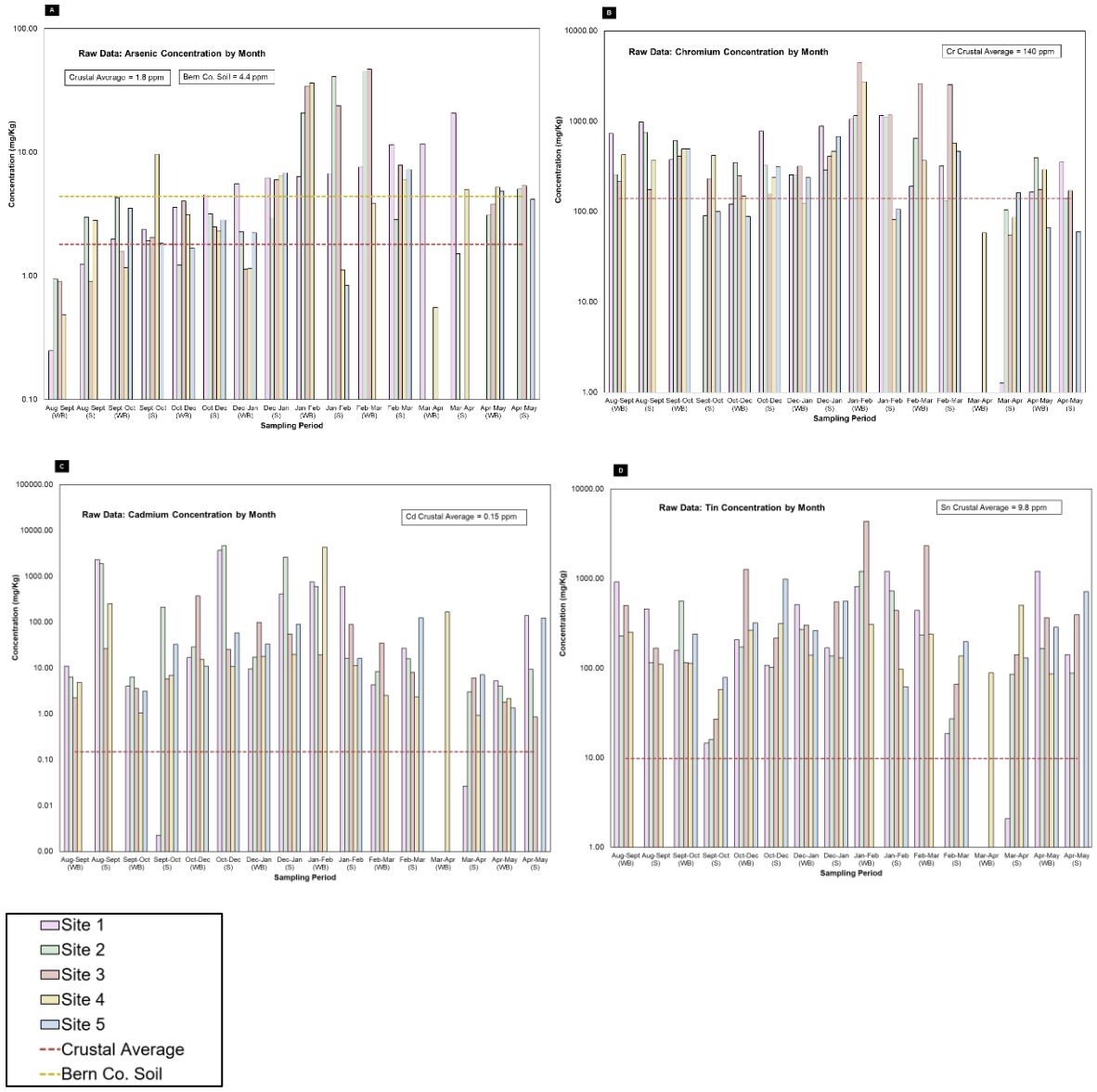

Figure 34. Raw concentration data (mg/kg) of elements in dust collected during each of the 8 sampling periods that are generally above the crustal averages. The raw data for arsenic (34A), chromium (34B), cadmium (34C), and tin (34D) are presented. The histogram bars are representative of the raw data at each site and the horizontal lines (red) represent the crustal average and Bernalillo County, NM, soil average (yellow). Data are also separated by settler (S) and windblown (WB) collector type.

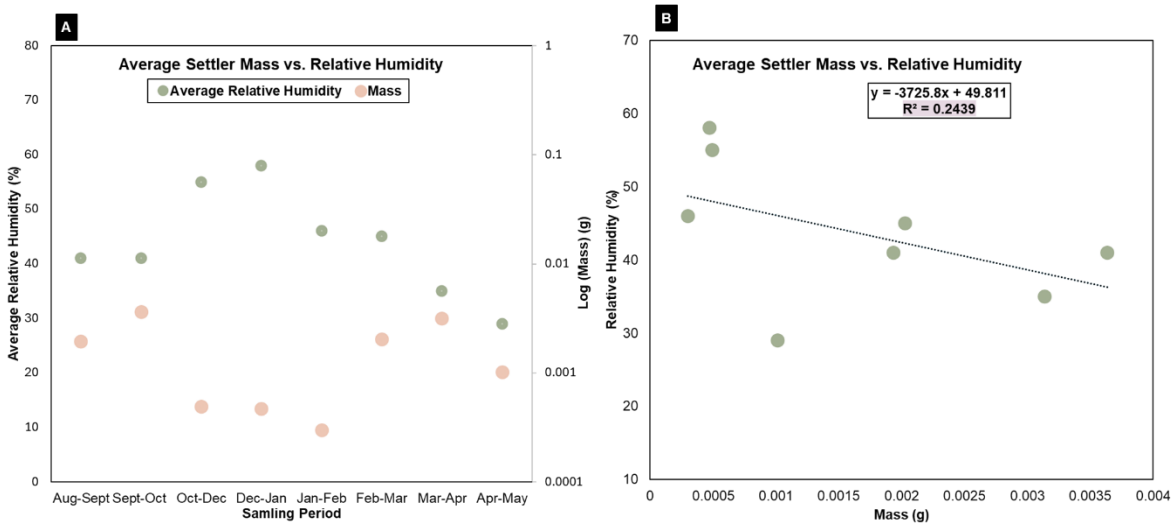

Figure 35. Plot of the average settler masses vs. the monthly average relative humidity. Figure 35A shows the average relative humidity near Pueblo of Laguna graphed against the logged average settler masses that were collected during each sampling period. This scatterplot shows that during periods of higher relative humidity, specifically from October to February, the average mass collected was lower. The line of best fit (y=-3725.8x + 49.811) found when graphing relative humidity against mass in Figure 35B produced a negative linear regression coefficient. This suggests that as relative humidity increased airborne mass decreases. However, the low R^2 (0.2439) value show that there no significant correlation between the variables in this dataset.

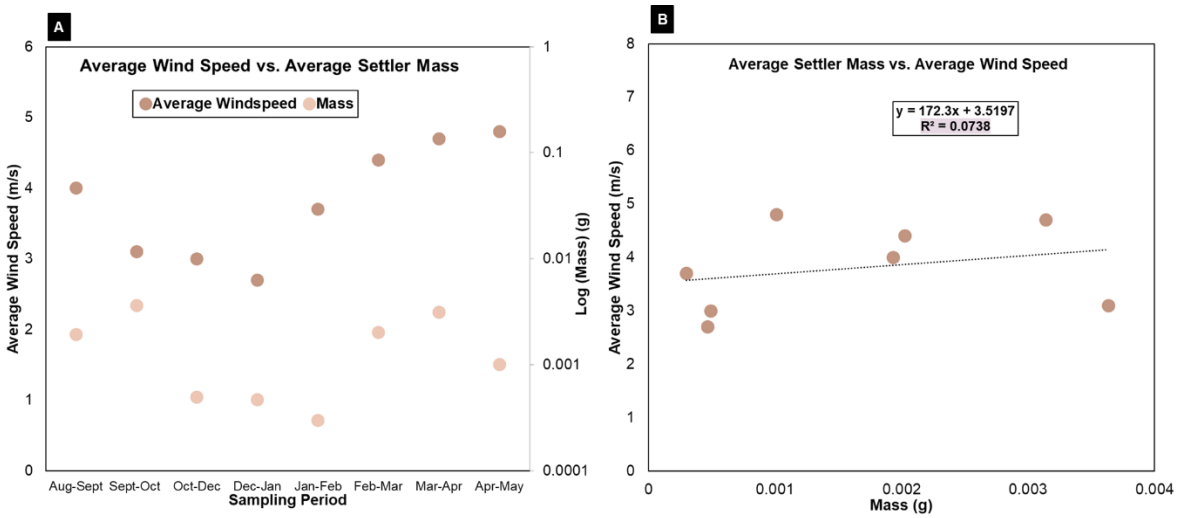

Figure 36. Plot of the average settler masses vs. the monthly average windspeed. Figure 36A shows the average windspeed near Pueblo of Laguna graphed against the logged average settler masses that were collected during each sampling period. Although the linear regression (y=172.3x + 3.5197) coefficient was positive, suggesting an increase in mass with average windspeed, the R^2 (0.0738) value produced from graphing the average windspeed by mass in Figure 36B show that there is no correlation between the variables.

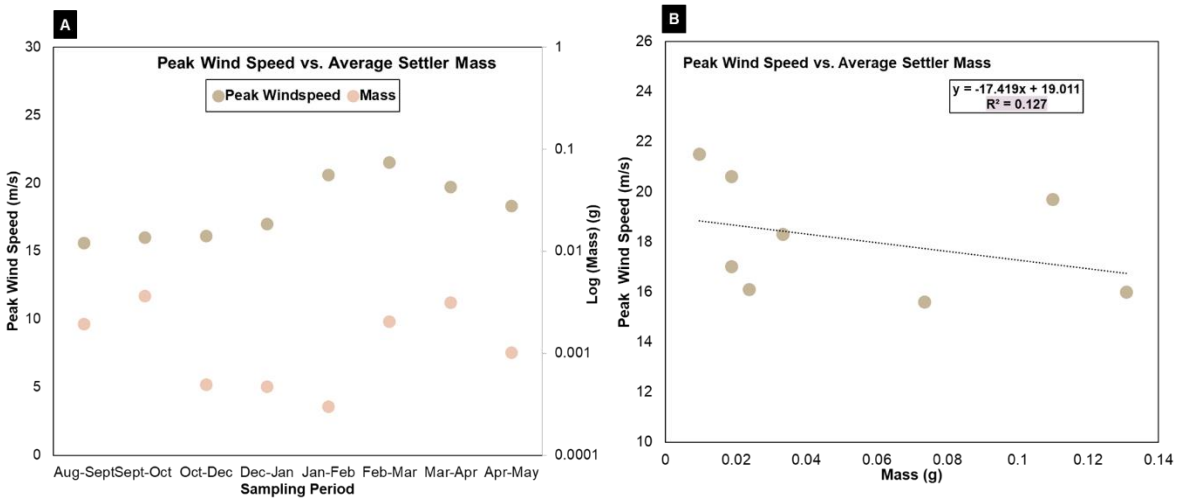

Figure 37. Plot of the average settler masses vs. the peak monthly windspeed. Figure 37A shows the peak windspeed near Pueblo of Laguna graphed against the logged average settler masses that were collected during each sampling period. The linear regression (y=-17.419x + 19.011) coefficient and the low R^2 (0.127) value produced from graphing the peak monthly windspeed by mass in Figure 37B shows that there is no significant correlation between the variables. The changes seen in the amount of mass collected over the sampling periods are not correlated to monthly peak windspeed.

Sample Period	*Deployment Date*	*Retrieval Date*	*Total Days in Field*
August-September	August 14, 2023	September 20, 2023	38
September-October	September 20, 2023	October 25, 2023	36
October-December	October 25, 2023	December 11, 2023	48
December-January	December 11, 2023	January 19, 2024	40
January-February	January 19, 2024	February 19, 2024	32
February-March	February 19, 2024	March 26, 2024	37
March-April	March 26, 2024	April 29, 2024	35
April-May	April 29, 2024	May 31, 2024	33

Table 1. Showing data for each of the 8 sampling periods. The sampling ran from August 2023 to May 2024. Deployment date is when new filters were placed in the collectors and the retrieval date is when they were taken back from the field. During the retrieval dates, new filters were also placed in the collectors. The sampling period is also defined by the number of days the filters were out in the field, which was used to normalize the mass data.

Filter #	Site	Sampling Period	Elements Identified by EDS
2	1	Aug-Sept	O, Ca, Cr, Fe, Ni, Mg, Al, Si, K,
6	3	Aug-Sept	O, Ca, Si, Fe, Cr, Na, Ni, Mg, Mn, Al, Cl, K, Ce, Cu, Zn, Sn, P, Ti
9	5	Aug-Sept	O, Si, Al, Na, Ni, Fe, Cr, Ti, Mg, K, Zr,
10	5	Aug-Sept	O, Fe, Si, Cr, Ni, Mg, Ti, Al,
14	2	Sept-Oct	O, S, Si, Al, Mg, Ti, Fe, Ni, Cr,
15	3	Sept-Oct	O, Na, Ca, Zn, Cu, Ti, Al, Si, Cr, Fe, Ni, K, Ce,
18	4	Sept-Oct	O, S, Si, Fe, Cr, Ni,
27	3	Oct-Dec	O, Si, Cr, Ni, Si, Mg, Al, Fe, Ce, La, P
28	4	Oct-Dec	O, Si, Ca, Al, Fe, Cu, Zn, Mg, Ba, Mg,
41	5	Dec-Jan	O, Si, Fe, Na, Al, S, K, Fe, Ca, Cl, Mg, Ti, Fe, Cu, Zn
44	2	Jan-Feb	O, Si, Al, Mg, Ti, Fe, Cr, Ni
46	3	Jan-Feb	O, Si, Mn, Fe, S, Cu
53	1	Feb-Mar	O, Ca, Si, Al, Mg, Ti, Cr, Fe, Ni, Cu, Zn, P, Co
55	2	Feb-Mar	O, Si, K, Fe, Al, Mg, S, Cu, Zn, P, Ni, Cr,
73	1	Apr-May	O, Si, K, Fe, Al, Mg, Fe, Cr, Ni,
77	3	Apr-May	O, Si, K, Zr, Cu, Zn
79	4	Apr-May	O, Si, Al, Sn, Cr, Ni, Fe, Ti, Mg, Al, Cu, S, Co

Table 2. Table showing the different samples that were analyzed using scanning electron microscopy (SEM). The Filter # is the identifier used when the samples were placed out in the field and are correlated to the site and sampling period that they are from. The SEM analysis spanned each of the 5 different sites as well as the 8 different sampling periods. The composition of the dust grains was qualitatively analyzed using energy dispersive spectroscopy (EDS). EDS results are present in the last column of the table and show the common elements found throughout the dust grains.

Month	*Average Relative Humidity (%)*	*Average Windspeed (m/s)*	*Peak Windspeed (m/s)*
August 2023	41	4.0	15.6
September 2023	41	3.1	16.1
November 2023	52	2.9	15.6
December 2023	55	3.0	16.1
January 2024	58	2.7	17.0
February 2024	46	3.7	20.5
March 2024	45	4.4	21.5
April 2024	35	4.7	19.7
May 2024	29	4.8	18.3

Table 3. Compilation of the average relative humidity, average windspeed, and peak windspeed close to Pueblo of Laguna, New Mexico, during each of the different sampling dust sampling periods. This data was collected from the National Weather Service. These different weather variables were examined to determine if there was a correlation between them and the collected mass.

Site	*Location*	*Coordinates*	*Elevation (m)*
Site 1	Main Pit	35.14431, -107.342254	1857
Site 2	Main Pit	35.13958, -107.33685	1824
Site 3	Main Pit	35.12938, -107.33597	1827
Site 4	North Pit	35.13443, -197.37017	1828
Site 5	South Pit	35.12393, -107.37265	1828

Table 4. Compilation of the geographical information of each of the five sites. Each of the different “sites” are associated with one of the three major pits in the Jackpile Mine. The coordinates of those locations as well as the elevation are also present.

REFERENCES

"Abandoned Uranium Mines and the Navajo Nation." EPA, Aug. 2017.

"Jackpile-Paguate Uranium Mine Laguna Pueblo." Agency for Toxic Substances and Disease Registry (ATSDR), 29 Nov. 2017.

5 benefits of using brass in automotive manufacturing (2023) *Thin Metal Sales*. Available at: https://www.thinmetalsales.com/blog/5-benefits-of-using-brass-in-automotive-manufacturing/#:~:text=Because%20of%20its%20superior%20resistance,stronger%20than%20their%20aluminum%20counterparts. (Accessed: 13 December 2023).

Abanades, Stéphane, Gilles Flamant, and Daniel Gauthier. "Kinetics of heavy metal vaporization from model wastes in a fluidized bed." *Environmental science & technology* 36.17 (2002): 3879-3884.

Abdesselam Abdelouas; Uranium Mill Tailings: Geochemistry, Mineralogy, and Environmental Impact. *Elements* 2006;; 2 (6): 335–341. doi: https://doi.org/10.2113/gselements.2.6.335

Adams, S. S., Curtis, H. S., Hafen, P. L., & Salek-Nejad, H. (1978). Interpretation of postdepositional processes related to the formation and destruction of the JACKPILE-paguate uranium deposit, northwest New Mexico. *Economic Geology*, *73*(8), 1635–1654. https://doi.org/10.2113/gsecongeo.73.8.1635

Agency for Toxic Substances and Disease Registry (ASTDR), Jackpile-Paguate Uranium Mine Laguna Pueblo Laguna, Cibola County, New Mexico (2017).

Agency for Toxic Substances and Disease Registry, Where is Cadmium Found?, (2005).

Agreement signed for Reclamation of Jackpile Mine, New Mexico. U.S. Department of the Interior Indian Affairs. (n.d1986, December 12.). Retrieved December 1, 2022, from https://www.bia.gov/as-ia/opa/online-press-release/agreement-signed-reclamation-jackpile-mine-new-mexico

Avasarala, Sumant, et al. "Effect of bicarbonate and oxidizing conditions on U (IV) and U (VI) reactivity in mineralized deposits of New Mexico." *Chemical geology* 524 (2019): 345-355.

Barceloux, Donald G., and Donald Barceloux. "Molybdenum." *Journal of Toxicology: Clinical Toxicology* 37.2 (1999): 231-237.

Benin, Andrea L., et al. "High concentrations of heavy metals in neighborhoods near ore smelters in northern Mexico." *Environmental Health Perspectives* 107.4 (1999): 279-284.

Bexfield, Laura M., and L. Niel Plummer. "Occurrence of arsenic in ground water of the Middle Rio Grande Basin, central New Mexico." *Arsenic in Ground Water: Geochemistry and Occurrence*. Boston, MA: Springer US, 2003. 295-327.

Bi, Xiangyang, et al. "Environmental contamination of heavy metals from zinc smelting areas in Hezhang County, western Guizhou, China." *Environment international* 32.7 (2006): 883-890.

Blake J., Avasarala, S., Artyushkova, K., Ali, A-M., **Brearley, A.J.**, Shuey, C., Robinson, Wm. P. Nez, C., Bill, S. Lewis, J., Hirani, C., Lezama-Pacheco, J.S. and Cerrato, J. M. (2015) Elevated concentrations of U and co-occurring metals in abandoned mine wastes in a Northeastern Arizona Native American community. *Environmental Science & Technology* ***49***, 8506–8514.

Bowell, Robert J., et al. "The environmental geochemistry of arsenic—an overview—." *Reviews in Mineralogy and Geochemistry* 79.1 (2014): 1-16

Brearley, A. (n.d.). NIEHS METALS Superfund Center Phase II Background.

Brown, Reid Douglas. *Geochemistry and Transport of Uranium-Bearing Dust at Jackpile Mine, Laguna, New Mexico*. MS thesis. New Mexico Institute of Mining and Technology, 2017.

Brugge, D., Dasaraju, A., Lu, Y.Q., Dayer, B. (2015). The externalized costs of uranium mining in the United States. In: Merkel, B., Arab, A. (eds) Uranium - Past and Future Challenges. Springer, Cham. https://doi.org/10.1007/978-3-319-11059-2_35

Buchtela, K. "Radiochemical Methods|gamma-Ray Spectrometry☆." *Reference Module in Chemistry, Molecular Sciences and Chemical Engineering*, vol. 3, 2019, pp. 15–22., https://doi.org/10.1016/b978-0-12-409547-2.11333-2.

Campa, AMS de la, et al. "Impact of abandoned mine waste on atmospheric respirable particulate matter in the historic mining district of Rio Tinto (Iberian Pyrite Belt)." (2011): 1018-1023.

Cannon, Helen L., and Vernon Emanuel Swanson. *Contributions of major and minor elements to soils and vegetation by the coal-fired Four Corners Power Plant, San Juan County, New Mexico*. No. 75-170. US Geological Survey, (1975).

Cediel-Ulloa A, Isaxon C, Eriksson A, Primetzhofer D, Sortica MA, Haag L, Derr R, Hendriks G, Löndahl J, Gudmundsson A, Broberg K, Gliga AR. Toxicity of stainless and mild steel particles generated from gas-metal arc welding in primary human small airway epithelial cells. Sci Rep. 2021 Nov 8;11(1):21846. doi: 10.1038/s41598-021-01177-7. PMID: 34750422; PMCID: PMC8575907.

Cediel-Ulloa, Andrea, et al. "Toxicity of stainless and mild steel particles generated from gas–metal arc welding in primary human small airway epithelial cells." *Scientific Reports* 11.1 (2021): 21846.

Cepriá, G., E. García-Gareta, and J. Pérez-Arantegui. "Cadmium yellow detection and quantification by voltammetry of immobilized microparticles." *Electroanalysis: An International Journal Devoted to Fundamental and Practical Aspects of Electroanalysis* 17.12 (2005): 1078-1084.

Cooke, Gail, et al. "Analysis of Particulate Matter (PM10 and PM2. 5) Exceedances Caused by High Winds April 2001–June 2001 Doña Ana County, New Mexico." (2001): 1-13.

Cortie, M.B., McEwan, J.J. and Enright, D.P. (1996) 'Materials selection in the mining industry: old issues and new challenges', *Journal of the Southern African Institute of Mining and Metallurgy* , 96(4), pp. 145–155. Available at: https://hdl.handle.net/10520/AJA0038223X_2375.

Councell TB, Duckenfield KU, Landa ER, Callender E. Tire-wear particles as a source of zinc to the environment. Environ Sci Technol. 2004 Aug 1;38(15):4206-14. doi: 10.1021/es034631f. PMID: 15352462.

Csavina J, Field J, Taylor MP, Gao S, Landázuri A, Betterton EA, Sáez AE. A review on the importance of metals and metalloids in atmospheric dust and aerosol from mining operations. Sci Total Environ. 2012 Sep 1;433:58-73. doi: 10.1016/j.scitotenv.2012.06.013. Epub 2012 Jul 4. PMID: 22766428; PMCID: PMC3418464.

Csavina, Janae, et al. "A review on the importance of metals and metalloids in atmospheric dust and aerosol from mining operations." *Science of the Total Environment* 433 (2012): 58-73.

Csavina, Janae, et al. "Metal and metalloid contaminants in atmospheric aerosols from mining operations." *Water, Air, & Soil Pollution* 221 (2011): 145-157.

Deditius, Artur P., Satoshi Utsunomiya, and Rodney C. Ewing. "The chemical stability of coffinite, USiO4· nH2O; 0< n< 2, associated with organic matter: A case study from Grants uranium region, New Mexico, USA." *Chemical Geology* 251.1-4 (2008): 33-49.

Diawara, Moussa M., et al. "Arsenic, cadmium, lead, and mercury in surface soils, Pueblo, Colorado: implications for population health risk." *Environmental Geochemistry and Health* 28 (2006): 297-315.

Diawara, Moussa M., et al. "Arsenic, cadmium, lead, and mercury in surface soils, Pueblo, Colorado: implications for population health risk." *Environmental Geochemistry and Health* 28 (2006): 297-315.

Donald E. Owen, Walters, Lester J., Jr., and Ronald G. Beck New Mexico Geology, v. 6, n. 3 pp. 45-52, Print ISSN: 0196-948X, Online ISSN: 2837-6420. https://doi.org/10.58799/NMG-v6n3.45

El Hayek, Eliane, et al. "Uptake and toxicity of respirable carbon-rich uranium-bearing particles: insights into the role of particulates in uranium toxicity." *Environmental science & technology* 55.14 (2021): 9949-9957.

Elena S. Craft, Aquel W. Abu-Qare, Meghan M. Flaherty, Melissa C. Garofolo, Heather L. Rincavage & Mohamed B. Abou-Donia (2004) DEPLETED AND NATURAL URANIUM: CHEMISTRY AND TOXICOLOGICAL EFFECTS, Journal of Toxicology and Environmental Health, Part B, 7:4, 297-317, DOI: 10.1080/10937400490452714

Environmental Protection Agency. (2017, October 20). *Jackpile-paguate uranium mine site profile*. EPA. Retrieved December 1, 2022, from https://cumulis.epa.gov/supercpad/SiteProfiles/index.cfm?fuseaction=second.cleanup&id=0607033

Environmental Protection Agency. (n.d.). *Air Quality Dispersion Modeling-Alternative Models*. EPA. Retrieved December 1, 2022, from https://www.epa.gov/scram/air-quality-dispersion-modeling-alternative-models

Environmental Protection Agency. *The Legacy of Abandoned Uranium Mines in the Grants Mineral Belt, New Mexico,* https://www.epa.gov/sites/default/files/2015-08/documents/uranium-mine-brochure.pdf. Accessed 27 Feb. 2023.

EPA (2013) 'Support Document for the Revised National Priorities List Final Rule-Jackpile-Paguate Uranium Mine'. EPA.

EPA (2016) 'Overview of the Current Hazard Ranking System'.

Esworthy, Robert. "Air quality: EPA's 2013 changes to the particulate matter (PM) standard." Washington, DC, USA: Library of Congress, Congressional Research Service, 2013.

Forth, L. (1970) *Stainless steel and the mining industry, https://specialpipingmaterials.com*. Available at: https://specialpipingmaterials.com/stainless-steel-and-the-mining-industry/ (Accessed: 13 December 2023).

Gao, Jintao, et al. "Recovery of crown zinc and metallic copper from copper smelter dust by evaporation, condensation and super-gravity separation." *Separation and Purification Technology* 231 (2020): 115925.

Gimeno-Adelantado, J. V., and F. Bosch-Reig. "Identification of inorganic pigments from paintings and polychromed sculptures immobilized into polymer film electrodes by stripping differential pulse voltammetry."

Gonzalez–Maddux, Cristina, et al. "Elemental composition of PM2. 5 in Shiprock, New Mexico, a rural community located near coal–burning power plants and abandoned uranium mine tailings sites." *Atmospheric Pollution Research* 5.3 (2014): 511-519.

Guney, Mert, Robert P. Chapuis, and Gerald J. Zagury. "Lung bioaccessibility of contaminants in particulate matter of geological origin." *Environmental Science and Pollution Research* 23 (2016): 24422-24434.

Guo, Xue-yi, et al. "Copper and arsenic substance flow analysis of pyrometallurgical process for copper production." *Transactions of Nonferrous Metals Society of China* 32.1 (2022): 364-376.

Hahladakis, John N., et al. "An overview of chemical additives present in plastics: Migration, release, fate and environmental impact during their use, disposal and recycling." *Journal of hazardous materials* 344 (2018): 179-199.

Heather E. Jamieson, Stephen R. Walker, Michael B. Parsons, Mineralogical characterization of mine waste, Applied Geochemistry, Volume 57,2015, Pages 85-105, ISSN 0883-2927, doi: https://doi.org/10.1016/j.apgeochem.2014.12.014

Hettiarachchi, Eshani, et al. "Mineralogy controlled dissolution of uranium from airborne dust in simulated lung fluids (SLFs) and possible health implications." *Environmental science & technology letters* 6.2 (2018): 62-67.

Hettiarachchi, Eshani, et al. "The fate of inhaled uranium-containing particles upon clearance to gastrointestinal tract." *Environmental Science: Processes & Impacts* 24.8 (2022): 1257-1266.

Jackpile-paguate uranium mine site profile (2017) *EPA.* Available at: https://cumulis.epa.gov/supercpad/SiteProfiles/index.cfm?fuseaction=second.Healthenv&id=0607033 (Accessed: 13 December 2023).

Jeong, Hyeryeong, and Kongtae Ra. "Source apportionment and health risk assessment for potentially toxic elements in size-fractionated road dust in Busan Metropolitan City, Korea." *Environmental Monitoring and Assessment* 194.5 (2022): 350.

John N. Hahladakis, Costas A. Velis, Roland Weber, Eleni Iacovidou, Phil Purnell, An overview of chemical additives present in plastics: Migration, release, fate and environmental impact during their use, disposal and recycling, Journal of Hazardous Materials,Volume 344, 2018, Pages 179-199, ISSN 0304-3894, https://doi.org/10.1016/j.jhazmat.2017.10.014.

Kim, Ki-Hyun, Ehsanul Kabir, and Shamin Kabir. "A review on the human health impact of airborne particulate matter." *Environment international* 74 (2015): 136-143.

Kok, Jasper F., et al. "The physics of wind-blown sand and dust." *Reports on progress in Physics* 75.10 (2012): 106901.

Kubier, Andreas, Richard T. Wilkin, and Thomas Pichler. "Cadmium in soils and groundwater: A review." *Applied Geochemistry* 108 (2019): 104388.

Lanteigne, Sonia, Michael Schindler, and Andrew McDonald. "Distribution of metals and metalloids in smelter-derived particulate matter in soils and mineralogical insights into their retention and release in a low-T environment." *The Canadian Mineralogist* 52.3 (2014): 453-471.

LaRosa-LoPresti, Savannah S.. "WINDBLOWN TRANSPORT OF TOXIC METALS IN AIRBORNE PARTICULATE MATTER NEAR THE JACKPILE-PAGUATE URANIUM MINE ON LAGUNA PUEBLO, NEW MEXICO." (2021). https://digitalrepository.unm.edu/eps_etds/297

Lewis J, Hoover J, MacKenzie D. Mining and Environmental Health Disparities in Native American Communities. Curr Environ Health Rep. 2017 Jun;4(2):130-141. doi: 10.1007/s40572-017-0140-5. PMID: 28447316; PMCID: PMC5429369.

Li, P. J., et al. "Temporal and spatial distribution patterns of heavy metals in soil at a long-standing sewage farm." *Environmental monitoring and assessment* 149 (2009): 275-282.

Lund, L. J., A. L. Page, and C. O. Nelson. *Movement of heavy metals below sewage disposal ponds*. Vol. 5. No. 3. American Society of Agronomy, Crop Science Society of America, and Soil Science Society of America, 1976.

Machado, A. T., et al. "Structural ceramics made with clay and steel dust pollutants." *Applied Clay Science* 51.4 (2011): 503-506.

McLemore, V. T., Frey, B. A., El Hayek, E., Hettiarachchi, E., Brown, R., Chavez, O., Paul, S., & Das, M. (2021). The jackpile-paguate uranium mine, grants Uranium District: Changes in perspectives from production to superfundsite. *Geology of the Mount Taylor Area*, 183–194. https://doi.org/10.56577/ffc-71.183

McLemore, Virginia T., et al. "Uranium Resources in the Grants Uranium District, New Mexico: An Update." *Geology of Route 66 Region: Flagstaff to Grants,* 2013*,* https://doi.org/10.56577/ffc-64.117.

Meyer, M. (2020, January 14). https://law.ucla.edu/sites/default/files/PDFs/Academics/Meyer-Paguate-Jackpile%20Mine.pdf. UCLA.

Miller, Casey, et al. "Interfacial Interactions of Uranium and HDPE in agricultural soil and their bioacummulation in Mentha arvensis." (2022).

Miller, Elizabeth. "'Like a Demon That's Always behind Us', the JACKPILE Mine Toxic Legacy Continues." *New Mexico In Depth,* 13 Feb. 2022, https://nmindepth.com/2021/like-a-demon-thats-always-behind-us-the-jackpile-mine-toxic-legacy-continues/.

Moench, R.H. and Schlee, J.S. (1967) 'Geology and Uranium Deposits of the Laguna District, New Mexico'. Washington: U.S. Atomic Energy Commission .

Moench, Robert Hadley, and John Stevens Schlee. *Geology and uranium deposits of the Laguna district, New Mexico*. No. 519. US Govt. Print. Off.,, 1967.

Montenegro, Victor, Hiroyuki Sano, and Toshiharu Fujisawa. "Recirculation of high arsenic content copper smelting dust to smelting and converting processes." *Minerals Engineering* 49 (2013): 184-189.

Morozesk, Mariana, et al. "Airborne particulate matter in an iron mining city: Characterization, cell uptake and cytotoxicity effects of nanoparticles from PM2. 5, PM10 and PM20 on human lung cells." *Environmental Advances* 6 (2021): 100125.

Patra, Aditya Kumar, Sneha Gautam, and Prashant Kumar. "Emissions and human health impact of particulate matter from surface mining operation—A review." *Environmental Technology & Innovation* 5 (2016): 233-249.

Pearce, Alexandra Rose. *Implications of Cryptic, Nonstoichiometric Uranium Mineralization on the Formation and Leachability of Sandstone-Hosted Uranium Ores, Grants District, New Mexico*. New Mexico Institute of Mining and Technology, 2020.

Popoola, L. T., S. A. Adebanjo, and B. K. Adeoye. "Assessment of atmospheric particulate matter and heavy metals: a critical review." *International Journal of Environmental Science and Technology* 15 (2018): 935-948..

Price, Lisa. “Assessment of Health and Environmental Impacts of Uranium Mining and Milling .” Environmental Protection Agency, Aug. 2010.

Richard Michael James, Mohamad Jamal Altamimi, The enhancement of friction ridge detail on brass ammunition casings using cold patination fluid,Forensic Science International, Volume 257, 2015, Pages 385-392, ISSN 0379-0738, https://doi.org/10.1016/j.forsciint.2015.10.004. (https://www.sciencedirect.com/science/article/pii/S0379073815004284)

S.M. Hall, B.S. Van Gosen, R.A. Zielinski,Sandstone-hosted uranium deposits of the Colorado Plateau, USA, Ore Geology Reviews,Volume 155, 023,105353, ISSN 0169-1368, https://doi.org/10.1016/j.oregeorev.2023.105353. (https://www.sciencedirect.com/science/article/pii/S0169136823000689)

Sanchez, Petra. “Jackpile-Paguate Uranium Mine.” EPA, 17 Sept. 2015.

Schindler, Michael, et al. "Mobilization and agglomeration of uraninite nanoparticles: A nano-mineralogical study of samples from the Matoush Uranium ore deposit." *American Mineralogist* 102.9 (2017): 1776-1787.

Seltenrich, Nate. "Cleaning Up after the Cold War: Experts Call for Action on Abandoned Uranium Mines on the Navajo Nation." *Environmental Health Perspectives* 129.9 (2021): 094001.

Shane Wero & Rena Martin (2021) Łeetso – Working and Living Within the Monster: A Cultural Resources Study of Navajo Habitations Within Former Uranium Mines in the Cove and Monument Valley Regions, KIVA, 87:3, 354-376, DOI: 10.1080/00231940.2021.1930648

Stovern, Michael, et al. "Windblown dust deposition forecasting and spread of contamination around mine tailings." *Atmosphere* 7.2 (2016): 16.

Suzuki, Keiko. "Characterisation of airborne particulates and associated trace metals deposited on tree bark by ICP-OES, ICP-MS, SEM-EDX and laser ablation ICP-MS." *Atmospheric Environment* 40.14 (2006): 2626-2634.

Thomson, Bruce. “The Environmental Legacy of Uranium Mining and Milling in New Mexico .” *New Mexico Geological Society*, 2021, https://doi.org/10.56577/FFC-71.

Turner, Andrew, and Montserrat Filella. "The role of titanium dioxide on the behaviour and fate of plastics in the aquatic environment." *Science of the Total Environment* 869 (2023): 161727.

United States Geological Survey (USGS), Arsenic in Coal (2005).

Velasco, Carmen A., et al. "Organic functional group chemistry in mineralized deposits containing U (IV) and U (VI) from the Jackpile Mine in New Mexico." *Environmental science & technology* 53.10 (2019): 5758-5767.

Victoria E. Burlakova, Ekaterina G. Drogan, Igor E. Uflyand, Alexey A. Milov, Boris S. Lukyanov, Wear products and tribochemical reactions during friction of a brass-steel pair, Wear, Volumes 462–463, 2020, 203517, ISSN 0043-1648, https://doi.org/10.1016/j.wear.2020.203517. (https://www.sciencedirect.com/science/article/pii/S0043164820309765)

Vouitsis, Ilias, et al. "Transport-related airborne nanoparticles: Sources, different aerosol modes, and their toxicity." *Atmospheric Environment* 301 (2023): 119698.

Xu, Da-Mao, et al. "Current knowledge from heavy metal pollution in Chinese smelter contaminated soils, health risk implications and associated remediation progress in recent decades: A critical review." *Journal of Cleaner Production* 286 (2021): 124989.

Yao, Wen-ming, et al. "Formation of arsenic− copper-containing particles and their sulfation decomposition mechanism in copper smelting flue gas." *Transactions of Nonferrous Metals Society of China* 31.7 (2021): 2153-2164.

Yao, Zhipeng, et al. "Numerical investigation of 700 C boiler flue gas thermal deviation based on orthogonal experiment." *Fuel* 295 (2021): 120510.

Yudovich, Ya E., and M. P. Ketris. "Arsenic in coal: a review." *International Journal of Coal Geology* 61.3-4 (2005): 141-196.

Zajzon, Norbert, et al. "Tracking magnetic pollutants by integrated mineralogical and magnetic analyses of airborne particles in urban environment." *Earth Environ. Sci* 8 (2013): 221-229.

Zeb, Bahadar, et al. "Variation in coarse particulate matter (PM10) and its characterization at multiple locations in the Semiarid Region." *Frontiers in Environmental Science* 10 (2022): 843582.

Zhang, F-S., M. Nanzyo, and K. Kimura. "Evaluation of cadmium and other metal losses from various municipal wastes during incineration disposal." *Environmental Pollution* 115.2 (2001): 253-260.

Zhang, Kai, et al. "Size distribution and source of heavy metals in particulate matter on the lead and zinc smelting affected area." *Journal of Environmental Sciences* 71 (2018): 188-196.